# On the Chronostratigraphy of Planetary Satellites and Asteroids

Absolute Surface Age Determination of Small Planetary Bodies:
Scaling the Lunar Crater Chronology System

vorgelegt von
Dipl.-Geol. Nico Schmedemann

Fachbereich Geowissenschaften
Freie Universität Berlin

Dissertation zur Erlangung des Grades
Doktor der Naturwissenschaften (Dr. rer. nat.)

Berlin, im Juli 2015

Hauptgutachter: Prof. Dr. R. Jaumann
Freie Universität Berlin
Institut für Geologische Wissenschaften
Fachrichtung Planetologie und Fernerkundung
und
Deutsches Zentrum für Luft- und Raumfahrt
Institut für Planetenforschung, Abt. Planetengeologie

Zweitgutachter: Prof. Dr. S. v. Gasselt
Freie Universität Berlin
Institut für Geologische Wissenschaften
Fachrichtung Planetologie und Fernerkundung

Tag der Disputation: 1. Dezember 2015

## Eidesstattliche Erklärung

Hiermit versichere ich, die vorliegende Arbeit selbstständig angefertigt und keine anderen als die angegebenen Quellen und Hilfsmittel benutzt zu haben.

Berlin, 2015

# Danksagung

Großer Dank gebührt dem zwischenzeitlich leider verstorbenen Herrn Prof. Dr. Gerhard Neukum (FU-Berlin) für die Vergabe des Themas und der damit verbundenen Einstellung als Wissenschaftlicher Mitarbeiter in der Fachrichtung Planetologie an der Freien Universität Berlin. Durch seine Beteiligung an zahlreichen aktiven Raumfahrtmissionen ergab sich für mich die Möglichkeit mit bisher unveröffentlichten Daten in den Projekten Cassini und Dawn zu arbeiten. Er hat mich oft dazu ermuntert neue Ideen im Detail an den vorhandenen Daten zu testen, mit früheren Ergebnissen zu vergleichen und dabei das große Bild nicht aus den Augen zu verlieren. Er bestand zudem auch auf starke Präsenz bei internationalen Konferenzen, die einen angeregten Gedankenaustausch mit anderen Fachkollegen ermöglichten, die oft auch grundsätzlich andere Ansichten vertreten haben.

Da Herr Prof. Dr. Neukum meine Arbeit nicht mehr betreuen kann, möchte ich mich bei Herrn Prof. Dr. R. Jaumann (Deutsches Zentrum für Luft und Raumfahrt, FU-Berlin) dafür bedanken, dass er sich für meine Arbeit als Betreuer und Erstgutachter bereit erklärt hat. In seiner Funktion als „Head of the Geoscience Working Group" im Dawnprojekt hatte er einen ganz besonderen Einblick in die Diskussionen rund um die Chronostratigrafie des Asteroiden Vesta, die ein wesentlicher Bestandteil dieser Arbeit ist.

Weiterer Dank gebührt Herrn Prof. Dr. S. van Gasselt (FU-Berlin) für die Übernahme der Zweitbegutachtung dieser Arbeit. Ganz besonderer Dank gilt ihm außerdem für die sehr hilfreichen Hinweise zur Planung, zur Struktur und zum Erscheinungsbild der Arbeit.

Als äußerst wertvoll empfand ich die langen und intensiven Diskussionen mit meinen Kollegen Dr. T. Kneissl, Dr. G. Michael und Dipl.-Geol. A. Neesemann über viele Details der Kraterverteilung und Chronologie auf Vesta aber auch über das eine oder andere Thema am Rande. Sehr hilfreiche Diskussionen schon zu Beginn meiner Arbeit bekam ich besonders von Dr. R. J. Wagner und Dipl.-Ing. T. Denk bezüglich des Cassini Projekts. Nicht vergessen möchte ich hierbei die Einführung in die Arbeit am Stereokomparator, die ich von Dr. S. C. Werner und Frau U. Wolf erhielt.

Großer Dank für die Unterstützung in Fragen der Informationstechnologie gebührt Dipl.-Geol. S. H. G. Walter. Das betrifft nicht nur die Instandhaltung des Bürorechners, sondern die gesamte Infrastruktur in unserer Fachrichtung. Aufwendige Rechnungen und die Bilddatenprozessierung für diese Arbeit sind auch auf den Servern der Fachrichtung gelaufen. Ebenfalls bedanken möchte ich mich bei Dipl.-Ing. Heike Rosenberg für die Unterstützung in der Cassinibilddatenverwaltung und die liebevolle Ausrichtung der Weihnachtsfeiern bei der sie von weiteren Mitgliedern unserer Arbeitsgruppe unterstützt wurde. Insgesamt möchte ich mich

bei der gesamten Arbeitsgruppe für die gute Zusammenarbeit und hilfsbereite Unterstützung bedanken.

Die aktive Arbeit im Dawn Team hat mir zudem gezeigt, dass die richtige Erkenntnis oft nicht ein Resultat eines vorgegebenen Arbeitsablaufs ist, sondern das Ergebnis eines mitunter lebhaften Austauschs von wissenschaftlichen Argumenten, die dazu anhalten, noch genauer und noch akribischer zu arbeiten.

Zum Abschluss gilt mein Dank auch meiner Familie und meinen Freunden, die immer fest an einen erfolgreichen Abschluss der Arbeit geglaubt haben.

## Abstract

Based on recent geologic research it appears that meteoritc bombardment is a major agent in the exogenic dynamics of Earth and other planetary bodies, especially in more ancient times (e.g. Neukum, 1984; Hildebrand et al., 1991; Gehrels, 1995; Becker et al., 2004 and Bottke et al., 2012). Furthermore, meteoritic bombardment is one of the few foreseeable natural hazards which mankind is able to prepare for to a certain degree. This is true predominantly for larger projectiles which orbital characteristics is known well ahead of a potential impact. Predicting impact risks, however, requires a deep understanding of numerous processes, which eventually result in such an event. Even the simple comparison between the Moon and the Earth shows for instance, that the time-dependent behavior of the projectile flux as well as the crater size-frequency distribution, is hard to investigate thoroughly on Earth alone.

This thesis aims to relate the understanding of the meteoritic bombardment in the Earth-Moon system to other dynamical regions of our Solar System. Resulting in a significant improvement in one of the key issues in the field of planetary sciences: the ability to date planetary surfaces from impact craters on bodies from the inner Solar System to the asteroid Main Belt and the giant planet satellites of the outer Solar System.

This tool is key in understanding the geologic history of the investigated bodies since the terminal phase of planetary accretion about 4 Ga ago until today. The cratering records of planetary bodies and the related projectile dynamics in the inner Solar System are relatively well known from vast sets of remote sensing data of the Moon, Mars and to a lesser degree, Mercury. In the case of the Moon, absolute calibration of the measured crater frequencies was possible by radiometric dating of returned lunar rock and soil samples. For bodies in the asteroid Main Belt and beyond, in the outer Solar System, the smaller sets of remote sensing data, limitations in observations of projectiles, and incomplete models of projectile dynamics complicate the interpretation of the cratering records and thus the understanding of the geologic history of respective planetary bodies.

The work presented in this thesis utilizes the lunar cratering record and adopts it with some customization for the investigated planetary bodies with significantly different impact environments than the Moon. By comparing the predictions of the lunar-like model and the observed cratering records at different locations in the Solar System (Martian satellite Phobos, Main Belt asteroids and Saturnian satellites) a significant increase in knowledge has been achieved about the projectiles' origin and their dynamical characteristics. Applying the lunar-like cratering models to surface areas that are related to major geologic events on the investigated bodies allowed for the exploration of their individual geologic histories as well as, partially, their dynamical histories. A comparison of the geologic histories of the planetary bodies across the Solar System also offers a possibility to understand the development of the Solar System in many different aspects. Such aspects are for

instance the projectile dynamics and collisional evolution of small bodies from the late stage planetary accretion until today. Stratigraphic relationships were used in order to test the lunar-like models and alternative models of other scientific working groups for consistency.

Results from the Saturnian satellites Mimas and Iapetus, the Main Belt asteroids Vesta, Lutetia, Ida and Gaspra as well as the Martian satellite Phobos studied in this work showed that they are consistent with a lunar-like impact history.

Under consideration of earlier work, the timing of youngest basin forming impact events on the Moon, Mars and the larger asteroids as well as the time of the Phobos capture and the catastrophic disruption of the precursor bodies of Ida and Lutetia lead to the conclusion of similar projectile flux characteristics at all of these bodies at the end of the heavy bombardment time period. During the first billion years of Solar System history the exponential decline in the Solar System-wide projectile flux could be interpreted as the tail of planetary accretion. In this respect the Saturnian system needs further analysis in order to find and properly date its youngest basin.

For the Saturnian satellites Mimas and Iapetus the crater distributions suggest a planetocentric and collisionally evolved source of projectiles with relatively low impact velocities. Mimas appears to have been geologically inactive since its surface accumulated the currently observable craters. The satellite shows the same crater retention age (~4.3 Ga) over its whole surface. Its largest crater, Herschel, formed about 4 Ga ago. Crater size-distributions on the asteroids Ida, Gaspra, Lutetia and Vesta clearly show a lunar-like behavior that has previously been discussed and was expected to be shallower at small sizes based on modelling of collisional cascades of asteroids. In the case of the geologically complicated asteroid Vesta, absolute crater retention ages of basin forming events show a high level of agreement with an independent radiometric chronometer. This particular result does not only imply a consistent conversion of the lunar cratering functions to Vesta, but also supports the underlying lunar chronology. Results from the Martian satellite, Phobos, suggest that the poorly understood formation of its grooves likely occurred more than ~3 Ga ago and that Phobos is probably a captured asteroid that has been in orbit about Mars since about 4 Ga.

# Kurzfassung

Die jüngere Geschichte geologischer Forschung hat die Erkenntnis wachsen lassen, dass Meteoriteneinschläge auf der Erde ein wesentlicher Faktor der exogenen Dynamik insbesondere auf der jungen Erde waren (z.B. Neukum, 1984; Hildebrand et al., 1991; Gehrels, 1995; Becker et al., 2004 und Bottke et al., 2012). Meteoriteneinschläge gehören zudem zu den wenigen Naturkatastrophen, auf die sich die Menschheit in einem gewissen Rahmen theoretisch vorbereiten kann. Dies gilt insbesondere für größere Projektile, deren Flugbahnen lange vor einem potenziellen Einschlag bekannt sind. Zur Vorhersage von Meteoriteneinschlagsrisiken ist ein sehr gutes Verständnis aller Faktoren notwendig, die zu einem solchen Ereignis führen. Schon der einfache Vergleich zwischen dem stark bekraterten Erdmond und der fast gar nicht bekraterten Erde zeigt, dass das zeitliche Verhalten, sowie die Größen - Häufigkeitsverteilung von Meteoriteneinschlägen aus statistischen Gründen nur sehr schwer direkt auf der Erde erforscht werden können.

Das Ziel dieser Arbeit ist es, das Verständnis des Meteoritenbombardements im Erde – Mond System in einen Bezug zum Bombardement in anderen Regionen des Sonnensystems und möglichen Projektilpopulationen zu setzen. Dabei wird die Methode zur Datierung planetarer Oberflächen durch Meteoriteneinschlagskrater vom inneren Sonnensystem auf die Körper des Asteroidengürtels und die Monde des äußeren Sonnensystems übertragen. Die vorliegende Arbeit liefert damit einen Beitrag in einem der zentralen Aufgabenfelder in der Planetologie.

Datierungen der planetaren Oberfläche sind der Schlüssel zum Verständnis der geologischen Entwicklung der untersuchten Körper seit der Endphase der Planetenentstehung vor etwa 4 Ga bis heute. Die Kraterverteilungen auf den Körpern des inneren Sonnensystems und die Dynamik der entsprechenden Projektile werden durch die umfangreichen fernerkundlichen Datensätze von Mond und Mars bereits gut verstanden. Für den Mond konnten die gemessenen Kraterhäufigkeiten mit radiometrisch datierten Boden- und Gesteinsproben kalibriert werden. Für die Körper außerhalb des inneren Sonnensystems, ist die Datenlage schwieriger und Modelle zur Projektilherkunft und -dynamik scheinen unvollständig zu sein, wodurch Interpretationen zur beobachteten Kraterverteilung und zur geologischen Entwicklung der Körper erschwert werden.

Die vorliegende Arbeit nutzt die lunare Kratergrößen - Häufigkeitsverteilung und passt sie als Model an die individuellen, zum Teil sehr stark vom Mond abweichenden, Einschlagsbedingungen der untersuchten Körper an. Durch den Vergleich der Vorhersagen der mondähnlichen Modelle mit den beobachteten Kraterverteilungen an verschiedenen Orten innerhalb des Sonnensystems (inneres/äußeres Sonnensystem und Asteroidengürtel) konnte ein deutlich verbessertes Verständnis zur Herkunft der Projektile und ihrer dynamischen Eigenschaften erlangt werden. Die Anwendung mondähnlicher Kraterverteilungsmodelle auf wichtigen geologischen Einheiten erlaubt die Untersuchung der

individuellen geologischen und z.T. dynamischen Entwicklung der betrachteten Körper. Der Vergleich signifikanter geologischer Ereignisse der einzelnen planetaren Körper im Sonnensystem lässt auch Rückschlüsse auf dessen Entwicklung als Ganzes zu. Mit Hilfe stratigrafischer Beziehungen wurden sowohl die mondähnlichen Kraterverteilungsmodelle als auch alternative Modelle auf ihre jeweilige Konsistenz getestet.

Die in der vorliegenden Arbeit von den Saturnmonden Mimas und Iapetus, den Hauptgürtelasteroiden Vesta, Lutetia, Ida und Gaspra und dem Marsmond Phobos gewonnenen Ergebnisse sind konsistent mit einer mondähnlichen Impaktgeschichte.

Unter Berücksichtigung früherer Arbeiten führt die zeitliche Einordnung der jüngsten beckenbildenden Einschlagsereignisse auf dem Mond, Mars und Vesta als auch die Zeit des Phoboseinfangs und der katastrophalen Zerstörung der Vorläuferkörper von Ida und Lutetia zu der Schlussfolgerung einer ähnlichen Entwicklung der Einschlagsrate mit exponentiell abnehmender Intensität auf allen diesen Körpern bis zum Ende der Periode starken Bombardements ca. 1 Ga nach Entstehung des Sonnensystems. Dieses zeitlich sehr ähnliche Verhalten des Meteoritenbombardements in großen Teilen unseres Sonnensystems, könnte als die auslaufende Akkretion der planetaren Körper interpretiert werden. In diesem Zusammenhang sollte das Saturnsystem noch weiter untersucht werden, um dort das jüngste Becken zu finden und korrekt zu datieren.

Bei den Saturnmonden Mimas und Iapetus weisen die Kraterverteilungen auf eine planetozentrische und kollisionsentwickelte Quelle der Projektile hin, die mit relativ niedrigen Geschwindigkeiten einschlagen. Mimas scheint geologisch inaktiv zu sein, seitdem die beobachtbaren Krater entstanden sind, da das gleiche Kraterretentionsalter (~4.3 Ga) auf der gesamten Oberfläche gefunden wurde. Sein größter Krater Herschel entstand vor etwa 4 Ga. Die Krater-Größenhäufigkeitsverteilungen auf den untersuchten Asteroiden Ida, Gaspra, Lutetia und Vesta zeigen eine deutlich mondähnliche Charakteristik, die schon in früheren Arbeiten diskutiert aber basierend auf Kollisionskaskadenmodellierungen bei kleinen Kratergrößen deutlich flacher erwartet wurde. Im Falle des Asteroiden Vesta zeigen absolute Kraterretentionsalter beckenbildender Ereignisse einen hohen Grad an Übereinstimmung mit einem unabhängigen radiometrischen Chronometer. Dieses wichtige Ergebnis impliziert zum einen die konsistente Übertragung der lunaren Chronologie- und Kraterproduktionsfunktion auf Vesta und zum anderen wird die zugrunde liegende lunare Chronologiefunktion damit indirekt bestätigt. Die Ergebnisse von Phobos legen nahe, dass die wenig verstandene Bildung seiner Furchensysteme vermutlich vor mehr als etwa 3 Ga stattfand und das es sich bei Phobos möglicherweise um einen vor ca. 4 Ga eingefangenen Asteroiden handelt.

# Content


**1 INTRODUCTION ..... 1**

1.1 Significance of chrono-stratigraphy and the role of radiometric ages for the determination of the geologic history of planetary bodies and the history of the Solar System ..... 1

1.2 Scope of this Work and Structure ..... 7

**2 DETAILS ON METHODOLOGY NOT INCLUDED OR REFERENCED IN THE PRESENTED PAPERS ..... 9**

2.1 Brief overview on the geology and astronomic relation of the investigated bodies ..... 9

*2.1.1 Phobos ..... 9*

*2.1.2 (951) Gaspra ..... 9*

*2.1.3 (243) Ida ..... 9*

*2.1.4 (21) Lutetia ..... 10*

*2.1.5 (4) Vesta ..... 10*

*2.1.6 Mimas ..... 10*

*2.1.7 Iapetus ..... 11*

2.2 Scaling error of projected imaging data between reference body surface and true body surface on irregularly shaped small bodies ..... 11

*2.2.1 Case Ida: ..... 11*

*2.2.2 Case Gaspra: ..... 12*

*2.2.3 Case Lutetia: ..... 12*

*2.2.4 Case Vesta: ..... 12*

2.3 Applicability of saturation or standard equilibrium distribution on small bodies ..... 14

*2.3.1 Highest crater frequencies on Vesta – in equilibrium? ..... 16*

2.4 Dependence of model ages on the shape of the production function ..... 17

*2.4.1 Fit range > 1 km (reference crater size) ..... 17*

*2.4.2 Fit range < 1 km (Reference Crater Size) ..... 18*

**3 THE AGE OF PHOBOS AND ITS LARGEST CRATER, STICKNEY ..... 21**

3.1 Introduction ..... **Fehler! Textmarke nicht definiert.**

3.2 Methodology ..... 23

*3.2.1 Measurements of crater size–frequency distributions ..... 23*

*3.2.2 Interpretation of crater distributions ..... 23*

*3.2.3 Randomness analysis ..... 24*

*3.2.4 Production function ..... 25*

*3.2.5 Chronology function ..... 27*

3.3 Results ..... 29

*3.3.1 Average surface to the west of Stickney ..... 29*

*3.3.2 The interior of Stickney ..... 31*

*3.3.3 Spatial randomness analysis ..... 36*

*3.3.4 Crater density asymmetry at apex and antapex points of orbital motion ..... 37*

3.4 Summary ..... 38

3.5 Acknowledgment ..... 40

**4 THE CRATERING RECORD, CHRONOLOGY AND SURFACE AGES OF (4) VESTA IN COMPARISON TO SMALLER ASTEROIDS AND THE AGES OF HED METEORITES ..... 41**

4.1 Introduction ..... **Fehler! Textmarke nicht definiert.**

4.2 Methodology ..... 43

*4.2.1 Crater counting ..... 43*

*4.2.2 Derivation of the crater production functions of asteroids* ..... *45*
*4.2.3 Discussion of alternative proposed chronology model* ..... *55*
4.3 Results: crater retention ages for key areas ..... 59
*4.3.1 Surface ages of Ida, Gaspra and Lutetia* ..... *60*
*4.3.2 Surface Ages of Vesta* ..... *61*
*4.3.3 Summary on crater retention ages of key areas on Vesta* ..... *79*
4.4 Comparison of vestan crater retention ages with radiometric $^{39}$Ar-$^{40}$Ar reset Ages of HED meteorites 83
4.5 Summary and discussion ..... 85
4.6 Acknowledgments ..... 89
4.7 Appendix - The Cratering Record, Chronology and Surface Ages of (4) Vesta in Comparison to Smaller Asteroids and the Ages of HED meteorites ..... 90
*4.7.1 Measurements on Small Asteroids* ..... *90*
*4.7.2 Additional Information about Counting Areas on Vesta* ..... *96*
*4.7.3 Major Impact Structures on Vesta (Fig. 4-36, 4-37)* ..... *110*

**5 MORPHOLOGY AND FORMATION AGES OF MID-SIZED POST-RHEASILVIA CRATERS – GEOLOGY OF QUADRANGLE TUCCIA, VESTA ..... 113**

5.1 Introduction and general geologic setting of quadrangle Av-13 ..... **Fehler! Textmarke nicht definiert.**
5.2 Methodology ..... 115
*5.2.1 Database and geologic mapping* ..... *115*
*5.2.2 Analysis of crater size–frequency distributions (CSFDs)* ..... *119*
*5.2.3 Morphometric measurements* ..... *123*
5.3 Mapping results ..... 125
*5.3.1 Cratered highlands material (ch)* ..... *125*
*5.3.2 Cratered plains material (cp)* ..... *127*
*5.3.3 Rheasilvia smooth material (Rs)* ..... *129*
*5.3.4 Rheasilvia ridge-and-groove material (Rrg)* ..... *129*
*5.3.5 Rheasilvia scarp wall material (Rsw)* ..... *131*
*5.3.6 Undifferentiated lobate material (ul)* ..... *132*
*5.3.7 Dark lobate material (dl)* ..... *133*
*5.3.8 Crater materials (uc, bc, dc, bcr, dcr, ccr)* ..... *133*
*5.3.9 Dark material (d)* ..... *134*
5.4 Geology and formation ages of prominent impact craters in Av-13 Tuccia ..... 135
*5.4.1 Geology of Tuccia and Eusebia craters* ..... *135*
*5.4.2 Geology of Vibidia and Galeria craters* ..... *142*
*5.4.3 Geology of Antonia crater* ..... *145*
5.5 Discussion ..... 149
*5.5.1 The age of Rheasilvia* ..... *149*
*5.5.2 Prominent mid-sized impact craters* ..... *150*
5.6 Conclusions ..... 154
5.7 Acknowledgments ..... 155
5.8 Appendix Supplementary data ..... 156

**6 OLIVINE OR IMPACT MELT: NATURE OF THE ''ORANGE'' MATERIAL ON VESTA FROM DAWN ..... 157**

6.1 Introduction ..... 158
6.2 Data description and processing ..... 160
*6.2.1 Orbits and resolution of FC and VIR data* ..... *160*
*6.2.2 FC color images processing* ..... *161*
*6.2.3 Visible and infrared mapping spectrometer data processing* ..... *162*
6.3 Data analysis ..... 163

*6.3.1 FC color ratios* ..... *163*
*6.3.2 VIR band parameters* ..... *164*
6.4 DESCRIPTION OF ORANGE MATERIAL ..... 165
*6.4.1 Types of orange material deposits: morphology and color properties* ..... *165*
*6.4.2 Mapping the distribution of the orange material* ..... *177*
*6.4.3 Formation age of Oppia and Octavia craters* ..... *181*
6.5 COMPOSITION OF THE ORANGE MATERIAL ..... 183
*6.5.1 Spectral band parameters* ..... *183*
*6.5.2 Pyroxene chemistry* ..... *185*
*6.5.3 Relationship with HEDs* ..... *185*
*6.5.4 Elemental composition of the orange regions* ..... *188*
6.6 ORIGIN OF THE ORANGE MATERIAL ..... 191
*6.6.1 Olivine option* ..... *191*
*6.6.2 Metal option* ..... *194*
*6.6.3 Impact melt/shock option* ..... *197*
6.7 CONCLUSION ..... 202
6.8 ACKNOWLEDGMENTS ..... 205
6.9 APPENDIX A ..... 205
*6.9.1 A.1. Details of the VIR data processing* ..... *205*
*6.9.2 A.2. Crater counting methodology* ..... *207*
*6.9.3 A.3. Crater counting sites description* ..... *207*
6.10 APPENDIX B. SUPPLEMENTARY MATERIAL ..... 208

**7 IMPACT CRATER SIZE – FREQUENCY DISTRIBUTION ON MIMAS AND THE AGE OF HERSCHEL ..... 213**

7.1 INTRODUCTION: ..... 213
7.2 METHODOLOGY ..... 214
7.3 IMAGE DATA AND MEASUREMENT AREAS ..... 217
*7.3.1 Image Data* ..... *217*
*7.3.2 Description of counting areas* ..... *217*
7.4 MEASUREMENTS ..... 220
7.5 SIZE-FREQUENCY DISTRIBUTION OF POSSIBLE PROJECTILE POPULATIONS IN THE SATURNIAN SYSTEM ..... 221
*7.5.1 Possible Projectiles* ..... *222*
*7.5.2 Derivation of strength to gravity values by a modified 1/g approach* ..... *226*
*7.5.3 Comparison between scaled projectile and observed projectile distributions* ..... *227*
*7.5.4 Apex-/Antapex asymmetry not observed* ..... *233*
7.6 CRATER CHRONOLOGY FUNCTIONS AND CRATER PRODUCTION FUNCTIONS FOR MIMAS AND IAPETUS ..... 234
*7.6.1 Crater Production Function* ..... *234*
*7.6.2 Crater Chronology Functions* ..... *237*
7.7 SURFACE AGES OF MEASURED UNITS ON MIMAS ..... 238
7.8 CONCLUSION ..... 242
7.9 ACKNOWLEDGEMENT ..... 244
7.10 APPENDIX – A - DATA TABLES ..... 245

**8 SUMMARY AND OUTLOOK ..... 257**

8.1 APPLICABILITY OF LUNAR-LIKE CRATER PRODUCTION AND CHRONOLOGY FUNCTIONS: ..... 257
*8.1.1 Phobos (chapter 3):* ..... *258*
*8.1.2 Main Belt asteroids (chapters 4, 5 and 6):* ..... *258*
*8.1.3 Mimas (chapter 7):* ..... *262*
8.2 OUTLOOK: ..... 265

**REFERENCES** ..... **269**

**CURRICULUM VITAE** ..... **I**

**PUBLICATIONS** ..... **III**

# List of Figures

*Fig. 1-1: Basic lunar observations:* ..... 2
*Fig. 1-2: Development of interpretations on the lunar cratering rate* ..... 3
*Fig. 1-3: Comparison of impact rates (left) and chronology functions (right)* ..... 5
*Fig. 2-1: Correction between reference and true body surfaces:* ..... 13
*Fig. 2-2: Standard lunar equilibrium distribution and crater frequencies on Ida, Gaspra and Lutetia:* ..... 15
*Fig. 3-1: Crater production and chronology functions for Phobos:* ..... 26
*Fig. 3-2: Area overview:* ..... 29
*Fig. 3-3: Map and crater plot of average surface to the west of Stickney:* ..... 31
*Fig. 3-4: Map and crater plot of area S1:* ..... 33
*Fig. 3-5: Map and crater plot of area S2:* ..... 35
*Fig. 3-6: Randomness Analysis:* ..... 36
*Fig. 3-7: Apex/Antapex Asymmetry Measurement:* ..... 38
*Fig. 4-1: Projectile populations:* ..... 49
*Fig. 4-2: Impact probability–Velocity distributions:* ..... 52
*Fig. 4-3: Lunar and asteroidal crater production functions:* ..... 54
*Fig. 4-4: Chronology functions:* ..... 59
*Fig. 4-5: Rheasilvia basin map and cumulative crater plot:* ..... 63
*Fig. 4-6: Rheasilvia central peak–Map and cumulative crater plot:* ..... 65
*Fig. 4-7: Tuccia quadrangle–Ridge and groove terrain–Map and cumulative crater plot:* ..... 66
*Fig. 4-8: Floor of Veneneia basin:* ..... 68
*Fig. 4-9: Heavily cratered terrain:* ..... 70
*Fig. 4-10: North pole area:* ..... 71
*Fig. 4-11: Ancient crater at 250°E/30°N:* ..... 73
*Fig. 4-12: Oppia ejecta blanket:* ..... 75
*Fig. 4-13: Octavia ejecta blanket:* ..... 78
*Fig. 4-14: Ejecta blanket of Antonia crater:* ..... 79
*Fig. 4-15: Map of vestan model ages for the lunar-like chronology:* ..... 82
*Fig. 4-16: Comparison of probability plots of Ar–Ar ages (Bogard, 2011) and crater retention ages:* ..... 84
*Fig. 4-17: Ida Crater Measurement:* ..... 92
*Fig. 4-18: Gaspra Crater Measurement:* ..... 94
*Fig. 4-19: Lutetia Crater Measurement:* ..... 96
*Fig. 4-20: Rheasilvia Basin:* ..... 97
*Fig. 4-21: Top of Central Peak of Rheasilvia:* ..... 97
*Fig. 4-22: The Tuccia Quadrangle – Ridge and Groove Terrain:* ..... 98
*Fig. 4-23: Floor of the Veneneia Basin:* ..... 98
*Fig. 4-24: Heavily Cratered Terrain North of the Equator:* ..... 99
*Fig. 4-25: Heavily Cratered Terrain North of the Equator:* ..... 100
*Fig. 4-26: HAMO2 imaging mosaic with superimposed additional North Pole mosaic* ..... 100
*Fig. 4-27: LAMO Measurement of the Ancient Crater Floor:* ..... 101
*Fig. 4-28: LAMO Measurement of the Elevated_Terrain_North (ETN):* ..... 101
*Fig. 4-29: LAMO Measurement of the Elevated_Terrain_South (ETS):* ..... 102
*Fig. 4-30: HAMO Measurements in Ancient Crater at 250°E/30°N:* ..... 102
*Fig. 4-31: Oppia Ejecta Blanket Northern Part:* ..... 103
*Fig. 4-32: Oppia Ejecta Blanket Southern Part:* ..... 103
*Fig. 4-33: Octavia Ejecta Blanket South-East:* ..... 104
*Fig. 4-34: Octavia Ejecta Blanket South:* ..... 104
*Fig. 4-35: Antonia Ejecta Blanket:* ..... 105

*Fig. 4-36: Global Topography of Vesta:* ..... *110*
*Fig. 4-37: Cumulative Crater Plot of impact structures ≥ 100 km:.* ..... *111*
*Fig. 5-1: Overview map of quadrangle Av-13 Tuccia.* ..... *114*
*Fig. 5-2: Tuccia quadrangle boundary (red) draped over Vesta's topography.* ..... *116*
*Fig. 5-3: LAMO-based geologic map of quadrangle Av-13 Tuccia.* ..... *117*
*Fig. 5-4: Topographic profiles and interpreted cross-sections across quadrangle Av-13* ..... *118*
*Fig. 5-5: Cumulative crater size–frequency distribution (CSFD) plots of global map units* ..... *126*
*Fig. 5-6: Type areas of material units.* ..... *128*
*Fig. 5-7: Interpreted correlation of map units as mapped in Fig. 5-3.* ..... *131*
*Fig. 5-8: Outcrop of dark material at the scarp of Vestalia Terra at 237.6°E and 30°S.* ..... *135*
*Fig. 5-9: Geology of Tuccia, Eusebia, Vibidia, Galeria, and Antonia.* ..... *137*
*Fig. 5-10: Clementine-type color ratio maps of Tuccia (A), Vibidia (B), Galeria (C), and Antonia (D)* ..... *138*
*Fig. 5-11: Topographic profiles and interpreted cross-sections* ..... *139*
*Fig. 5-12: Cumulative crater size–frequency distribution plots for the Tuccia and Eusebia Impact regions.* *141*
*Fig. 5-13: Cumulative crater size–frequency distribution plots* ..... *144*
*Fig. 5-14: Perspective view of Antonia crater.* ..... *146*
*Fig. 5-15: Color spectra of dark material (black) and bright material from the crater wall (light gray)* ..... *148*
*Fig. 5-16: Cumulative crater size–frequency distributions, production–function fits* ..... *153*
*Fig. 6-1: Perspective views of Oppia and Octavia craters.* ..... *166*
*Fig. 6-2: Perspective views of orange material that forms "pumpkin" patches on the surface of Vesta* ..... *168*
*Fig. 6-3: Perspective views of orange material that forms "pumpkin" patches on the surface of Vesta* ..... *170*
*Fig. 6-4: Close-up views of some orange patches at two different locations on Vesta.* ..... *171*
*Fig. 6-5: Perspective views of orange material found in crater rays of fresh craters* ..... *172*
*Fig. 6-6: Color ratio images of selected sites on the Moon* ..... *174*
*Fig. 6-7: (A) Average FC color spectra from HAMO1 phase* ..... *176*
*Fig. 6-8: Global maps of Vesta* ..... *179*
*Fig. 6-9: (A) Map of counting areas northeast and south of Oppia, outlined in white.* ..... *181*
*Fig. 6-10: (A) Map of counting areas southwest and southeast of Octavia, outlined in white.* ..... *182*
*Fig. 6-11: Plot of the Band I center versus BAR* ..... *184*
*Fig. 6-12: Plots comparing the composition derived from VIR* ..... *187*
*Fig. 6-13: Maps of (A) the fully corrected Fe counting rate and (B) neutron absorption on Vesta* ..... *189*
*Fig. 6-14: Fe abundances plotted against the high-energy gamma-ray derived Cp values* ..... *190*
*Fig. 6-15: Plots used to analyze the olivine option for the orange material.* ..... *193*
*Fig. 6-16: Plots used to investigate the presence of PGEs in the orange material.* ..... *196*
*Fig. 6-17: Plots used to test the affinity of shocked eucrites and impact melt with the orange material.* ..... *199*
*Fig. 7-1: Herschel, Morphology and Thermal Inertia Anomaly:* ..... *218*
*Fig. 7-2: Counting Areas:* ..... *219*
*Fig. 7-3: Plot of All Crater Counts:* ..... *221*
*Fig. 7-4: Target-separated comparison of scaled and observed projectile diameters:* ..... *228*
*Fig. 7-5: Density-separated comparison of calculated and observed projectile diameters:* ..... *230*
*Fig. 7-6: Iapetus', Mimas' and lunar crater production functions:* ..... *236*
*Fig. 7-7: Iapetus chronology calibration:* ..... *237*
*Fig. 7-8: Measurements and Crater SFD:* ..... *239*
*Fig. 7-9: Differential plot and fit of measurement A7:* ..... *240*
*Fig. 7-10: Measured Crater Frequencies and Chronologies:* ..... *242*
*Fig. 8-1: Comparison of crater retention ages* ..... *261*

# List of Tables

*Table 2-1: Reference Radii for Gaspra, Ida, Lutetia and Vesta and the Extreme Values of their Topography. 13*
*Table 3-1: Parameters for Converting the Production Function:.....26*
*Table 3-2: Coefficients of Phobos production functions for the Cases A and B. .....28*
*Table 3-3: Coefficients of Phobos' chronology functions for the Cases A and B.....29*
*Table 4-1: List of asteroid fly-bys by spacecraft other than Dawn. .....42*
*Table 4-2: Scaling parameters for conversion of the lunar crater production function to asteroids. .....51*
*Table 4-3: Coefficients of asteroid production functions: .....53*
*Table 4-4: Intrinsic collision probabilities ($P_i$; Fig. 4-2) for asteroids .....57*
*Table 4-5: Summary of model age data of the measured asteroids Ida, Gaspra and Lutetia. .....61*
*Table 4-6: Summary of surface model age data of the measured areas on Vesta: .....80*
*Table 4-7: Detailed statistics on fitted cumulative crater distributions: .....106*
*Table 4-8: Detailed statistics on fitted differential crater distributions: .....108*
*Table 5-1: CSFD measurements derived in quadrangle Av-13 Tuccia. .....120*
*Table 5-2: Morphometric parameters of prominent impact craters in quadrangle Av-13 .....124*
*Table 5-3: Geologic units mapped in the detail maps only. .....124*
*Table 6-1: List of FC filters with their band pass center, peak and full width at half maximum (FWHM).....160*
*Table 6-2: List of FC observational phases and their respective characteristics. .....161*
*Table 6-3: List of the 17 sites showing orange material in the FC Clementine maps .....184*
*Table 7-1: Image names and respective resolutions for measurements on Mimas. .....217*
*Table 7-2: Impact velocities: .....225*
*Table 7-3: Impact parameters:.....227*

# 1 Introduction

## 1.1 Significance of chrono-stratigraphy and the role of radiometric ages for the determination of the geologic history of planetary bodies and the history of the Solar System

The airburst of a 17 to 20 m diameter bolide, equivalent to an explosion of approximately 500 (±100) kt TNT (Brown et al., 2013), over the Russian city of Chelyabinsk with ~1200 injured people and the independent close fly-by of a ~50 m sized asteroid inside the geosynchronous orbit of the Earth on the same day in February 2013 draw the public attention to the cosmic neighborhood of our home, Earth. In the media response to these events questions were raised about a planetary defense strategy and the frequency and magnitude of such threats. The Chelyabinsk bolide disrupted within the atmosphere causing no significant impact crater. However, in the past larger meteorites have left impact structures on Earth's surface such as the ~1 km diameter Barringer crater, the ~25 km Ries crater, the ~150 km Chicxulub crater or the ~160 km Vredefort impact structure. The Earth Impact Database[1] currently lists 188 confirmed impact structures on Earth. On the Moon however, even a small amateur telescope reveals a much higher density of impact craters on its surface (Fig. 1-1). The dearth of impact craters on Earth is a result of the intense geologic activity resurfacing our planet continuously and erasing its cratering record.

From Fig. 1-1 it can also be determined that even on the Moon with heavily reduced geologic activity, there are areas with significantly lower crater density than other areas. The brighter lunar highlands are heavily cratered, while the darker lunar maria are much less cratered. The nature of the lunar craters was ambiguous (e.g. Gilbert, 1893) until, during the Apollo era, their origin as impact structures became more and more clear (e.g. Taylor, 1975; Neukum, 1984 and references therein). With the advent of highly successful lunar mapping spacecraft the lunar impact craters were systematically measured and their size-frequency distribution analyzed (e.g. Shoemaker and Hackman, 1962 and Baldwin, 1964). The differences in crater frequencies of the lunar highlands and the maria areas were interpreted as a result of different surface ages (e.g. Baldwin, 1964) allowing for the determination of relative stratigraphic relationships of geologic surface units. Theoretical analysis of impact probabilities of small bodies crossing the Earth orbit by Öpik (1960) led to initial lunar surface age estimates on the order of 4.5 Ga, which were subsequently revised under the assumption of higher impact rates in the past (e.g. Hartmann, 1966).

[1] http://www.passc.net/EarthImpactDatabase/Diametersort.html

Fig. 1-1: Basic lunar observations: Amateur image of the Moon in a small telescope taken as a webcam mosaic on 19.10.2003. It reveals the bright heavily cratered lunar highlands and the darker less cratered lunar maria. The image shows the waning Moon with North direction rotated to the right (image by the author).

With the United States Apollo and the USSR Luna sample return missions it became possible to calibrate the lunar cratering record at the sampling sites for absolute radiometric ages. Assuming an isotropic bombardment the calibrated crater size-frequency distribution also allowed for determination of absolute surface ages for the entire lunar surface. However, for technical reasons all sample return missions to the Moon targeted its nearside. The lunar nearside is dominated by several large impact basins (e.g. Wilhelms et al., 1987), the floors of which are covered with post impact volcanism basalts (e.g. Hiesinger et al., 2010). Except for the large South-Pole Aitken basin and a few smaller basins, the farside of the Moon is dominated by heavily cratered highlands (e.g. Wilhelms et al., 1987). The spatial dichotomy of lunar basins may already imply a biased sampling by the historic sample return missions.

Historic sampling of the top layer of the lunar regolith may cause a heavy overweight of samples originating in the upper lunar regolith i.e. the youngest major ejecta blanket. That bias in sampling lunar soil and rocks may have caused a still ongoing debate lasting since the early publications with respect to the geologic interpretation of lunar samples (e.g. Baldwin, 1974; Tera et al., 1974; Hartmann, 1975; Neukum, 1984; Haskin et al., 1998; Hartmann, 2003; Gomes et al., 2005; Tsiganis et al., 2005; Baldwin, 2006; Morbidelli et al., 2010; Bottke et al., 2012; Nimmo and Korycansky, 2012 and Fernandes et al., 2013). In fact, for most parts of the lunar nearside it is expected that the Imbrium impact event deposited hundreds of meters of ejecta (Haskin et al., 1998). Those ejecta are covered by thinner ejecta of subsequent smaller impacts and post mare basalt flows. Subsequent impact events large enough to excavate material from below the Imbrium ejecta blanket may provide samples of older large basin forming events. Such samples are continuously

reworked by ongoing impact gardening. It may be assumed that pre-Imbrian material is only a minority in the sample collection of Apollo and Luna missions. The resulting distribution in radiometric ages would show a major peak in surface ages corresponding to the Imbrium ejecta layer, which has been mostly sampled (Neukum, 1984).
The found distribution of radiometric ages among the lunar sample material led to the conclusion of a cataclysmic peak in impact rates of less ~200 Ma duration on the Moon and Earth around 3.9 Ga ago (Tera et al., 1974). This interpretation has been challenged by advocates of a smoothly decaying impact flux (e.g. Baldwin, 1974; Hartmann, 1975 and Neukum, 1984). Tera et al. (1974) present a schematic diagram, which shows how their view on the terminal lunar cataclysm evolved from pre-Apollo time to post-Apollo time (Fig. 1-2).

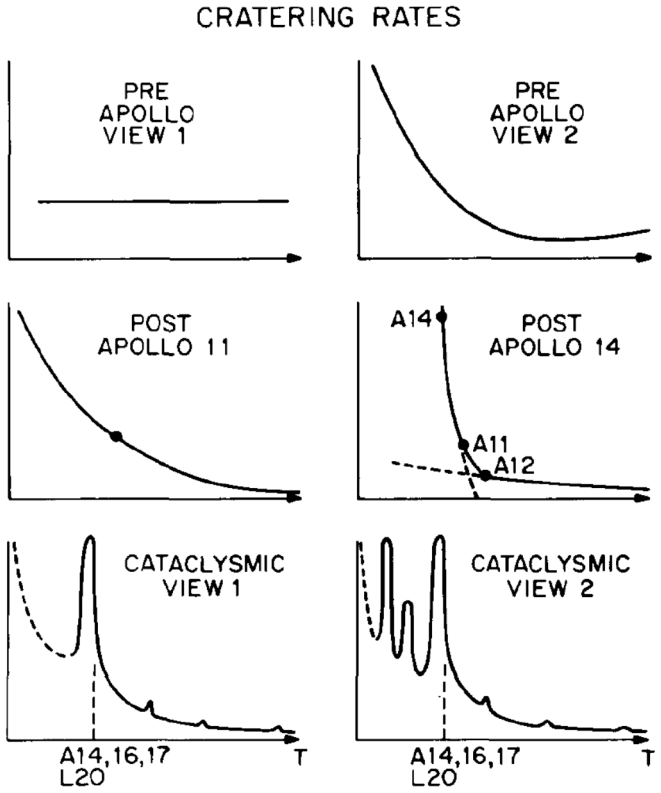


Fig. 1-2: Development of interpretations on the lunar cratering rate from pre-Apollo time through post-Apollo time and different views of a lunar cataclysm (Fig. taken from Tera et al., 1974). The vertical axis represents the impact rate on the Moon and the horizontal axis shows the age, starting on the left at the Moon-forming event until today (arrow-tip on the right).

The characteristics of the decay in the lunar impact flux has profound implications for the late stages of the Solar System formation. This becomes evident once the reason for a smooth decay or a spike in the lunar projectile flux is investigated. In fact there is a large variety of proposed scenarios that have been tested against observations not only for the Moon but for other Solar System bodies as well. Especially since the year 2005 there have been many publications referring to numerical simulations of orbital mechanics known as the Nice model (Gomes et al., 2005; Tsiganis et al., 2005 and Morbidelli et al., 2010).

The Nice model is a dynamical simulation of the outer Solar System that gives support for the initial idea of the terminal lunar cataclysm also termed as late heavy bombardment (LHB). Based on this model, predictions about the predominantly impacting projectiles were made with respect to their nature, timing and dynamical characteristics. In its initial form the Nice model proposed a high ratio of cometary projectiles in the inner Solar System around 3.9 Ga ago over a duration of a few tens of millions of years. That should have been caused by a resonance catastrophe between Jupiter and Saturn, which led to destabilization of the orbits of Uranus and Neptune and in some flavors of the model the order of Uranus and Neptune is switched. This event is accompanied by a destabilization of the small body populations in the asteroid Main Belt but even more in the Kuiper Belt beyond the orbit of Neptune. The initially more compact configuration of the outer Solar System changed into the one, which is currently observed. Due to inconsistencies with observations (e.g. O'Brien et al., 2006; Alexander et al., 2012; Fischer-Gödde and Becker, 2012; Nimmo and Korycansky, 2012 and Fernandes et al., 2013) the Nice model was adapted in a way that the spike in impact rates is much more extended (200-300 Ma), the predominant projectiles changed from comets to asteroids and the onset of the LHB was pushed back to 4.1 Ga (e.g. Bottke et al., 2012 and Morbidelli et al., 2012). Interestingly, the lunar chronology by Morbidelli et al. (2012) is nearly the same proposed by Neukum (1984) and Neukum and Ivanov (1994) for the time range from 4.1 Ga ago until today (Fig. 1-3).

Utilizing scaling laws that relate projectile diameters to crater diameters (e.g. Ivanov, 2001 and Holsapple et al., 2002) it is possible to derive crater production functions not only for the Moon but also for other planetary bodies. Also impact fluxes can be derived based on statistically derived impact probabilities from the current orbits of involved bodies (Öpik, 1960 and Bottke et al., 1994). This approach requires model assumptions for the early Solar System configuration and the respective predominant projectile populations. From this approach most of our knowledge about the geologic history of the other terrestrial planets and their satellites, the giant planets satellites and some asteroids is derived. Only on the Moon ground truth data from returned sample material at known locations can be used for absolute impact flux calibration, if accurately applied.

But even without knowing the actual time dependence of the impact flux for each body, in most cases it is possible to use crater frequency measurements in order to develop relative stratigraphies. This is possible for all bodies experiencing an isotropic bombardment but not for those with asymmetric impact geometries such as the retrograde orbiting satellite Triton in the Neptunian system, where a clear apex-/antapex asymmetry is evident (e.g. Dones et al., 2009). From relative stratigraphy we know for instance that Venus shows a relatively homogeneous surface age probably indicating episodic events of global volcanism, while Mars' heavily cratered southern highlands appear much older than the smooth plains in the northern lowlands indicative of regional resurfacing. Also on Mars the very low crater frequency on volcanic calderas and dunes may imply relatively recent geologic activity (Neukum et al., 2004). That is also true for the Jupiter moon Io which lacks any known impact craters and which is characterized by active sulfuric volcanism, as recorded by the Voyager, Galileo and New Horizons spacecrafts.

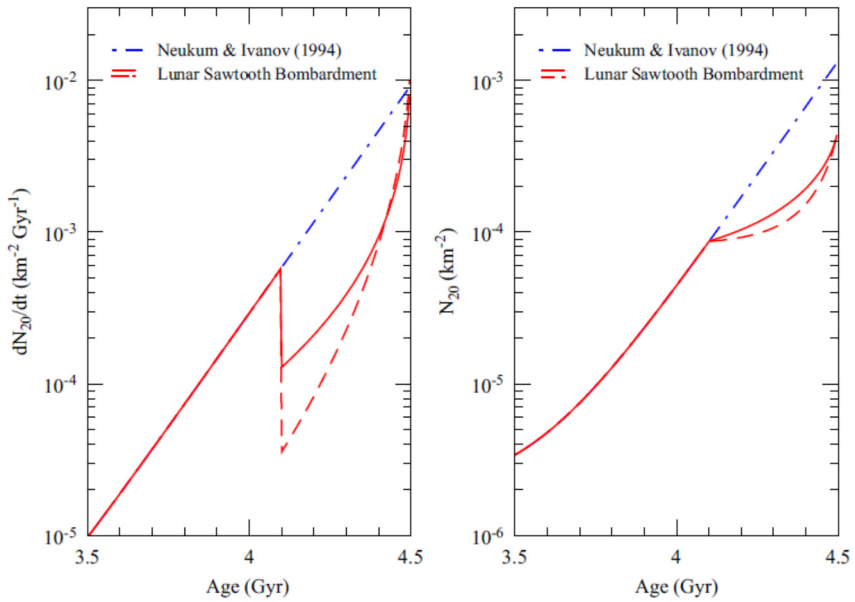


Fig. 1-3: Comparison of impact rates (left) and chronology functions (right) in the non-cataclysm view by Neukum and Ivanov (1994) and two modern flavors of a terminal lunar cataclysm by Morbidelli et al. (2012) during the first billion years after Solar System formation (Fig. taken from Morbidelli et al., 2012).

Furthermore, the South Pole area on Enceladus in the Saturnian System also shows much lower crater frequencies and thus lower crater retention ages (absolute model age since the last resurfacing event) than other areas of that body. On Iapetus the equatorial ridge system is as heavily cratered as the heavily cratered plains in between the basins. That and the ridge's interruption where basins are superimposed, indicate the high age of the ridge system that predates at least the youngest basins. On the large asteroid Vesta absolute surface ages are heavily debated but just from crater frequency measurements it can be determined that the floor of the large South Pole basin named Rheasilvia, is younger than its respective ejecta blankets (Schenk et al., 2012a and Schmedemann et al., 2014a). That may imply significant mass wasting processes inside the basin after it formed (Otto et al., 2013; Kneissl et al., 2014 and Schmedemann et al., 2014a). This collection of examples shows that relative stratigraphic relationships of geologic units can be analyzed by measuring crater frequencies.

If absolute crater retention ages are derived from various bodies in the Solar System in their individual dynamical environments, it may even be possible to decipher the late stages of planetary formation and specific impact flux related events in the Solar System history. Although both models for the lunar projectile flux discussed above are very similar on the Moon for the mentioned time frame from 4.1 Ga until today, they differ significantly in their underlying assumptions. While the Nice-model is based on dynamical models, which initially implied a terminal lunar cataclysm and showed a high dependence of the location of the target bodies within the Solar System, the competing model of a smoothly decaying lunar impact flux assumes a relatively stable Solar System with no terminal lunar cataclysm. As proposed by Neukum (1984), not only the inner Solar System but also the satellites of Jupiter and Saturn were cratered predominantly by Main Belt asteroids from planetocentric orbits. Thus, all of these bodies may have experienced impact fluxes similar to that at the Moon with similar time dependences but different absolute fluxes.

In order to verify which model is the more likely one, specific events in the geologic history of different bodies need to be analyzed. For instance, on the Moon Hartmann (1965a, b, 1970, 1972) and Neukum (1984; 2001) identified much higher impact rates before 3.5 Ga than since that time. If this behavior with similar timing could be identified on other bodies as well, it may support a smooth decay model with a largely stable late stage Solar System similar to the one proposed by Neukum (1984). If a lunar-like behavior in impact rates cannot be observed on other bodies this may point to a more complicated dynamical history possibly similar to the Nice model. An example for this case is the chronology model by O'Brien et al. (2014) for the Main Belt asteroid Vesta that is very different from the lunar-like model for ages > ~3 Ga.

For unambiguous results more surface samples not only from the Moon but also from other planetary bodies are required as well in order to correlate cratering data with independent radiometric ages. For the Moon a deep drilling project that penetrates the expected thick ejecta blankets of the younger large impact basins would be desirable in order to investigate their four-dimensional (lateral, vertical and temporal) relationships and their correlation to particular impact basins. However, some samples of other Solar System bodies already exist in meteorite collections. The problem here is that besides the Moon and Mars it appears all other meteorites are pieces of asteroids and the sample locations are largely unknown. About 6% of all meteorites on Earth belong to the HED (Howardite – Eucrite – Diogenite) class which is likely derived predominantly from the large Main Belt asteroid Vesta (e.g. Binzel and Xu, 1993). The Dawn mission at Vesta (e.g. Russell et al., 2012) revealed that the asteroid is dominated by two large impact basins in the southern hemisphere. These massive impact events are probably recorded in radiometric ages of Vesta-derived meteorites (Bogard and Garrison, 2003 and Bogard, 2011). Such signals in radiometric ages can be correlated with the respective crater retention ages. As for Mars, a recent publication (Werner et al., 2014) claims the identification of the source region of shergottite meteorites that allowed the authors to verify the impactor flux in the early history of Mars.

The main conclusion of what has been said so far is that measurements of crater frequencies are a powerful tool for understanding stratigraphic relations between various geologic units on a planetary body that allows for relative dating specific geologic events. Absolute dating of surface units however requires sophisticated knowledge about the projectile flux for the various planetary bodies over a large fraction of the Solar System history. For best results the cratering chronology needs to be calibrated with an independent and reliable technique such as radiometric dating of rock samples. Only for the Earth and the Moon are the required data available for such a calibration but difficulties in lunar data interpretation and scarcity of impact craters on Earth leave behind ambiguity. Absolute surface dating on other bodies based on lunar/Earth-derived calibrated cratering chronologies always depend on certain assumptions and models of the respective projectile characteristics (density, impact velocity, flux) at the body in question. If for some reason the absolute age of a cratered surface is known to some degree, this information can be used to derive unknown parameters of the impacted projectiles

(e.g. chapter 7). That in turn could provide information about the projectile source region during the Solar System history.

## 1.2 Scope of this Work and Structure

The scope of this work is to utilize the lunar crater production function and the lunar crater chronology function published by Neukum (1984) and Neukum and Ivanov (1994) for absolute surface dating on smaller planetary bodies with lower surface gravity as well as a different dynamical environment. For this aim both functions are scaled to the impact conditions at the respective target bodies. The validity of the scaled functions is tested against numerous measurements of the crater size-frequency distribution on the Martian satellite Phobos, the Main Belt asteroids Vesta, Lutetia, Ida and Gaspra and the Saturnian satellites Mimas and Iapetus. These bodies were selected because of their good coverage by high-resolution image data which allows to extract statistically representative data, their particular location in the Solar System as well as the ability to distinguish between dynamical characteristics of possible projectile populations. Results are compared with published work and in the case of Vesta even correlated with radiometric data of Vesta derived HED meteorites.
This work is based on five publications submitted to the journals "Planetary and Space Science" and "Icarus". Except for the manuscript in chapter 7 (in review) all papers are published. The Author of this thesis, Nico Schmedemann, is leading author of the publications presented in chapters 3, 4 and 7. Following the title of each publication in chapters 3 – 7, is a note about the work the author did for the respective publication. In chapter 2 information and methodologies are detailed that are not presented in the papers. The necessity to explain these methods became apparent during several discussions within the Dawn team. Therefore, these methods and respective examples are related to irregular asteroid-like bodies. Presented papers in which the author of this thesis is lead author investigate the reasoning for lunar-like production and chronology functions, present the derivation and resulting coefficients for crater production and chronology functions and apply the functions to sample areas in order to derive absolute model ages for major surface units that are key in understanding the geologic history of the respective bodies. These papers are presented in chapter 3 "The age of Phobos and its largest crater, Stickney", chapter 4 "The cratering record, chronology and surface ages of (4) Vesta in comparison to smaller asteroids and the ages of HED meteorites" and chapter 7 "Impact Crater Size – Frequency Distribution on Mimas and the Age of Herschel". In the context of the Dawn mission the remaining chapter 5 "Morphology and formation ages of mid-sized post-Rheasilvia craters – Geology of quadrangle Tuccia, Vesta", and chapter 6 "Olivine or impact melt: Nature of the "Orange" material on Vesta from Dawn" demonstrate, how crater retention ages based on the derived lunar-like functions are used in concert with other flavors of remote sensing data in order to piece together a global understanding of the investigated body.

In chapter 8 a conclusion is given about major results as well as yet unsolved issues. The latter point is part of an outlook of work that needs to be conducted in the future.

# 2 Details on methodology not included or referenced in the presented papers

## 2.1 Brief overview on the geology and astronomic relation of the investigated bodies

### 2.1.1 Phobos

Phobos is the inner one of the two natural Martian satellites. Due to its close orbit about Mars inside the Mars-synchronous orbit and within the Roche-limit, Phobos is exposed to substantial tidal forces that will cause further decay of its orbital height and which will ultimately lead to its disruption and impact of the debris on Mars within the astronomically near future. As detailed in chapter 3 the origin and dynamic history of Phobos is largely unknown and subject to scientific discussion. Relative stratigraphy suggests that the large crater Stickney formed before or contemporary with the groove system. The formation of the groove system is also under scientific discussion (e.g., Ramsley and Head III, 2013 and Murray and Heggie, 2014). Phobos' low density of ~ 1.9 g/cm³ (Willner et al., 2014) suggests low density materials and/or a rubble-pile like characteristics of this ~23 km diameter irregular body. The composition of Phobos is still uncertain (Pieters et al., 2014). It was hypothesized that the Kaidun meteorite is probably derived either from Ceres or Phobos (Zolensky and Ivanov, 2003).

### 2.1.2 (951) Gaspra

Gaspra is an S-type Main Belt asteroid and probably member of the Flora family (Chapman et al., 1996b). With its semi-major axis of 2.2 AU Gaspra is located within the inner asteroid Main Belt. Gaspra has a diameter of about 12 km and a density of roughly 2.7 g/cm³ (Thomas et al., 1994). Because of its size and shape Gaspra is likely a remnant of a collision event that separated Gaspra from its precursor parent body. Crater retention ages suggest the break up occurred roughly 200 Ma ago (Chapman et al., 1996b). The collisional life time of Gaspra was estimated at ~ 500 Ma (Bottke et al., 1994).

### 2.1.3 (243) Ida

Similar to Gaspra, Ida is an S-type Main Belt asteroid (Veverka et al., 1996). Ida is about 32 km in diameter with a density of about 2.6 g/cm³ and highly irregular shape (Thomas et al., 1996). Thus, Ida is probably a remnant of an asteroidal break up event as well. This is supported by Ida's location in the phase space of the Koronis family in the outer Main Belt. Crater retention ages suggest a breakup of the Ida precursor body around 2 Ga ago (Chapman et al., 1996a). The age of the

possible break up event is updated to about 3.5 Ga in chapter 4. Ida's semi-major axis is about 2.9 AU.

### 2.1.4 (21) Lutetia

With about 100 km diameter Lutetia is about 3 times larger than Ida and large enough that it could have escaped catastrophic disruption over the age of the Solar System (Bottke et al., 2005b and Sierks et al., 2011b). It is listed as M-type Main Belt asteroid orbiting the Sun at a semi-major axis distance of 2.4 AU. Thus, Lutetia is an object of the inner Main Belt. A crater cluster at its North Pole exposes a number of boulders suggesting a relatively recent formation of the respective craters. Presumably older craters show smoothed morphologies indicating resurfacing processes due to seismic shaking and/or ejecta blanketing due to neighboring impacts and landslides caused by high relief topography. Lutetia shows several sets of lineaments that might be impact related (Thomas et al., 2012). The relatively high density of 3.4 g/cm³ may suggest a low porosity and/or high density materials in the subsurface (Pätzold et al., 2011). Thus, Lutetia could be the heavily battered remains of a partially differentiated body (Weiss et al., 2012).

### 2.1.5 (4) Vesta

With a mean diameter of about 514 km, after (1) Ceres and (2) Pallas, Vesta is the third largest object in the Main Belt and the second most massive. Vesta circles the Sun at a distance of about 2.4 AU. The vestan geology is dominated by two large impact basins in the southern hemisphere. The older basin, named Veneneia, is tectonically related to a trough system named Saturnalia Fossae that is about 30° inclined with respect to the equator. Veneneia has a diameter of about 400 km. The younger basin, named Rheasilvia, is tectonically related to an equatorial trough system named Divalia Fossae. Rheasilvia has a diameter of about 500 km (Jaumann et al., 2012b). The determination of the basin formation ages is extensively discussed in chapters 4 and 5. Hydrocode modelling of the Rheasilvia impact suggest that it caused global resurfacing (Bowling et al., 2013).
The internal distribution of mass indicates that Vesta is a differentiated body (Russell et al., 2012). Vesta is the only known larger Main Belt asteroid with a basaltic crust. Thus, most of the HED meteorites found on Earth are believed to originate on Vesta (McCord et al., 1970; e.g. Binzel and Xu, 1993 and Scott et al., 2009).

### 2.1.6 Mimas

Mimas is the innermost of the mid-sized Saturnian satellites. It circles Saturn in a locked rotation at a distance of about 185 600 km. Its diameter is about 400 km. Mimas' density of a little more than 1 g/cm³ (Thomas et al., 2007) suggests a composition vastly dominated by water ice, that is also found almost

uncontaminated on the satellite's surface (Filacchione et al., 2010). The satellite shows an anomaly in thermal inertia on a global scale (Howett et al., 2011).

### 2.1.7 Iapetus

Iapetus is the outermost of the mid-sized Saturnian satellites. It circles Saturn in a locked rotation at a distance of about $3.6x10^6$ km. Its diameter is about 1400 km. Similar to Mimas Iapetus' density of slightly more than 1 g/cm³ (Thomas et al., 2007) suggests a composition dominated by water ice, that is heavily contaminated with organic materials on the satellite's surface (Filacchione et al., 2010). Iapetus shows a major color dichotomy between its leading and trailing hemisphere (Denk et al., 2010). Along its equator Iapetus features a ridge about 20 km high that is interrupted by large impact basins (Porco et al., 2005).

## 2.2 Scaling error of projected imaging data between reference body surface and true body surface on irregularly shaped small bodies

Global imaging as well as topographic data is often published with reference to a sphere even in the case of irregular bodies (e.g. Roatsch et al., 2012). Thus, surface measurements are performed with respect to a reference sphere. Due to the often highly irregular shape of small bodies some areas are below and other areas are above the spherical reference body. Therefore, feature sizes are distorted and measured with slightly incorrect sizes, in case they vertically divert from the reference sphere. Features below the reference surface appear too large, features above appear too small. Here the expected errors for Ida, Gaspra, Lutetia and Vesta are quantified. Projected crater size errors are proportional to the ratio of the radii of the true body and the reference body at a specific location. Errors of projected area sizes are proportional to the squared ratio of the radii of the true body and the reference body. The largest possible scaling errors between true body surface and the surface of the reference body are indicated for each asteroid in Fig. 2-1 and tabulated in Table 2-1. Fig. 2-1 also shows inlays of the cross sections for each asteroid and the respective reference spheres. The cross-section meridian was chosen such that it contains the broadest possible range of true body radii based on available topographic models. That does not necessarily mean that such a meridian contains the absolute largest and smallest body radius. The vertical axis in the cross-section diagrams is always the z-axis of the Cartesian coordinate system of each body. That direction also correlates to the body's rotation axis.

### 2.2.1 Case Ida:

The radii of the fit ellipsoid for Ida as given by Thomas et al. (1996) are 29.9 x 12.7 x 9.3 km³. In ArcGIS, our preferred mapping tool, the imaging data is projected on a reference sphere with a mean radius of 15.7 km as it was derived by Thomas et al. (1996). Thomas et al. (1996) also provide a digital elevation model (DEM) and a

basemap, which is rectified and projected to the reference sphere. The used Ida DEM and basemap are provided by the "Small Body Shape Models V2.1"[2] data collection of the Planetary Data System. These data were used as reference in order to rectify the Galileo imaging data for the crater measurements. The basemap has a ground resolution of about 25 m/pixel in its best resolved areas.

### 2.2.2 Case Gaspra:

The diameters of the principal axis of Gaspra as given by Thomas et al. (1994) are 18.2 x 10.5 x 8.9 km³. A mean radius of 6.1 km as it was derived by Thomas et al. (1994) is used for the reference sphere on which the imaging data were projected in ArcGIS. As for Ida the DEM and basemap for Gaspra is taken from the "Small Body Shape Models V2.1" data collection of the Planetary Data System.
The basemap is rectified and projected to the reference sphere. It has a ground resolution of about 55 m/pixel. This basemap is used in order to rectify the Galileo imaging data for crater measurements.

### 2.2.3 Case Lutetia:

The dimensions of Lutetia are (121+/-1) x (101+/-1) x (75+/-13) km³ (Sierks et al., 2011b). Thus, an average radius of 49.5 km is used for the reference sphere on which the imaging data is projected in ArcGIS. Sierks et al. (2011b) provide a basemap, which is rectified and projected to the reference sphere. This basemap is used in order to rectify the Rosetta imaging data used for crater measurements. The DEM of Lutetia is described by Preusker et al. (2012a).

### 2.2.4 Case Vesta:

The radii of the best-fit ellipsoid for Vesta are 286.3 x 278.6 x 223.2 km³ (Preusker et al., 2012b). Roatsch et al. (2012) provide a Dawn HAMO (High Altitude Mapping Orbit) basemap, which is rectified and projected to a reference sphere with 255 km radius. This basemap with ~70 m/pixel ground resolution and the digital elevation model by Preusker et al. (~93 m/pixel lateral resolution) is used for low resolution crater measurements down to approximately 500 m crater size. For high resolution crater counts down to about 50 m crater size imaging data from the Dawn Low Altitude Mapping Orbit (LAMO) with about 20 m/pixel ground resolution is used.

[2] http://sbn.psi.edu/pds/asteroid/EAR_A_5_DDR_SHAPE_MODELS_V2_1/

Table 2-1: Reference Radii for Gaspra, Ida, Lutetia and Vesta and the Extreme Values of their Topography. The four columns on the right side indicate the respective distortion of crater and area sizes.

| Body | Radius of Reference Sphere [km] | Minimum below Reference Sphere [km] | Maximum above Reference Sphere [km] | True Crater Size/Measured Crater Size Minimum [%] | True Crater Size/Measured Crater Size Maximum [%] | True Area Size/Measured Area Size Minimum [%] | True Area Size/Measured Area Size Maximum [%] |
|---|---|---|---|---|---|---|---|
| **Gaspra** | 6.10 | -1.96 | 4.70 | 67.87 | 177.05 | 46.06 | 313.46 |
| **Ida** | 15.70 | -12.40 | 15.36 | 21.02 | 197.83 | 4.42 | 391.38 |
| **Lutetia** | 49.50 | -14.30 | 17.20 | 71.11 | 134.75 | 50.57 | 181.57 |
| **Vesta** | 255.00 | -43.05 | 38.01 | 83.12 | 114.91 | 69.09 | 132.03 |

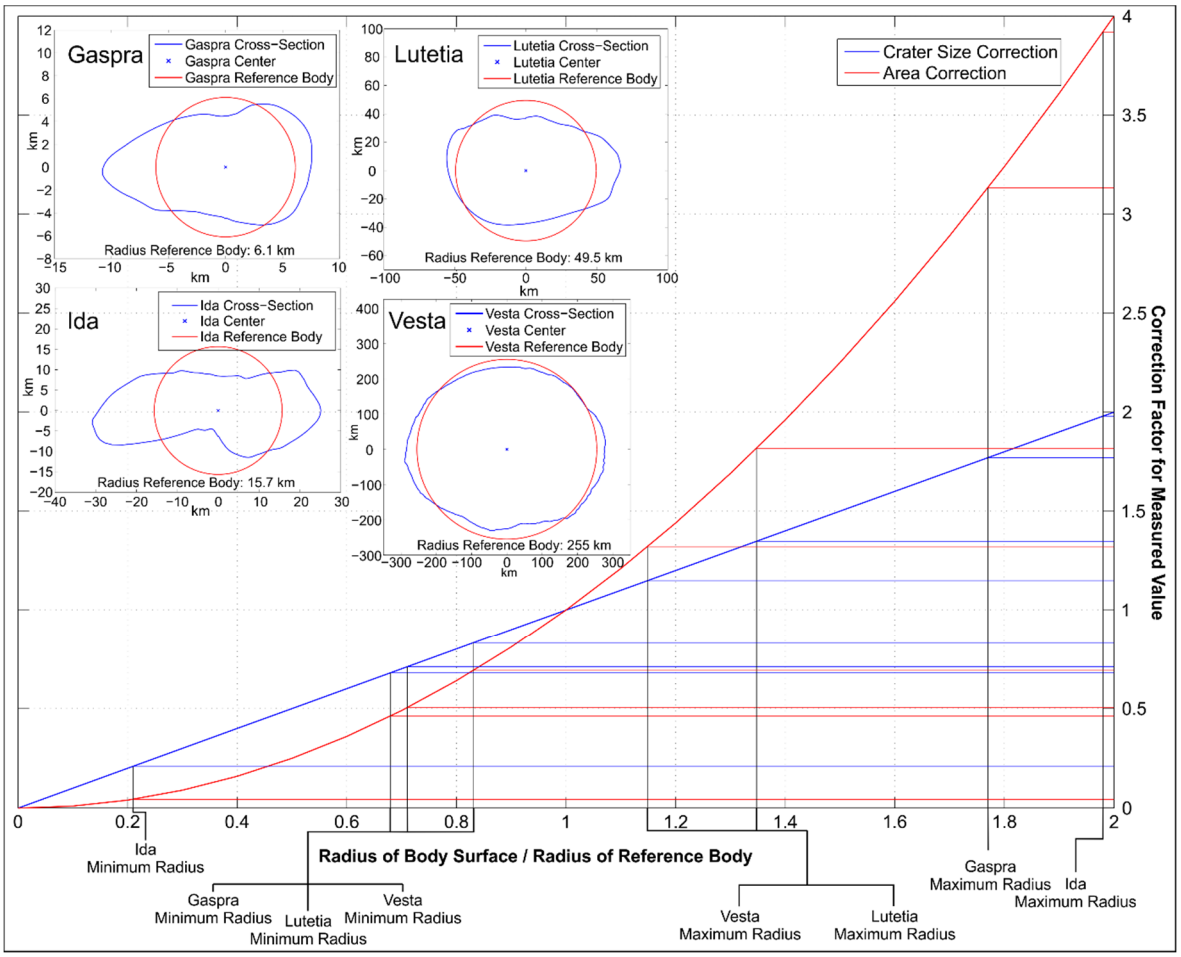


Fig. 2-1: Correction between reference and true body surfaces: Inlays: True body cross-sections along the topographically most variable meridian for Gaspra, Ida, Lutetia and Vesta are given as blue outlines. Respective reference spheres are indicated as red outlines with the same center as the true-body cross-sections. Main Panel: Minimum and maximum radii for each of the four asteroids are given as ratio with respect to the radii of the reference spheres along the x-axis. The y-axis gives the correction factor for crater sizes (blue) and areas (red) with respect to the ratios indicated along the x-axis. Vesta as largest body shows the smallest diversions (<20%) from the spherical reference body. Diversions for Lutetia, the second largest body in this selection are up to ~40%. Gaspra's reference sphere diverts up to ~80% from the true body surface. Ida's highly irregular shape diverts up to a factor of about ~2 from its reference sphere. This extreme difference results in a factor of two incorrect crater sizes and a factor of ~4 incorrect areas.

## 2.3 Applicability of saturation or standard equilibrium distribution on small bodies

Crater saturation (e.g. Hartmann, 1984 and Richardson, 2009) or standard lunar equilibrium distribution (Neukum and Dietzel, 1971 and Neukum, 1984) describes a change of slope from initially steep (-3 cumulative or -4 differential) crater distributions towards a shallower cumulative -2 slope (differential: -3 slope) for small crater diameters (< ~10 km). On the discussed asteroids the scaled lunar-like production function becomes flatter than -2 cumulative slope for craters > ~10 km diameter. Thus, a comparison to the standard lunar equilibrium distribution (in the following text: "equilibrium distribution") is only meaningful below ~10 km crater size. Equation (2.1) gives the equilibrium distribution as presented by e.g Neukum and Dietzel (1971), Neukum et al. (1975) and Neukum (1984).

$$N = 10^{1.1} D^{-2} \qquad \text{(D [km], N [1/km²]; Neukum, 1984)} \qquad (2.1)$$

The equilibration effect occurs during ongoing cratering of already densely cratered surfaces. It is interpreted as the point where there is a statistical balance between the obliteration and formation of craters by the impact process. The obliteration includes not only the geometrical overlap of crater rims but also incorporates ejecta blanketing and crater degradation by seismic shaking (Thomas and Robinson, 2005).

Small bodies are characterized by low escape velocities. Thus, impact ejecta are partly lost to space and contribute less to surface blanketing. On small bodies seismic shaking maybe the more dominant process of crater degradation compared to ejecta blanketing (Thomas and Robinson, 2005). Crater degradation by seismic shaking also appears to be influenced by surface gravity, in a way that it becomes more localized with increasing surface gravity (Richardson, 2013).

Where the crater production function is shallower or equal to a -2 cumulative slope, a crater distribution could also reach quasi-equilibrium where its shape would not be affected such that it would resample the initial production distribution. A surface model age derived from such a distribution would only represent a minimum age of the respective surface (e.g. Neukum and Dietzel, 1971 and Chapman and McKinnon, 1986).

Crater distributions on small bodies may not be in equilibrium or saturation although they plot already above the conventional lines of equilibrium or saturation on the Moon (Chapman et al., 1996b and Hartmann and Gaskell, 1997). Small fresh craters measured on asteroids (chapter 4) are typically below the lunar equilibrium distribution for small craters (Neukum and Dietzel, 1971). But if heavily degraded craters are also taken into account the measurements are sometimes above the lunar equilibrium distribution for small craters as shown for Ida, Gaspra and Lutetia in Fig. 2-2. The case for Ida shows the distribution for all craters almost parallel to the line of equilibrium for diameters ≤ 1 km. The distribution of only the fresh craters appears slightly steeper than the equilibrium down to crater sizes of ~500 m. Thus, the actual position of the equilibrium may be a function of the crater detection limit. Higher crater frequencies from recent crater counts compared to older ones are also

reported by Fasset et al. (2012) for the Moon. Recent data sets are of much better data quality than at the time when lines of equilibrium or saturation were empirically determined on the Moon. Even if old data sets are digitally enhanced and analyzed more craters may become visible, especially if they are degraded by some processes. The slope of the equilibrium function appears not to be affected and is probably a better indication of crater equilibrium than the absolute position of an equilibrium function.

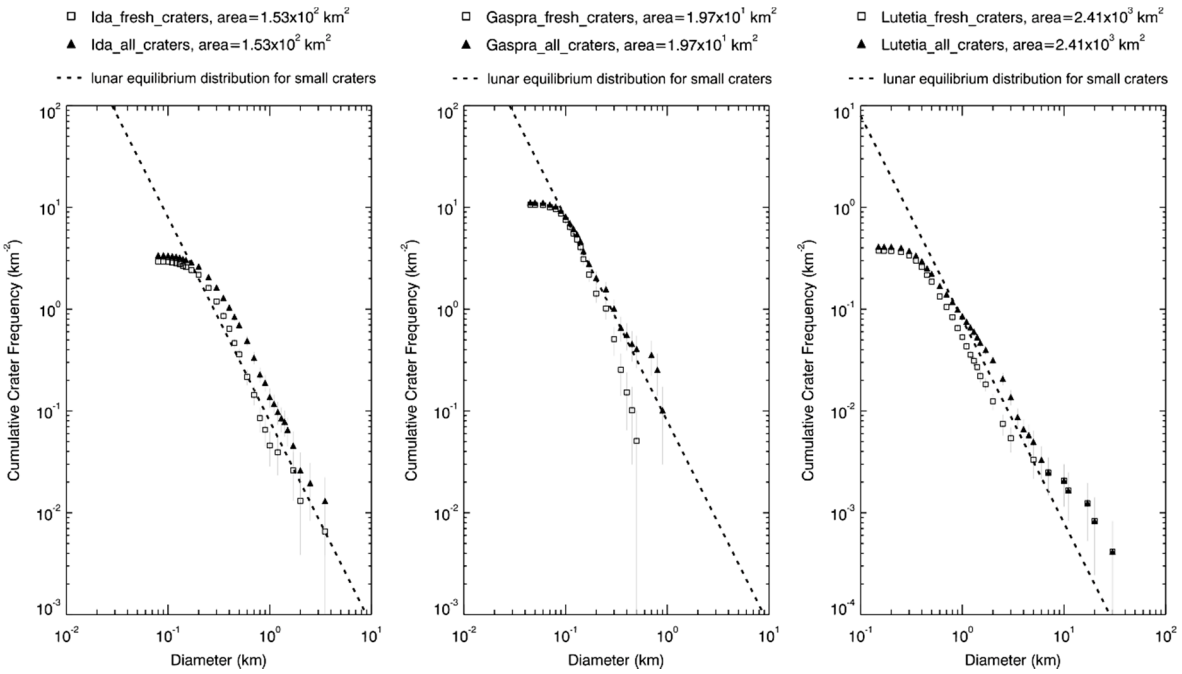


Fig. 2-2: Standard lunar equilibrium distribution and crater frequencies on Ida, Gaspra and Lutetia: Open squares represent measurements of fresh and pristine craters only. Filled triangles show measurements of all craters, including degraded ones. While fresh craters plot close to the lunar equilibrium distribution (dashed line), measurements including degraded craters plot mostly above the lunar equilibrium. In the case of Ida (left panel) the distribution for all craters above equilibrium seem to follow a -2 slope, while the fresh craters < 1 km, because of crossing the equilibrium, appear to show a slightly steeper distribution than the equilibrium. This may indicate a sensitivity of the vertical position of the equilibrium function with respect to the crater detection limit. In the case of Gaspra (center panel) the fresh crater distribution plot below the lunar equilibrium function for craters ≥ 200 m. The distribution for all craters < 400 m follows closely the equilibrium, while two bins at 7 and 8 km plot clearly above the equilibrium (total number of craters in these two bins is statistically insignificant). In the case of Lutetia fresh craters seem to be in equilibrium below the lunar equilibrium function between 500 m and 3 km crater size. The distribution of all craters < 2 km is shallower than the equilibrium slope (cumulative: -2). Although above the actual lunar equilibrium function, craters ≥ 2 km show a wavy distribution and as presented in Fig. 4-19 they are in reasonably good agreement with a lunar-like crater distribution which is scaled to Lutetia. Thus, these craters appear not to be in equilibrium yet.

### 2.3.1 Highest crater frequencies on Vesta – in equilibrium?

Fig. 2-3 shows two crater distributions from heavily cratered terrains on Vesta. The presented measurements indicate that the oldest terrains on Vesta show small crater distributions above the lunar equilibrium. In this size range an equilibrated crater distribution should follow a straight slope of -2 cumulative or -3 differential. The shown examples could be interpreted as being in production but in fact a vertically shifted lunar equilibrium function is also consistent with the crater distribution ≥ 1 km. Crater frequencies < 1 km show deficiencies due to resurfacing, resulting in a shallower than -2 slope (cumulative). Therefore, it cannot be ruled out, that an age of ~3.8 Ga, which is derived from the example measurement for crater sizes < 10 km is only a lower boundary for the real surface age.

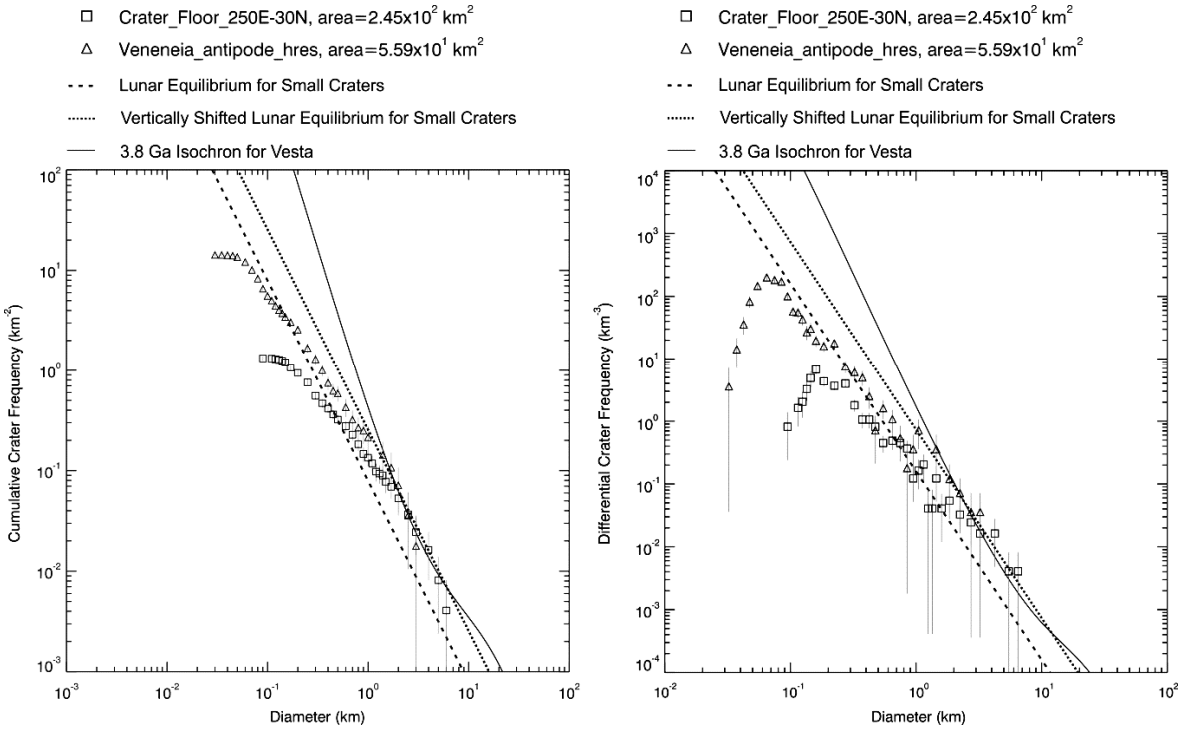


Fig. 2-3: Comparison of equilibrium and production crater distribution of small craters on oldest vestan surface: Cumulative (left) and differential (right) plots of highest crater frequencies < 10 km crater size found on Vesta. In both cases the solid line represents the 3.8 Ga isochron which is the reference in case the measurements are not in equilibrium. The dotted line is the vertically shifted lunar equilibrium function (actual lunar equilibrium – dashed line). In the diameter range in question it is not clear whether the measurement follows the plotted isochron or the shifted equilibrium function. Thus, an age of ~3.8 Ga can be interpreted as a minimum for the densly cratered terrains in the northen hemisphere of Vesta.

Neukum (1984) reported that the diameter range of craters in equilibrium propagates to larger diameters with increasing exposure age of a given surface. For craters < 10 km diameter with a steep sloping production function, that is a direct result of the shrinking crater formation rate with increasing crater diameter. Therefore, a crater distribution in equilibrium at small diameters could still be in production at larger crater diameters.

## 2.4 Dependence of model ages on the shape of the production function

The crater production function is used in order to relate the frequencies of arbitrary crater diameters of a given measurement to the respective crater frequency at the crater diameter for which the chronology function of the measured body is calibrated. Publications presented in this thesis use chronology functions calibrated to 1 km crater diameter. Exceptions from this rule are the Zahnle chronology models (Fig. 7-10; Zahnle et al., 2003) presented in chapter 7. In case a measurement contains craters in the size bin of 1 km this value can be used for dating the surface in the respective counting area without knowing the production function. However, in that case statistical errors are usually larger than fitting several crater size bins. Moreover, not all measurements contain craters inside the 1 km crater bin and require an appropriate crater production function that allows to fit crater frequencies at any measured diameter range, where the function is defined, in order to derive the related crater frequency at 1 km diameter. The shape of the production function heavily depends on the model of the primary projectile distribution. The following examples related to the Dawn mission at Vesta illustrate the effect of slight differences in the crater production function with respect to the resulting model ages. In both cases the chronology functions are identical at the age range in question. One of the production functions (Vesta-Rev4; Schmedemann et al., 2014a) is detailed in chapter 4. The production function by Marchi et al. (2014) was never published with its coefficients. However, in 2013 D.P. O'Brien, one of the co-authors of Marchi et al., provided a data table of their production function from which the coefficients of the polynomial of 11-th degree were derived in order to use this function with the craterstats software (Michael and Neukum, 2010). Both production functions have been used in order to determine surface ages on Vesta. They produce different model ages up to a factor of ~5 depending on the crater sizes used. These differences are the result of slightly different shapes of the production functions that are caused by the underlying model of the impacting projectile population. While Schmedemann et al. assume the same projectile population that impacted the lunar surface, Marchi et al. assume a projectile distribution that resembles the average asteroid Main Belt with slope extrapolation for unobservable small asteroids of at least 2 orders of magnitude in diameter. The reasons why the average Main Belt solution is probably less accurate than the lunar-like one is detailed in chapter 4.

### 2.4.1 Fit range > 1 km (reference crater size)

In Fig. 2-4 a measurement from the Rheasilvia ridge and groove terrain (detailed in chapter 4 and 5) is fitted in a diameter range larger than the reference diameter of 1 km. Because the slopes of the production functions differ somewhat from each other around 1 km diameter, we get two different cumulative crater frequencies in the sense that the steeper lunar-like production function gives higher crater frequencies and thus higher model ages for the same measurement in the same fit range.

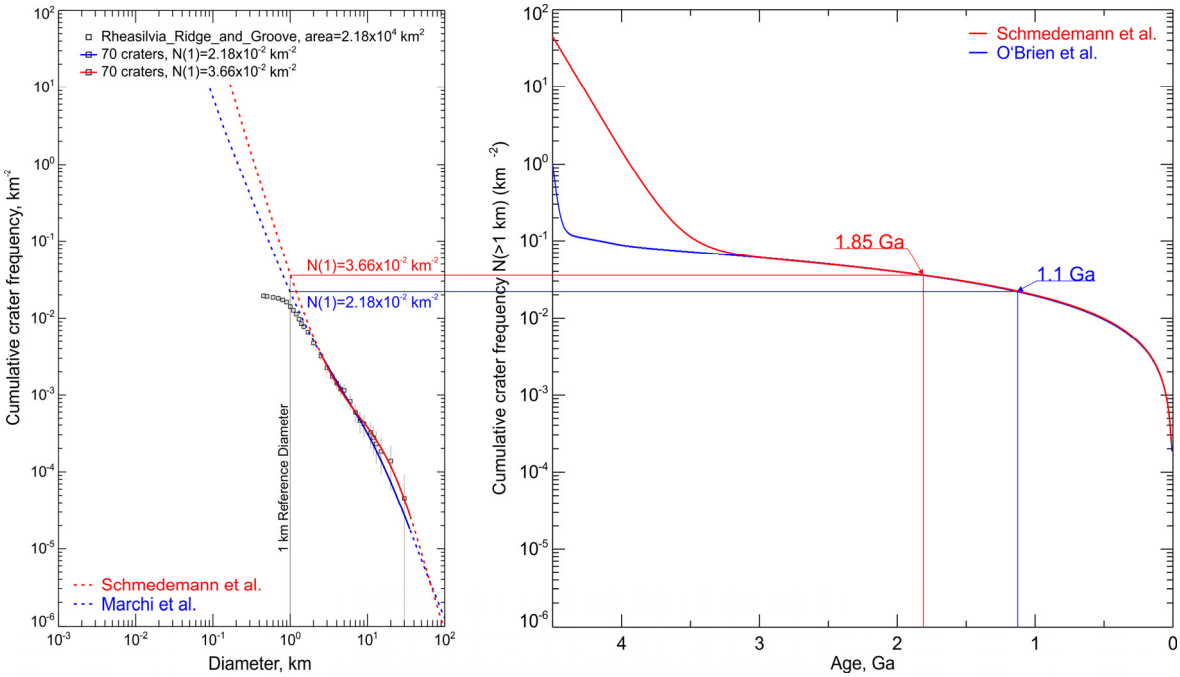


Fig. 2-4: Comparison of production function for craters > 1 km: Left: Plot of the cumulative crater distribution of the Rheasilvia ridge and groove terrain - open black squares (detailed in chapter 4 and 5). Production functions for Vesta Rev4 by Schmedemann et al. (2014a) - red dashed curve and the production function used by Marchi et al. (2014; provided by D.P. O'Brien, 2013) - blue dashed curve are fitted to the measurement given by the open black squares in the same diameter range (fitted diameter range – solid curves). Blue and red horizontal lines represent cumulative crater frequencies at 1 km crater diameter for the respective production functions. Right: Plot of the Vesta chronology functions by O'Brien et al. (2014) - blue and lunar-like (Schmedemann et al., 2014a) - red. The vertical axis of the chronology plot is equal to the vertical axis of the crater distribution plot on the left. The interceptions of the blue and red horizontal lines (measured cumulative crater frequencies at 1 km diameter) give the model ages for both chronologies. Vertical red line - model age for crater production function from Schmedemann et al. (2014a). Vertical blue line - model age for crater production function used by Marchi et al. (2014; provided by D.P. O'Brien, 2013).

### 2.4.2 Fit range < 1 km (reference crater size)

Analog to the previous example but for the case of fitting the production function to a measurement smaller than the reference diameter of 1 km, the steeper lunar-like production function results in lower crater frequencies and thus lower model ages (Fig. 2-5).

Within the Dawn team the combination of the production function by Marchi et al. (2012c) and Marchi et al. (2014) and the chronology function by O'Brien et al. (2014) has been termed "asteroid flux system", while production and chronology functions by (Schmedemann et al., 2014a) were termed "lunar-like system" or "lunar-derived system". Williams et al. (2014b) discuss the chronostratigraphy of Vesta using absolute ages of both systems. Significant differences in model ages of analyzed areas on Vesta are only partly caused by the presented differences in the used production functions. Other reasons are the geologic interpretation of the used counting areas, for crater frequencies > ~0.065 $km^{-2}$ or respectively model ages > ~3 Ga the much different shape of the used chronology function, and the ratio between

identified craters and identifiable craters. Such issues are further discussed in chapter 4.
With respect to the different shapes of used production functions similar issues also exist for absolute model ages at Phobos and in the outer Solar System. In the case of Phobos two different sets of production and chronology functions are described in chapter 3. In chapter 7 for the example of Mimas the lunar-like production function is compared with the significantly different production functions by Zahnle et al. (2003) and the observed crater distribution.

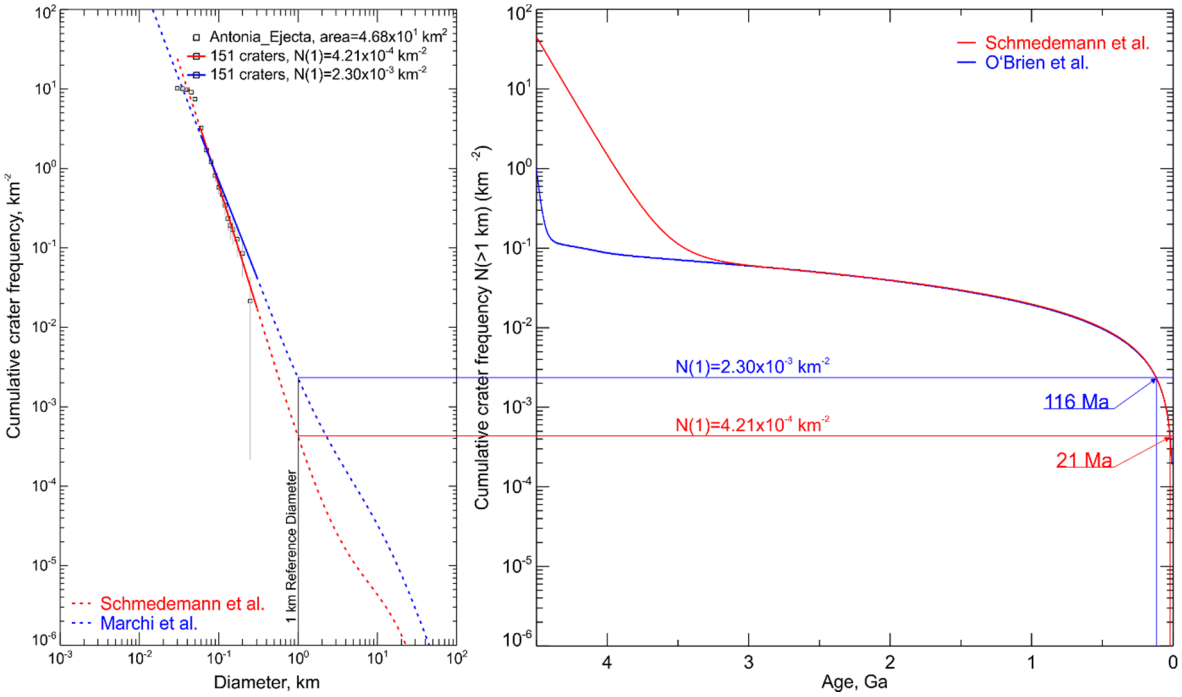


Fig. 2-5: Comparison of production function for craters < 1 km: Left: Plot of the cumulative crater distribution of the Antonia ejecta blanket (detailed in chapter 4 and 5). Colors and functions are the same as in Fig. 2-4. Right: Chronology functions – colors and functions are the same as in Fig. 2-4.

# 3 The age of Phobos and its largest crater, Stickney

by N. Schmedemann, G. Michael, B. A. Ivanov, J. Murray and G. Neukum (2014), published in Planetary and Space Science (http://dx.doi.org/10.1016/j.pss.2014.04.009).
The first author of the manuscript selected and mapped the counting areas, did the crater measurements, derived the lunar-like crater-production and chronology functions, interpreted the measurements and results, prepared the figures and the manuscript. The co-authors were involved in discussing the manuscript.

# 4 The Cratering Record, Chronology and Surface Ages of (4) Vesta in Comparison to Smaller Asteroids and the Ages of HED meteorites

by N. Schmedemann, T. Kneissl, B. A. Ivanov, G. G. Michael, R. Wagner, G. Neukum, O. Ruesch, H. Hiesinger, K. Krohn, T. Roatsch, F. Preusker, H. Sierks, R. Jaumann, V. Reddy, A. Nathues, S.H.G. Walter, A. Neesemann, C. A. Raymond and C. T. Russell (2014), published in Planetary and Space Science (http://dx.doi.org/10.1016/j.pss.2014.04.004). The published article is complemented by suplementory online material (SOM), which is presented in sub-chapter 4.7.
The first author of the manuscript selected and mapped the counting areas if not mentioned otherwise, did the crater measurements if not mentioned otherwise, derived the lunar-like crater-production and chronology functions, interpreted the measurements and results, prepared the figures and the manuscript. The co-authors were involved in discussing the manuscript.

# 5 Morphology and formation ages of mid-sized post-Rheasilvia craters – Geology of quadrangle Tuccia, Vesta

by T. Kneissl, N. Schmedemann, V. Reddy, D.A. Williams, S.H.G. Walter, A. Neesemann, G.G. Michael, R. Jaumann, K. Krohn, F. Preusker, T. Roatsch, L. Le Corre, A. Nathues, M. Hoffmann, M. Schäfer, D. Buczkowski, W.B. Garry, R.A. Yingst, S.C. Mest, C.T. Russell and C.A. Raymond (2014), published in Icarus (http://dx.doi.org/10.1016/j.icarus.2014.02.012).
The author of this thesis (N. Schmedemann) was responsible for the derivation of the lunar-like crater-production- and chronology function, involved in the analysis of crater-size frequency distributions and was deeply involved in the discussion of the maunscript.

# 6 Olivine or impact melt: Nature of the ‘‘Orange’’ material on Vesta from Dawn

by Lucille Le Corre, Vishnu Reddy, Nico Schmedemann, Kris J. Becker, David P. O'Brien, Naoyuki Yamashita, Patrick N. Peplowski, Thomas H. Prettyman, Jian-Yang Li, Edward A. Cloutis, Brett W. Denevi, Thomas Kneissl, Eric Palmer, Robert W. Gaskell, Andreas Nathues, Michael J. Gaffey, David W. Mittlefehldt, William B. Garry, Holger Sierks, Christopher T. Russell, Carol A. Raymond, Maria C. De Sanctis, Eleonora Ammanito, published in Icarus (http://dx.doi.org/10.1016/j.icarus.2013.08.013).

The author of this thesis (N. Schmedemann) was responsible for the selection and mapping of the counting areas, derivation of the lunar-like crater-production- and chronology function, determination of crater retention ages by measuring and analysis of crater-size frequency distributions and preparation of figures and parts of the manuscript presented in sections 6.4.3, 6.9.2 and 6.9.3. The autor was further involved in the discussion about the stratigraphic position of the orange material and layer thickness estimations.

# 7 Impact crater size – frequency distribution on Mimas and the age of Herschel

Manuscript by Nico Schmedemann, Roland J. Wagner, Gregory G. Michael and Tilmann Denk in revision for Icarus.
The first author of the manuscript selected and mapped the counting areas, did the crater measurements, compared projectile distributions, derived the lunar-like crater-production and chronology function, interpreted the measurements and results, prepared the figures and the manuscript. The co-authors were involved in discussing the manuscript.

**Abstract:** In this paper we mainly discuss results of crater counting from 9 areas on Mimas. The crater counting revealed crater size-frequency distributions created by members of a collisionally evolved impactor family like the one which bombarded the lunar surface. For the age determination we used chronologies based on published work for various types of impactors. We (i) measured the crater size-frequency distribution on Mimas between 0.4 and 130 km, (ii) derived scaling parameters for conversion between projectile and crater sizes for Mimas and Iapetus, (iii) compared crater-derived projectile size-frequency distributions for 3 dynamical cases with size-frequency distributions of Kuiper Belt Objects, comets and Main Belt asteroids, (iv) determined a crater production function and cratering chronology for one of the dynamical cases, (v) estimated the age of the crater Herschel and the heavily cratered plains for 3 different chronology functions.

## 7.1 Introduction:

The investigation of the geologic history of the Saturnian satellites and the processes of the early outer solar system are two major goals of the Cassini mission (Porco et al., 2004). On February 14, 2010 a close flyby of the Cassini spacecraft at Mimas revealed the most detailed images ever taken of this innermost of the midsized Saturnian satellites. High resolution images were taken with the Cassini ISS instrument (Porco et al., 2004), at image scales of up to 92 m/pixel. Compared with the best data available prior to this flyby there was an increase of image resolution by a factor of about 4. The main target during this flyby was the large crater Herschel on Mimas' leading side at 3° north/ 117° west and its vicinity. Although Herschel is the most prominent crater on Mimas, its diameter of 135 km (Thomas et al., 2007) is well below the maximum possible (240 km) without disrupting the 400 km diameter icy body (Leliwa-Kopystynski et al., 2008).
Crater counting of previously unresolved small craters inside the Herschel crater and on the proximal ejecta blankets allows the investigation of the crater size-

frequency distribution at small sizes and eventually the dating of the Herschel impact event relative to the surrounding heavily cratered plains. By application of a cratering chronology function absolute cratering model ages can also be derived from crater counts (e.g. Neukum, 1984; Neukum, 1985; Neukum and Ivanov, 1994; Zahnle et al., 1998; Zahnle et al., 2003; Neukum et al., 2006 and Michael and Neukum, 2010).
For the dating technique knowledge of the predominant projectile population i.e. the underlying impact crater size - frequency distribution (SFD) and the impact rates are required. These data determine models for the production function and chronology. In the literature no consensus has been reached with respect to the main impactor source in the Saturnian system and the related orbital dynamics of the projectiles (Neukum, 1984; Zahnle et al., 2003 and Dones et al., 2009).
In this context, the addition of the small crater production size - frequency distribution from the recent flyby to the already known distribution of larger craters is valuable. The interior of crater Herschel and its ejecta blanket are appropriate areas to measure the small crater SFD of post-Herschel impacts.
Crater SFDs inside or close to larger craters can be affected by secondary cratering. Typical indications for this are herringbone patterns, crater chains or clustered craters possibly associated with rays (Neukum, 1984; Bierhaus et al., 2001 and Werner et al., 2009). Such features are well preserved in the surroundings of the ray crater Inktomi on Rhea (Wagner et al., 2011 and Bierhaus et al., 2012). Bierhaus et al. (2012) also states that secondary cratering on Mimas is unlikely, because of the low surface gravity of Mimas. This would allow for a few distant secondaries only, while most of the secondary projectiles go into an orbit about Saturn. Most of these sesquinary projectiles (Alvarellos et al., 2005 and Bierhaus et al., 2012) should have reimpacted on Mimas, producing a steep size distribution of small craters. This, however, was not observed by Bierhaus et al. (2012).
In this work we present our results of crater counting in the Herschel area and compare it to measurements of the heavily cratered plains of Mimas. Furthermore, we compare the derived crater derived projectile size–frequency distribution of Mimas with that one of Iapetus and potential projectile populations such as Kuiper Belt Objects, comets and asteroids. We develop crater production and chronology functions for Mimas and Iapetus and give absolute and relative ages for Herschel crater with respect to the heavily cratered plains using the lunar-like (Neukum, 1984, 1985; Neukum et al., 2005 and Neukum et al., 2006) and Zahnle (Zahnle et al., 2003) chronology models.

## 7.2 Methodology

Image processing:
In order to measure impact crater sizes we use Cassini ISS imaging data (Porco et al., 2004). Raw images are corrected for artifacts caused by radiometry and compression. The resulting images are enhanced by a slight unsharp masking and usually cut off where the observation angle is below 10°. Finally the images are

rectified to align with a global mosaic (basemap) (Roatsch et al., 2009 and Roatsch et al., 2013a).
For the image processing we use the ISIS software environment (e.g. Becker et al., 2013). If craters are already well resolved (rim to rim >10 pixel) on the basemap, no additional images are used for the crater counting. This is not just time-saving but also reduces errors due to misalignments and thus enhances our ability to compare different measurements.
Mapping:
The mapping task is conducted using the ESRI ArcGIS software package. It provides the necessary tools for mapping craters and counting areas. For a more convenient workflow, we use the "CraterTools" plug in, developed by Kneissl et al. (2011). CraterTools allows for map projection independent measurements of surface features, reducing measurement errors caused by projection distortions. Area outlines as well as identified craters are managed as shapes in the shapefile format. Thus we have good control on the status of the measurements and the ability to cross check measurements with other co-workers.
The definition of the counting area has significant impact on the measurement. Following for instance Shoemaker and Hackman (1962), Neukum (1984) or Wilhelms et al. (1987) we keep the counting areas in each case inside a single geologic unit, that was formed by a single or related process(es). Our definition of a geologic unit by this means is based on the surface morphology. In the case of highly similar counting results from different areas which were emplaced by the same event the measurements can be combined for better statistics. We do not combine measurements of surfaces showing different cratering characteristics which would disturb the resulting crater SFD.
Areas dense in crater chains or clustered craters are excluded from the counting areas to avoid secondary craters. Based on crater measurements on the Cerberus Plains on Mars and a theoretical work, Werner et al. (2009) found that an additional contribution of visually well identifiable Zunil-secondary craters affected the standard model crater retention age of the Cerberus Plains by less than the statistical uncertainty. Works by Ivanov (2006) and Richardson (2009) also suggest a predominance of primary craters at least on planetary bodies in the inner Solar system. However, in the Saturnian system so-called sesquinary projectiles (e.g. Dones et al., 2009 and Bierhaus et al., 2012) may be an issue. It may be possible that significant cratering by sesquinary projectiles manifests as a steep crater distribution similar to secondary cratering. Due to their dynamical characteristics sequinary projectiles predominantly re-impact their source body (Alvarellos et al., 2005) but should be widely dispersed across its surface. A steep crater distribution, possibly caused by sesquinary craters, is present on Tethys (Schmedemann et al., 2014b).

Data analysis: The crater diameters which have been measured and exported from ArcGIS into a text file are binned and displayed with the software "craterstats" (Michael and Neukum, 2010). In general, we present plots conforming to suggestions made by (Arvidson, 1979). Although square-root 2 binning is recommended by that publication we use a pseudo-log binning for higher

resolution data plots. The pseudo-log binning has 18 intervals per decade with pseudo-logarithmic spacing (Neukum, 1984). Its higher resolution compared to the square-root 2 binning is useful for example in order to determine the positions of slope changes in the crater distribution with higher accuracy, which is important in analyzing differences between crater distributions. Due to the larger number of potential tie points it also is better suited for piecewise alignment of individual measurements in order to construct a combined crater SFD from several separate measurements of one body as demonstrated by e.g. Neukum and Wise (1976), König (1977), Neukum (1984) and Werner (2005). Craterstats is used to derive surface model ages from measured crater size-frequency distributions by fitting a crater production function to the measured crater distribution and converting the measured crater frequency into an absolute age based on a chronology function. That is detailed for instance in Neukum (1984) and Michael and Neukum (2010).
Chronology functions relate crater frequencies to model ages. Depending on the nature of the main impactor source, we here apply two primarily different chronologies in order to derive model ages.
The lunar-like model (Neukum, 1984, 1985; Neukum and Ivanov, 1994 and Neukum et al., 2006) applies a chronology which is derived from the lunar chronology, which in turn has been derived from radiometric dating of lunar rock samples and measured crater frequencies at the sample sites. The asteroid Main Belt is assumed as the main impactor source for the inner solar system and the Main Belt itself (e.g. Neukum and Ivanov, 1994; O'Brien and Greenberg, 2005; Strom et al., 2005; Ivanov, 2008; Massironi et al., 2009 and Schmedemann et al., 2014a). Neukum (1984, 1985, 1997); Neukum et al. (1998); Neukum et al. (2005) and Neukum et al. (2006) suggested a projectile source with high similarities to the asteroid Main Belt for the satellites of the jovian and Saturnian system. Thus, the crater SFDs are highly similar to the asteroid body SFD (e.g. Neukum, 1985 and Schmedemann et al., 2010) but shifted on the diameter axis, due to the impact scaling between projectiles and their respective craters. The lunar-like chronology function is adapted for the different impact fluxes on the respective target bodies.
The Zahnle model (Zahnle et al., 2003) assumes a predominantly cometary source of impactors at a nearly constant flux. This model is valid mainly for younger ages (e.g. Kirchoff and Schenk, 2010). This is caused by the high uncertainty of the cometary flux in the early solar system history. This model provides two chronologies where the cases A and B differ in the impactor flux as well as the impactor size-frequency distribution at small sizes. In this model planetocentric debris expelled from primary impacts also play an important role in the Saturnian system.

An overview of these models is given in (Dones et al., 2009).

## 7.3 Image data and measurement areas

### 7.3.1 Image data

Table 7.1 gives the names of the measurements, image numbers and resolution of the images used for crater counting on Mimas. The images we used range in scale between 92 and 392 m/pixel resolution. All measurements described in this work were performed on the Mimas basemap (Roatsch et al., 2009 and Roatsch et al., 2013a) or on images aligned to it. For the map projection of Mimas, we used a two-axial ellipsoid with 207.4 km semi-major axis and 190.6 km semi-minor axis, following Thomas et al. (2007).
Since the SPICE-based image rectification of the ISIS image processing is often offset to the respective basemap features, we re-rectifed the ISIS processed images to realign them with the basemap. Therefore, the lower resolution images of this flyby have been re-rectified to the Mimas basemap, while higher resolution images were re-rectified to the lower resolution images, respectively.
Crater Herschel is about 130 km in diameter, as it appears on the basemap. Thomas et al. (2007) give 135 km for the Herschel diameter while Leliwa-Kopystynski et al. (2008) use 145 km. However, images processed in ISIS, using the latest SPICE-Kernel dataset from the flyby in mid-February 2010, match well with the used basemap.

Table 7-1: Image names and respective resolutions for measurements on Mimas.

| Image number | Resolution [m/pixel] | Measurements |
|---|---|---|
| N1644777693 | 92 | A7 |
| N1644777828 | 95 | A1, A3 |
| N1644778567 | 116 | A4, A5, A2 |
| N1644781312 | 200 | A6 |
| N1501645855 | 392 | A8 |
| Basemap (Roatsch et al., 2009; Roatsch et al., 2013a) | 216 (equator) | A9 |

### 7.3.2 Description of counting areas

We selected the counting areas on a geomorphologic basis. Each counting area is inside a geologic unit, which we took to have been formed at one distinct point in time and is characterized by a homogenous surface morphology. We mapped the counting areas to the best of our abilities in such a way that the areas do not cross the borders of geologic units or the borders of images with changing resolution, which could affect the crater statistics.
Herschel is a complex crater with a central peak (Fig. 7-1).

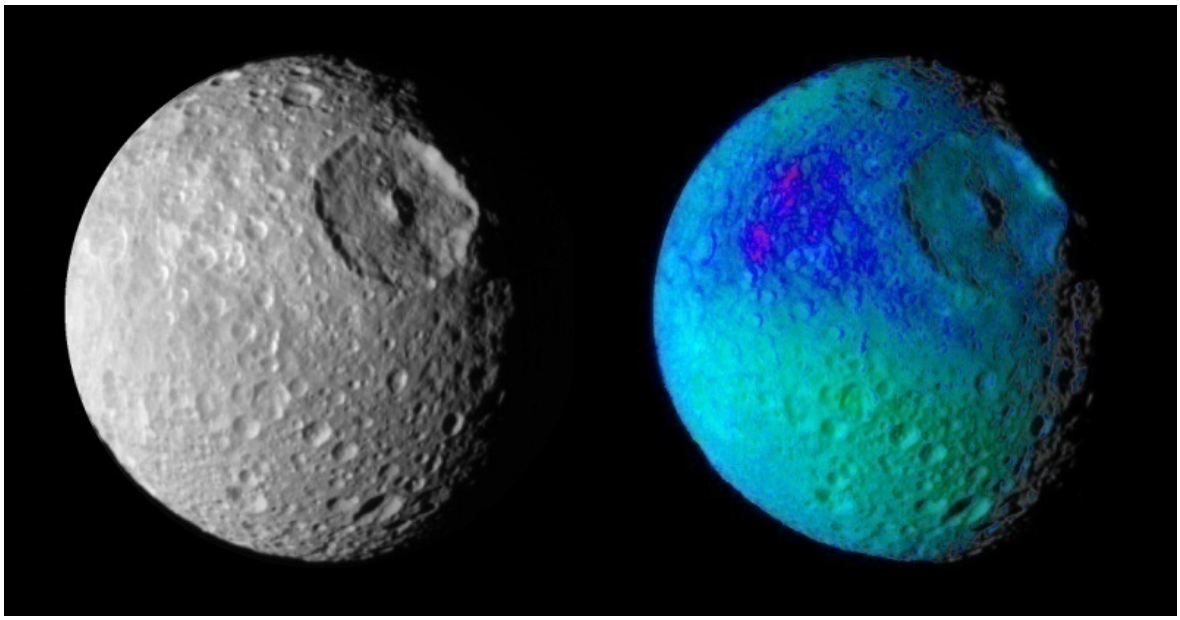

Fig. 7-1: Herschel, Morphology and Thermal Inertia Anomaly: Crater Herschel on Mimas with central peak. The darker blue area is likely a part of a high-amplitude thermal inertia anomaly (Howett et al., 2011) off the western crater rim of Herschel, visible in the false color (ultraviolet, green and infrared) image (right). (NASA/JPL/Space Science Institute, PIA06257).

Its shape is close to a circle but it is slightly elongated in the NW-SE direction, while shortened along the perpendicular direction at a ratio of about 1.09. An older Cassini ISS image from 2005 shows a possible trace of the 'pacman' structure which has been found to be a part of a high-amplitude thermal inertia anomaly (Howett et al., 2011) westward of Herschel in false colors (Fig. 7-1). Besides the central peak, which is also elongated in the NW-SE direction, the interior of Herschel displays several distinguishable features.

Fig.7-2 depicts a map of all the areas where crater frequency measurements were conducted on Mimas. The region of measurement "A1" shows a part of the crater floor with little or no cover by impact ejecta. Inside this measurement area only a few post-Herschel impact craters are clearly visible.

The crater floor NE of the central peak is characterized by an undulating topography. The measurement which probed this particular area is "A2". The nature of this unit is uncertain but could represent some kind of frozen impact melt (pers. comm. C. C. Porco, 2010).

In the southern part of Herschel there is significant mass wasting in the form of slumped terraces. This mass wasting might have happened shortly after the impact, when the transient crater relaxed. The respective measurement in this area is named "A3". This area was also heavily resurfaced during the impact und now displays a post-impact cratering record.

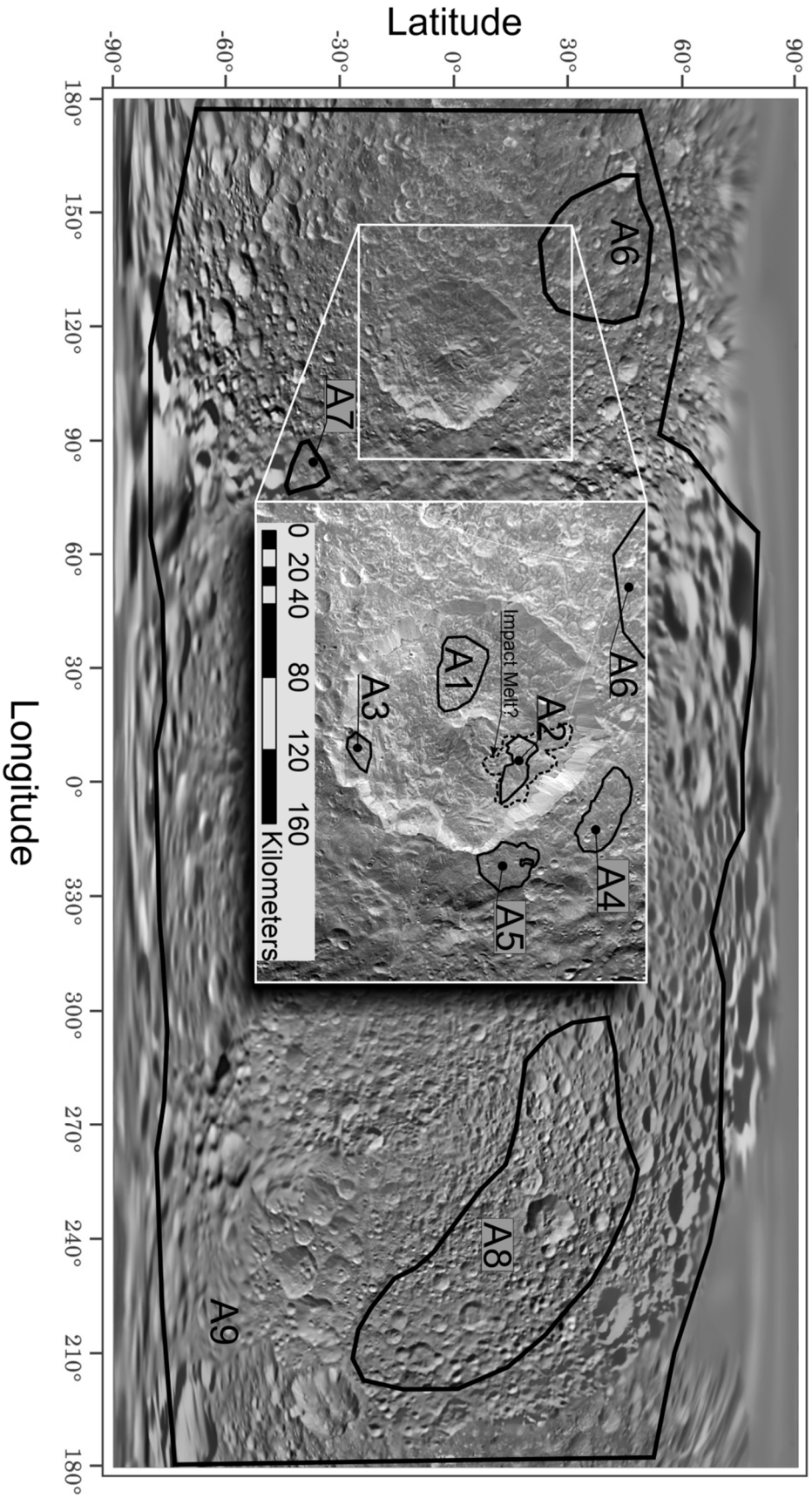


Fig. 7-2: Counting Areas: Areas of crater counting A1 – A9 (black outlines). The inlay gives a magnification of the crater Herschel area and the respective counting areas. Basemap: Roatsch et al. (2009) and Roatsch et al. (2013a).

Outside crater Herschel but close to its NE crater rim, a morphologic unit of smooth appearance was probed by crater counting with two measurements ("A4" and "A5"). The morphology of this smooth unit seems to be similar to rampart craters often found on Mars (Mutch and Woronow, 1980) but such features are also known from icy satellites such as Ganymede (Horner and Greeley, 1982) and Dione (Wagner et al., 2006). In any case the target materials seem to be rich in volatile material like water ice, which is also the case for Mimas' surface (e.g. Filacchione et al., 2010).
Further away from crater Herschel in NW direction, the measurement "A6" probes an area which was not resurfaced during the Herschel impact to a great extent. This area represents the presumably older, heavily cratered plain around Herschel and thus the underlying stratigraphic horizon.
A similar measurement ("A7") was made SE of Herschel crater. In this area large craters from an underlying stratigraphic horizon are also visible, while small craters are depleted by some process(es). A7 is located roughly one Herschel diameter away from the center of Herschel. Hence, this area is at the margin of the classical continuous ejecta blanket (e.g. Melosh, 1989).
Far away from the Herschel impact site, a large part of a heavily cratered plain ("A8") was measured on Mimas' trailing side (Fig. 7-2). This measurement contains a high number of midsized to large craters and gives a good representation of one of the oldest areas on Mimas.
The largest area ("A9") of crater counting on Mimas comprises almost the entire surface area of the satellite where at least the largest craters are sufficiently resolved for crater counting (Fig. 7-2). The main purpose of this measurement is to sample the crater SFD at the largest crater diameter ranges, in order to construct a general crater SFD for Mimas from measurements of all available crater sizes (Appendix A1-A9).

## 7.4 Measurements

Tables A1-A9 in Appendix A give the measured impact crater size-frequency distributions of the described areas in detail. An overview of the measurements is presented as cumulative plots in Fig. 7-3. All measurements are terminated towards smaller crater diameters by a so-called "roll-over". This indicates systematic undercounts of craters mostly close to the resolution limit of the respective image. The roll-over is also influenced by illumination conditions and surface morphology. If higher resolution images were available for the same geologic unit, crater diameters from the higher resolution counts were used. For the age determination we neglected the roll-over sections and fit the crater production function only to that part of the measurements which presumably is not disturbed by issues related to image quality, geologic processes or secondary/sesquinary cratering. Crater distributions influenced by secondary or sesquinary cratering usually show steeper size distributions than pure background primary craters, while the other mentioned issues usually lead to kinks in the measured distribution with lower crater

frequencies in specific size ranges (Neukum, 1984; e.g. Werner, 2005 and Schmedemann et al., 2014a).
The crater size–frequency distributions of areas A1-A5 appear relatively similar and thus indicate similar ages. Especially, the measurements A2, A3 and A5 plot almost on top of another within the error bars. They also cover almost the same range in crater diameter. Hence, these measurements can be merged for better statistics and clarity. The merged data will be labeled as A235 (Appendix A235) and is representative for younger Herschel impact resurfaced areas. A235 serves for comparison with older areas i.e. the heavily cratered plains.
The areas A6 through A9 range over about 2.5 orders of magnitude in crater diameter. The small vertical offsets of measurements sharing the same range of crater diameters also indicate a similar cratering history of these surface units.

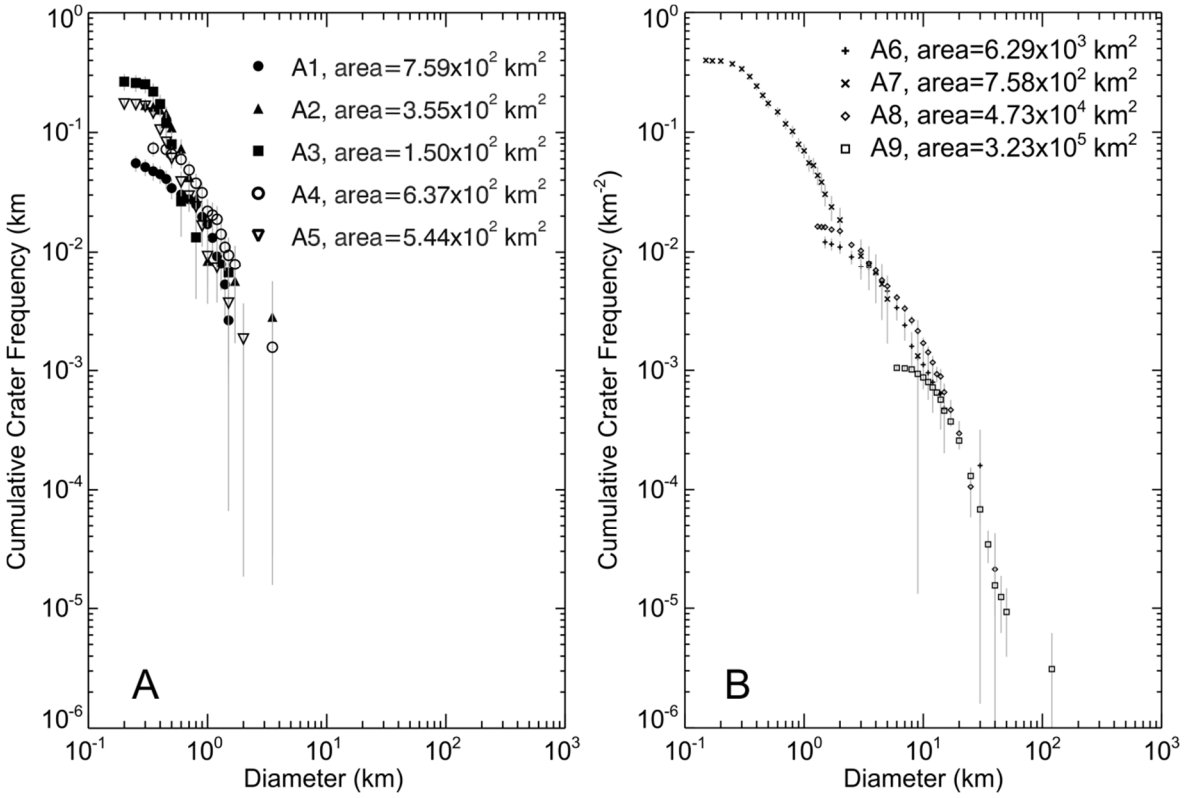


Fig. 7-3: Plot of All Crater Counts: Measurements of highly resurfaced areas due to the Herschel impact (A) and of the almost unaffected heavily cratered plains (B).

## 7.5 Size-frequency distribution of possible projectile populations in the Saturnian System

In this section we compare the theoretical size distribution of impactor populations derived from the measured cratering record of Mimas with published projectile populations such as comets and Kuiper Belt objects as well as Main Belt asteroids. The observed crater SFD on the target bodies is expected to have a similar shape like the responsible main impactor population but should be scaled to larger

diameters according to the respective impact conditions. This relationship has already been used as a strong argument in the identification of Main Belt asteroids as the main impactor source in the inner solar system (e.g. Neukum and Ivanov, 1994; Ivanov et al., 2002; O'Brien and Greenberg, 2005; Strom et al., 2005 and Ivanov, 2008).
Possible impactor populations for the Saturnian satellites have been described by e.g. Dones et al. (2009), Zahnle et al. (2003) and Neukum (1985). We compare the SFD of cometary, Kuiper Belt and asteroidal projectiles with the theoretical projectile distribution derived from impact conditions and the observed crater SFD on Mimas and Iapetus, the outermost regular midsized Saturnian satellite. The comparison of Mimas with Iapetus helps to constrain the dynamics of the main impactor source. The conversion between crater and projectile sizes is based on scaling laws (Ivanov, 2001 and Ivanov, 2008).
Heliocentric and high eccentricity planetocentric impactors should differ significantly in their impact velocity from co-orbital to low eccentricity planetocentric projectiles. Due to the focusing effect of Saturn and the consequential higher impact velocity, the related crater scaling should result in larger craters on Mimas compared to Iapetus. Low eccentricity, co-orbital projectiles impact with very low velocities, close to the escape velocity of the target body. At such low velocities scaling laws start to break down and our results may only be rough approximations of the true values. If the impact velocity is dominated by the escape velocity of the target bodies, much smaller variation in crater sizes between Mimas and Iapetus are expected compared to the cases of heliocentric and high eccentricity projectiles. Bierhaus et al. (2012) estimate a minimum velocity on the order of ~200 m/s at which secondary or sesquinary projectiles form craters. Mimas's escape velocity is slightly below this threshold. Thus, if Mimas is impacted by co-orbital projectiles, a significant fraction of this population may leave no craters behind. Only craters formed by more eccentric projectiles at higher impact velocities may be visible in the cratering record of Mimas.

### 7.5.1 Possible projectiles

Comets: Comets can be divided into several groups according to their orbital characteristics (e.g. Levison and Duncan, 1997; Dones et al., 2009 and Weiler et al., 2011). The two major categories are nearly isotropic comets (NIC) and Jupiter-family comets (JFC). Weiler et al. (2011) describe a flat distribution at small sizes for both categories (Fig. 7-4). Dones et al. (2009) argue for ecliptic comets (Jupiter-family comets, Centaurs, Scattered Disk Objects) as the chief source for primary craters in the outer solar system. The cometary size – frequency distribution published by Weiler et al. (2011) is re-digitized and presented in Fig. 7-4.
Kuiper Belt Objects (KBO): KBO are a probably large group of small bodies beyond the orbit of Neptune (e.g. Jewitt and Luu, 1993; Levison and Duncan, 1997 and Dones et al., 2009). In order to determine the body SFD of KBO we used absolute magnitude data from the JPL Solar System Dynamics Small-Body Database Browser (Giorgini et al., 1996) in November 2011. We further assumed a geometric albedo of 6% for all bodies between 30 and 50 AU and derived the body diameter following

Tedesco et al. (1992). We also re-digitized the data published by (Fraser et al., 2008). Both data sets are shown in Fig. 7-4.
In a qualitative way the body SFD of comets and KBO seem to be very similar in their overlapping region between 30 and about 150 km diameter. It is not clear if this is also true for smaller sizes, because of the limited observation of KBO and distant NIC. Weiler et al. (2011) suggest a shallow projectile size distribution as shown in Fig. 7-4 among small NIC even in their source region, the Oort cloud. Furthermore, volatile rich bodies like KBO and comets are losing significant amounts of material due to sublimation processes and splitting events while traveling the inner parts of the solar system. Thomas et al. (2013) estimated a global vertical ablation of the JF Comet 9P/Tempel 1 of about 30 cm per orbit. This implies: Once comets are affected by thermal sublimation processes, their SFD has been changed by non-collisional processes and therefore they do not reflect the original SFD. In relation to its volume a small comet will lose more material than a large comet, because of the higher surface area to volume ratio. This might be one explanation for the prominent deficiency of small comets (e.g., Zahnle et al., 2003 and Weiler et al., 2011). At large sizes (>50 km) KBO show changing slopes in their SFD. This may be the result of a collisional evolution. Analysis of typical collision velocities and frequencies following Bottke et al. (1994) show collision velocities of less than half of that among MBA and collision frequencies about 4 orders of magnitude less than those of typical MBA. These circumstances as well as the much more volatile composition may imply a different SFD of KBO than that of MBA (O'Brien and Greenberg, 2003). A detailed view on the SFD of KBO at small sizes presumably will be available from the cratering record of Pluto and Charon, which will be investigated in July 2015 by the New Horizons Mission.
Main Belt Asteroids (MBA): MBA have been determined to be the main impactor source in the inner solar system (e.g. Neukum and Ivanov, 1994; Ivanov et al., 2002; O'Brien and Greenberg, 2005 and Ivanov, 2008). For dynamical reasons MBA are believed to provide only a tiny contribution to the projectile distribution in the Saturnian system (e.g. Dones et al., 2009; Kirchoff and Schenk, 2010; Schenk and Murphy, 2011 and Richardson et al., 2012). However, e.g. Neukum (1985), Neukum et al. (1998), Neukum et al. (2005) and Neukum et al. (2006) argue for asteroids as the main impactor source in the Jovian and Saturnian system due to similarities in the size-frequency distribution of Main Belt asteroids and the observed crater distribution. Since the MBA SFD is not uniform throughout the Main Belt (Tedesco et al., 2005 and Elía and Brunini, 2007) we use the MBA SFD which is most similar to the crater SFD on the inner Solar system bodies. This is the case for MBA between 2.1 AU (inner edge of Main Belt) and 2.825 AU (5:2 mean motion resonance with Jupiter). That section of the Main Belt contains the highest radial densities of asteroids and also contains the three most efficient resonance gaps in the Main Belt (Gladman et al., 1997). As was done for the KBO, we determined the body SFD of MBA by utilizing the absolute magnitude data from the JPL Solar System Dynamics (JPL SSD) Small-Body Database Browser in November 2011 and calculated a moving average geometric albedo with a bin size of 1 AU based on bodies with known geometric albedo. For bodies with unknown diameter we derive the body diameter after (Tedesco et al., 1992) by utilizing the determined floating average

geometric albedo for the respective position in the Main Belt. If diameters were available in the mentioned JPL SSD dataset we used those values. In Fig. 7-4 we plot the size-distribution of all asteroids >5 km (observational completeness) in the semi-major axis range of 2.1 – 2.825 AU. The SFD of unobservable small asteroids is given by the extension of the asteroidal SFD towards smaller diameters by the SFD of lunar projectiles derived from the lunar crater SFD following crater scaling relations by Ivanov (2001) and Ivanov (2008). Schmedemann et al. (2014a) point out that there is a difference in distribution slopes between the modelled small body Main Belt population and the observed small crater population on the Main Belt asteroids and inner solar system bodies. Observed small crater distributions show steeper slopes around -3.5 cumulative (e.g., Neukum and Ivanov, 1994; Chapman et al., 1996a and Chapman et al., 1996b) compared to values of around -2.5 cumulative derived from collisional cascade simulations (e.g. Dohnanyi, 1969; Williams and Wetherill, 1994 and Tanaka et al., 1996). Schmedemann et al. (2014a) link this disagreement to increasingly higher mobility towards smaller projectile diameters, which are more influenced by radiation forces such as the YORP- and Yarkovsky effects.
MBA are expected to be much more stable against thermal influences of the inner Solar System than comets and thus they show the wavy size distribution of a collisionally evolved projectile population (e.g. Bottke et al., 2005a) and are much less influenced by thermal effects than comets.
Based on Dones et al. (2009) we calculate typical impact velocities (Eq. 7.1) for the three described groups of projectile populations and use the results in order to determine the projectile distributions from the measured crater SFD by application of scaling laws. We use the corrected version (Ivanov, 2008) of scaling laws by Ivanov (2001). In Eq. 7.1 $U_{mean}$ is the average impact velocity of the projectile, $v_{orb}$ is the orbital velocity of the target body, $v_\infty$ is the velocity of the projectile entering the Saturnian system and $v_{esc}$ is the escape velocity of the target body.

$$U_{mean} = (3{v_{orb}}^2 + {v_\infty}^2 + {v_{esc}}^2)^{1/2} \text{ (Dones et al., 2009)} \quad (7.1)$$

Table 7.2 lists the projectile velocities derived from Eq. 7.1 for various dynamical cases. We have two heliocentric cases where we took $v_\infty$=3 km/s from Dones et al. (2009) but also present a case with $v_\infty$=12.05 km/s, which should be the $v_\infty$ for bodies having their aphelion at 45 AU in the central Kuiper Belt. This value is derived from the squared difference of the solar escape velocity at the distances of Saturn ($v_{esc}$=13.6 km/s) and the Kuiper Belt ($v_{esc}$=6.3 km/s). We further calculated two planetocentric cases. The planetocentric - high eccentricity case would apply to the outer irregular Saturnian satellites but is very similar to the heliocentric case with $v_\infty$=3 km/s. Therefore, we are not going to discuss the planetocentric - high eccentricity case separately. The second planetocentric case is the low velocity endmember for planetocentric projectiles. In this case projectiles are nearly on the same orbit as the target body. This configuration is actually observed for lagrangeian satellites in the Saturnian system in the cases of Polydeuces and Helene in relation to Dione as well as Telesto and Calypso in relation to Tethys.

Table 7-2: Impact velocities: Mean projectile impact velocities on Mimas and Iapetus for various dynamic cases. $v_{esc}$ and $v_{orb}$ are taken from Bierhaus et al. (2012) and (Dones et al., 2009) respectively.

| Target | velocity at infinity [km/s] | orbital velocity [km/s] | escape velocity [km/s] | Mean impact velocity [km/s] | Dynamical Case |
|---|---|---|---|---|---|
| Mimas | 12.05 | 14.32 | 0.159 | 27.58 | Heliocentric (12 km/s approach velocity) |
| Iapetus | 12.05 | 3.27 | 0.572 | 13.33 | |
| Mimas | 3 | 14.32 | 0.159 | 24.98 | Heliocentric (3 km/s approach velocity) |
| Iapetus | 3 | 3.27 | 0.572 | 6.43 | |
| Mimas | 0 | 14.32 | 0.159 | 24.80 | Planetocentric – high eccentricity |
| Iapetus | 0 | 3.27 | 0.572 | 5.69 | |
| Mimas | 0 | 0 | 0.159 | 0.16 | Planetocentric – co-orbital |
| Iapetus | 0 | 0 | 0.572 | 0.57 | |

Table 7.3 summarizes the parameters we used to convert the observed crater sizes into projectile sizes by application of scaling laws (Eq. 7.2). Scaling laws convert projectile diameters into crater diameters and vice-versa. These calculations take into account impact velocities and various physical and material properties of the target and the impacting bodies.

$$\frac{D_t}{D_P\left(\frac{\delta}{\rho}\right)^{0.43}(v\sin\alpha)^{0.55}} = \frac{1.21}{[(D_{sg}+D_t)g]^{0.28}} \qquad (7.2)$$

Eq. (7.2): after Ivanov (2001); corrected by Ivanov and Hartmann (2007) and by Ivanov (2008) as his Eq. (8).

$g$ is the surface gravity, $D_P$ is the projectile diameter, v is the impact velocity, α is the impact angle, δ is the projectile density, ρ is the target density, $D_{sg}$ is the diameter of the strength to gravity transition and $Dt$ is the diameter of the transient crater. In an additional equation Ivanov (2001) calculates the relation between the diameter of the transient crater and the final crater diameter in the case of complex craters with diameters larger than the simple to complex transition diameter.
The used projectile densities of 0.6 g/cm³ and 2 g/cm³ are average estimates for comets and asteroids, respectively. The simple to complex and strength to gravity transitions cannot be converted by a simple 1/g approach (Pike, 1980) from basaltic bodies such as the Moon or the large asteroid Vesta, because of the different scaling in icy targets. For instance, this becomes clear if the simple to complex transition for Mimas is derived by a straightforward 1/g approach from the simple to complex transition on the Moon (15 km; Ivanov, 2001). The result would be ~380 km for the smallest complex crater on Mimas. As outlined above the largest crater on Mimas is the 135 km large Herschel crater, which clearly shows a central peak and thus is of complex character. Even the 64 km crater Arthur on Mimas shows a small central

peak. Presumably Arthur is only slightly above the transition size from simple to complex. We can use the simple to complex transition on Iapetus (15 km; Dones et al., 2009), the surface gravities of Iapetus and Mimas (0.223 m/s², 0.064 m/s²; Bierhaus et al., 2012) and the 1/g approach in order to calculate the simple to complex transition on Mimas. Scaling from one icy body to another should not be as problematic as scaling from basaltic to icy bodies. As expected the result of 53 km is slightly below the size of crater Arthur.

### 7.5.2 Derivation of strength to gravity values by a modified 1/g approach

Unfortunately the strength to gravity values are known neither for Iapetus nor Mimas. But we can use the values for Vesta (simple to complex transition ~70 km, surface gravity 0.25 m/s²; e.g. Schmedemann et al., 2014a) in order to calculate a modified surface gravity for Iapetus and Mimas, which incorporates the different scaling in the icy target material. We choose Vesta instead of the Moon because its size and surface gravity is closer to Iapetus and Mimas. Eq.(7.3) calculates the modified 1/g and Eq. (7.4) is used to calculate the strength to gravity transition on Mimas. Equations for Iapetus are analog. $g_{Vesta}$ is the vestan surface gravity, $g_{Mimas\_mod}$ is the modified surface gravity of Mimas, $SC_{Vesta}$ is the simple to complex transition on Vesta and $SC_{Mimas}$ is the simple to complex transition on Mimas.

$$\frac{1/g_{Vesta}}{SC_{Vesta}} = \frac{1/g_{Mimas\_mod}}{SC_{Mimas}} \tag{7.3}$$

Using the modified surface gravity of Mimas we can use the classic 1/g approach by Pike (1980) to convert the strength to gravity transition from Vesta (sgVesta=1.94 km; Schmedemann et al., 2014a) to Mimas ($sg_{Mimas}$) or Iapetus, respectively. The results are given in Table 7-3.

$$\frac{1/g_{Mimas\_mod}}{sg_{Mimas}} = \frac{1/g_{Vesta}}{sg_{Vesta}} \tag{7.4}$$

Table 7-3: Impact parameters: Used parameters for conversion of crater sizes into projectile sizes for the Moon, Mimas and Iapetus. If not indicated otherwise target densities, cometary projectile density, surface gravity and simple to complex transition were taken from Dones et al. (2009), Bierhaus et al. (2012) or were calculated (see text above). The impact angle is chosen for the most probable case of 45° (Gilbert, 1893).

| | **Mimas** | **Iapetus** | **Moon** |
|---|---|---|---|
| **target density [g/cm³]** | 0.9 | 0.9 | 1.8 (Vasavada et al., 2012) |
| **projectile density [g/cm³] Comets/Asteroids** | 0.6/2 | 0.6/2 | 2 |
| **impact velocity [km/s]** | Mean impact velocity | Mean impact velocity | 17.5 (Ivanov, 2008) |
| **impact angle [°]** | 45 | 45 | 45 |
| **surface gravity [m/s²]** | 0.0636 | 0.223 | 1.62 |
| **strength to gravity transition [km]** | 1.46 | 0.42 | 0.3 |
| **simple to complex transition [km]** | 52.6 | 15 | 15 (Ivanov, 2001) |

### 7.5.3 Comparison between scaled projectile and observed projectile distributions

Fig. 7-4 shows comparative R-plots of projectile sizes calculated from measured craters on Mimas, Iapetus and the Moon as well as observed projectile SFD of comets, KBO and MBA for the dynamical cases mentioned above (Table 7-2). The black open circles represent the measured crater SFD of Mimas (this work) and Iapetus (Schmedemann et al., 2007; Schmedemann et al., 2009 and Denk et al., 2010) for comparison. Individual measurements were vertically normalized in order to put measurements of younger units (usually smaller craters) to the same isochron of the old areas (predominantly large craters). Measurements are normalized based on measured crater frequencies in overlapping diameter bins. This procedure (see also Section 6) is described in e.g. Neukum and Wise (1976), König (1977), Neukum (1984) and Werner (2005). We applied a slight smoothing of the datasets to reduce noise. The low pass filter is a floating average across 3 neighboring crater size bins which preserves the general shape of the SFD. Both crater datasets show a distinct humpback feature around 15 km crater size, which is also observed by Kirchoff and Schenk (2010) not only on Mimas and Iapetus, but on other midsized Saturnian satellites as well. From the measured crater distributions we calculate the respective projectile sizes based on three predefined dynamical models (Table 7-2) and scaling laws utilizing impact properties as shown in Table 7-2 and 7-3. We compare this calculated projectile SFD with observed SFD of KBO, comets and MBA extended by the lunar projectile distribution.

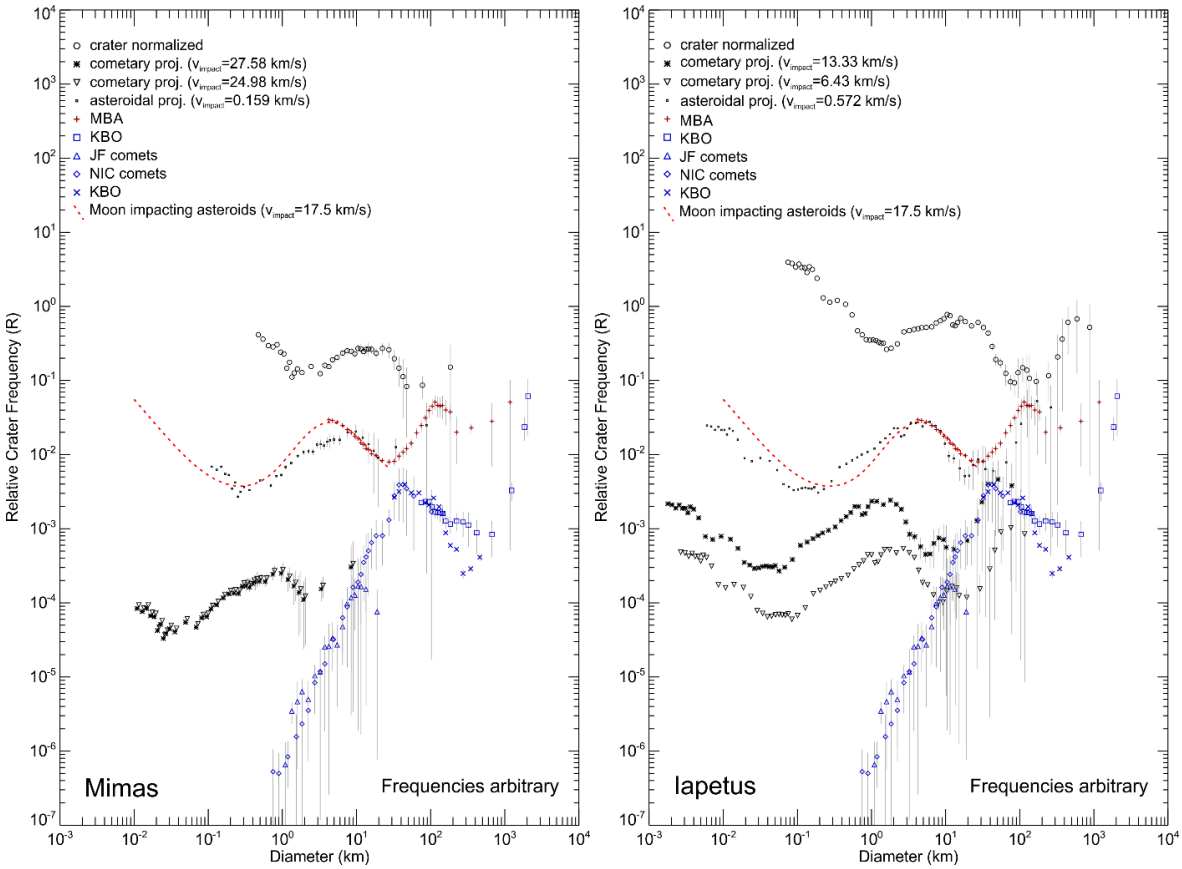


Fig. 7-4: Target-separated comparison of scaled and observed projectile diameters: All datasets are slightly smoothed by a floating average across 3 neighboring bins in order to reduce noise. Left panel ('Mimas'): crater and respective projectile sizes for Mimas. Right panel ('Iapetus'): crater and respective projectile sizes for Iapetus. Black open circles - R-Plots of measured crater SFDs, black dots, asterisks and inverted triangles - projectile SFDs for the three dynamic cases of Table 7-2 with densities of cometary projectiles of 0.6 g/cm³ for high eccentric or heliocentric impactors and densities of asteroidal projectiles of 2 g/cm³ for nearly co-orbital impactors. Red '+' signs - asteroid body SFD between 2.1 and 2.825 AU, red dashed line - lunar crater SFD scaled to projectile sizes and vertically aligned to the observed asteroid body SFD, open blue squares - Kuiper Belt Object (KBO) SFD based on JPL Solar-System Dynamics database (http://ssd.jpl.nasa.gov/sbdb_query.cgi), blue crosses - re-digitized Kuiper Belt Object (KBO) SFD by Fraser et al. (2008), open blue triangles and diamonds - cometary body SFD by Weiler et al. (2011) with "JF" indicating Jupiter family comets (blue triangles) and "NIC" nearly isotropic comets (blue diamonds). The vertical positions of all datasets are arbitrary for better visibility and comparability.

The following section about the interpretation of the data shown in Fig. 7-4 and Fig. 7-5 is speculative but points out some important dynamical characteristics of projectiles in the Saturnian system.

*Mimas:* On Mimas the derived projectile distribution for the case of cometary projectiles (highly eccentric planetocentric and heliocentric cases) decreases in R-value between 0.7 and 2 km nucleus size towards larger diameters in the presented R-plot of Fig. 7-4. This part is related to the humpback structure in the crater distribution on Mimas. Statistics for larger diameters is sparse and is not well suited for the purpose of comparison. Observed cometary nuclei in the same diameter range show an opposite behavior. They clearly show a relative monotonic increase towards larger sizes until about 40 km where they reach a local maximum.

If we compare the distribution of derived asteroidal projectiles on nearly co-orbital orbits with the observed Main Belt asteroid (MBA) SFD extended by the distribution of Moon impacting asteroids, we find reasonably good similarity in the statistically relevant diameter range of about 100 m to 20 km. This includes the humpback feature in both distributions. We observe a shift of the derived asteroidal projectile distribution towards larger diameters by a factor of ~2 with respect to the observed Main Belt distribution. Co-orbital projectiles on Mimas are calculated with Mimas' escape velocity as impact velocity. According to Bierhaus et al. (2012) the value of only about 160 m/s may be too low in order to form craters on Mimas. Therefore, co-orbital projectiles may not form craters on Mimas. Only projectiles on higher eccentric orbits and thus higher impact velocities might be able to form craters on Mimas. At higher impact velocities the respective impact craters would be larger and thus the derived projectile sizes are smaller, in better agreement with the observed Main Belt body SFD extended by the lunar projectile distribution.

*Iapetus:* Because of its larger size Iapetus also holds larger craters and thus the theoretical projectile distributions give statistically relevant information over a broader size range. The derived SFD of cometary projectiles on heliocentric orbits ($v_{impact}$=13.33 km/s) is in reasonably good agreement with the observed SFD of KBO and NIC in the size range of approximately 15 to 80 km. Also highly eccentric cometary projectiles ($v_{impact}$=6.43 km/s) would be somewhat in agreement with the observed SFD of KBO and NIC but not as good as for the heliocentric case. However, below ~15 km projectile size the observed cometary SFD (JF and NIC) divert significantly from the two cases of the derived projectile distributions for cometary projectiles impacting Iapetus. The cometary SFD shows no sign of a humpback feature in the range from 0.7 to 15 km nucleus size. For the crater derived cometary projectiles impacting Iapetus a significant part of the humpback feature is expected in the range of about 0.7 to 10 km diameter with a slight diameter shift depending on the dynamical case (heliocentric orbit or highly eccentric planetocentric orbit).

As for Mimas, for Iapetus we also find a much better agreement between the crater derived asteroidal projectile SFD and the observed MBA SFD extended by the SFD of Moon impacting asteroids. For Iapetus both distributions show generally similar characteristics between ~10 m and 200 km projectile size. In a detailed view there are some differences such as a misfit of the minimum around 100 m by a factor of ~3 or the minimum at ~30 km. At the 30 km minimum the derived projectile distribution on Iapetus shows a minor peak within a larger minimum that is not observed in the asteroid Main Belt SFD. This feature could be the result of a mixed projectile population, which is dominated by an asteroid-like population for smaller diameters (< ~30 km) and for larger diameters (> ~30 km) is dominated by cometary projectiles. As pointed out above, in this size range there is good agreement with NIC. Lower frequencies of cometary projectiles towards smaller sizes may result in a relative predominance of asteroid-like projectiles in the Saturnian system even though their absolute number is very low. On the other hand it could also be the result of the same kind of projectile but under two dynamical setups, which would result in a bimodal velocity distribution. An example for this situation could be the

case if Iapetus is impacted by co-orbital and highly eccentric projectiles such as irregular satellites at the same time.
If we assume that Mimas and Iapetus are impacted by the same projectile population, we would expect that for one dynamical model the derived projectile distributions for both target bodies are almost identical. This analysis is done in Fig. 7-5.

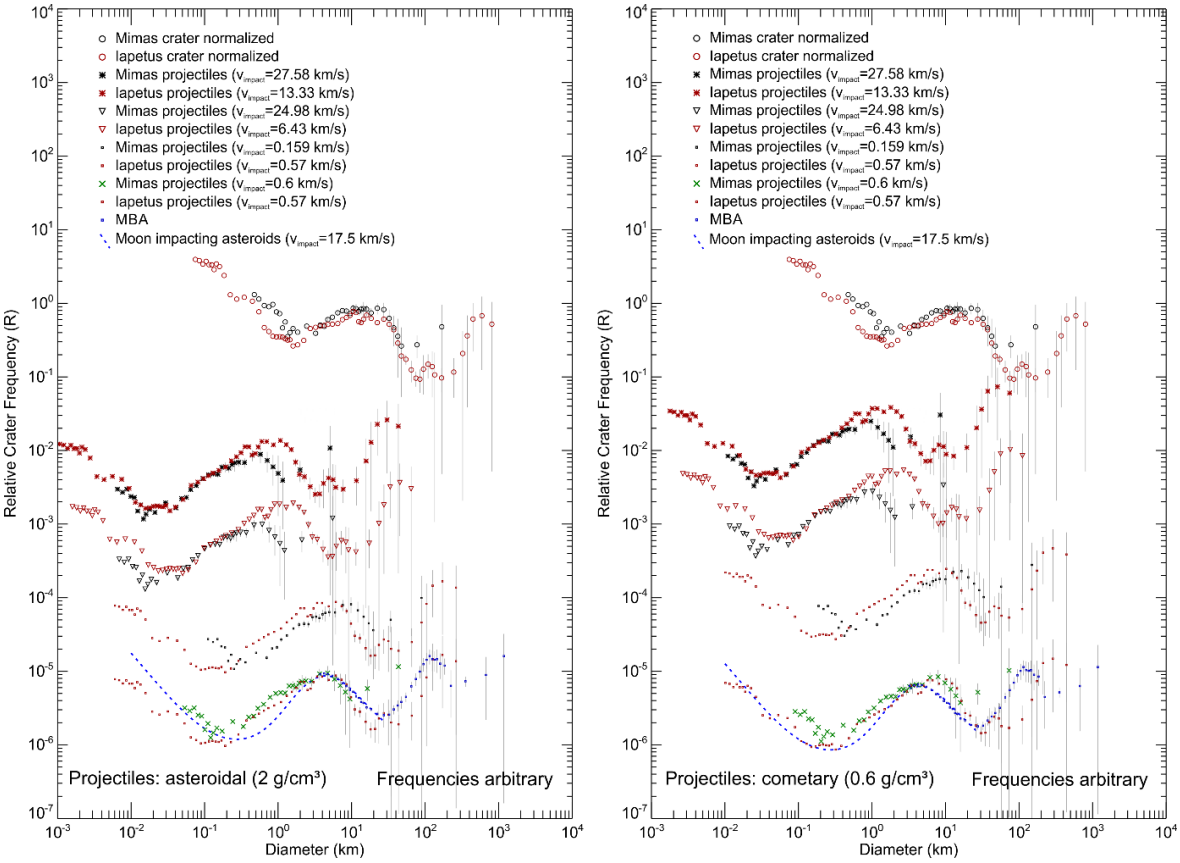


Fig. 7-5: Density-separated comparison of calculated and observed projectile diameters: All datasets are slightly smoothed by a floating average across 3 neighboring bins in order to reduce noise. Frequencies are arbitrary. Crater and projectile distributions are spacially grouped together for their respective dynamical case which is underscored by symbols. Open circles - R-Plots of measured crater SFDs, dots, asterisks and inverted triangles - projectile SFDs for the three dynamic cases of Table 7-2. In the lowest group Iapetus' and Mimas' projectiles, both at similar impact velocities of ~0.6 km/s, are compared with the SFD of MBA (2.1-2.825 AU) extended by the distribution of Moon impacting asteroids (blue dashed line and blue dots). Regardless of the projectile density the dynamical setup of the lowest group gives the best correlation between projectiles impacting Mimas and Iapetus. This solution also shows significant similarity to the projectile distribution impacting the Earth's Moon.

In Fig. 7-5 both plots show the measured crater distribution of Mimas and Iapetus grouped together. For the derived projectile distributions only minor differences are observable between the two panels, each panel shows one density case in order to discriminate between cometary (density=0.6 g/cm³) and asteroid-like (density=2 g/cm³) projectiles. The measured crater SFD are very similar to each other and are not showing a diameter shift of the distinctive humpback feature against each other as would be expected for a heliocentric main impactor source due to the focusing effect of Saturn. As a result, dynamical cases for heliocentric or high eccentricity

planetocentric projectiles do not compare as well as the crater distributions. However, it appears that there is a high agreement in the two projectile distributions of Mimas and Iapetus in the heliocentric case at small diameters around the minimum at 20 or 40 m depending on the projectile density. Even if we are dealing with more than one projectile source, it is not clear why predominantly smaller projectiles should impact from heliocentric orbits while large projectiles may have their source inside the Saturnian system. Large projectiles appear to impact at significantly lower velocities as indicated by higher similarity (humpback feature) for the co-orbital case (lowest impact velocities).

The case for very slow impacting co-orbital projectiles, still shows some disagreement between calculated projectile distributions of Mimas and Iapetus. Here we see an offset of about a factor of 2 in diameter direction between the two distributions. As mentioned above, projectiles impacting Mimas at its very low escape velocity may not form craters at all. Thus, it may be possible that only faster projectiles are recorded in the cratering record of Mimas.

The lowermost group in Fig. 7-5 is representing the co-orbital case for Iapetus' projectiles ($v_{impact}$=570 m/s) while Mimas' projectiles impact with 600 m/s, which is well above its escape velocity. Hence in both cases impact velocities are very similar which results in a similar projectile distribution too. For comparison we also show the MBA SFD between 2.1 and 2.825 AU extended by the size distribution of lunar projectiles. Here the comparison of projectiles with higher or lower density with the MBA SFD reveals small but interesting differences.

With projectile densities of 2 g/cm³ (i.e. asteroids) and the MBA SFD maximum in the humpback feature vertically normalized to the respective feature in the calculated projectile distributions, there is good agreement with Mimas' projectiles for the smallest shown sizes around the minimum in relative frequencies at ~200 m diameter. For the same sizes the fit of Iapetus' projectiles is worse because it falls below the MBA SFD. The opposite is true for the case with lower density projectiles (0.6 g/cm³) resembling cometary densities.

The distribution minimum around 20 km diameter is not well covered by Mimas' projectile sizes. However, in the higher density case the minor peak in Iapetus' projectile distribution falls together with the minimum in the MBA distribution. In the lower density case this minimum in Iapetus' SFD is shifted towards larger diameters such that its left part coincides with the absolute minimum of the MBA. For diameters larger than the local peak in Iapetus' projectile distribution there is not a really good agreement with the MBA. As outlined before in this section heliocentric comets may be the dominant projectile source.

Both density cases show an excess of projectile frequencies with respect to the MBA SFD in the range between the small diameter minimum and the humpback maximum. We speculate that this excess in projectiles could be the trace of sesquinary projectiles. Schmedemann et al. (2014b) found indications for sesquinary craters on Tethys below ~5 km diameter roughly consistent with the size range of increased crater frequencies at Mimas and Iapetus. For the diameter range between the humpback maximum and the large diameter minimum it depends on the density case whether there is excess (0.6 g/cm³) or paucity (2 g/cm³) of projectiles.

From this analysis we summarize for projectiles in the Saturnian system:

On Iapetus craters > ~100 km may be formed by heliocentric projectiles with low density and cometary-like size-frequency distribution. Because of monotonic decreasing relative frequencies of comets towards smaller diameters, craters < ~100 km on Mimas and Iapetus are formed predominantly by an asteroid-like projectile population, which SFD is characterized by a collisional evolution. Even if asteroid-like objects enter the Saturnian system in extremely low numbers, they still might outnumber small comets.

Per previous point small projectiles are predominantly asteroid-like projectiles implying densities of ~2 g/cm³. Assuming correct scaling also low projectile densities of 0.6 g/cm³ appear to be able to explain the observed data. If such low densities can be attributed to KBO it may imply that these objects indeed show a collisional evolution similar to the MBA. This would also imply a much more massive KBO population than is observed today. This is based on the fact that collisional frequencies between observed KBO are about four orders of magnitudes lower than between asteroids inside the asteroid Main Belt, according to calculated collision frequencies following Bottke et al. (1994). Asteroidal densities of ~2 g/cm³ would be in agreement with Mimas' co-orbital projectiles but there is less agreement to those of Iapetus. However, having different projectile densities at Iapetus and Mimas would require a more complex projectile model that explains increasing projectile densities going from the outer satellites towards the inner ones. This could be achieved e.g. by tidal disruption of projectiles. It may be possible, that good consistency for the low projectile density of 0.6 g/cm³ is rooted in wrong crater scaling at icy targets and in reality projectiles are of higher density.

Between the small diameter minimum and the humpback maximum both Mimas and Iapetus show an excess of crater frequencies. Schmedemann et al. (2014b) found indication of sesquinary cratering on Tethys in a similar size range. Thus, it may be possible that the observed slight excess of crater frequencies on Mimas and Iapetus could be caused by sesquinary cratering as well.

The SFD of KBO in the diameter range of the humpback feature and at smaller diameters is unknown today. Thus, we cannot discriminate between the populations of MBA and KBO yet. Based on the approach of Levison and Duncan (1997) it might be thinkable that projectiles of both populations rendezvous slowly with the Saturnian system and smoothly drift into the system at the Lagrange points of that system supported by complex changes in the gravimetric field due to interaction of the Sun, the large planets as well as the Saturnian satellites. Long term orbital evolution may place the captured objects into low eccentric orbits about Saturn. As a retrograde satellite Phoebe is most likely a captured object. Its eccentricity is moderate with ~0.16. Its density (~1.6 g/cm³) is more similar to asteroids than it is similar to comets. On the other hand there are a couple of low density objects on circular orbits as well such as the heavily battered Hyperion. Much less battered Calypso, Helene and Telesto are low density co-orbital objects of the midsized satellites Tethys and Dione. Densities of Hyperion and the co-orbital satellites are comparable to those of comets (Thomas, 2010) while the midsized satellites are at least twice as dense (~1 g/cm; Thomas, 2010). The co-orbital satellites are probably not of cometary origin or underwent significant resurfacing because of their high albedo.

Because of the given uncertainties and the high similarity of the observed crater distribution on the Saturnian satellites with the MBA SFD extended by lunar projectiles we follow Neukum (1985) and Neukum et al. (2006) and assume MBA as main projectile source for craters < ~100 km in the Saturnian system for the remainder of this paper. Based on that assumption we also assume a lunar-like time dependent behavior of the projectile flux at the Saturnian satellites.

### 7.5.4 Apex-/Antapex asymmetry not observed

In literature it is well known that Saturnian satellites do not show a pronounced apex-/antapex asymmetry (Neukum, 1985; e.g. Zahnle et al., 2001; Zahnle et al., 2003 and Dones et al., 2009). One explanation often expressed is a saturated cratering record that could obscure an apex-/antapex asymmetry. It is somewhat unlikely that large craters of tens of km in diameter are in saturation given the overall low impact frequency in the Saturnian system. For instance, if the surface of Iapetus had been saturated by large craters and even basins, its equatorial ridge would have been completely obliterated and not just partially as is observed. Another favored explanation is the hypothesis that a fluid subsurface layer allows the surface to rotate around the otherwise tidally locked satellite. This explanation may be reasonable for bodies such as Titan or Enceladus where strong evidence for subsurface liquids has been found. But the color dichotomy on Iapetus and its shape of an ellipsoid of a fast rotating (16 h; Castillo-Rogez et al., 2007) body are at odds with a drifting surface of the satellite. Its shape implies that Iapetus has probably been completely frozen since ~4.4 Ga (Castillo-Rogez et al., 2007). Its color dichotomy needs at least 1 Ga in order to develop (Spencer and Denk, 2010) and under permanent surface drift the dichotomy should have been smeared out just as the apex-/antapex crater frequencies would have been. Such a smeared-out color dichotomy is not observed. Following an attempt by Horedt and Neukum (1984), Zahnle et al. (2001) and Morota et al. (2008), Schmedemann et al. (2014c) give in their Eq. (6) a theoretical estimation of the apex-/antapex ratio. That approach gives for Iapetus an apex-/antapex asymmetry on the order of a factor of ~3.6 and for Mimas a factor of ~34 would be expected for their current orbit about Saturn for heliocentric projectiles (Table 7-2). As discussed previously, the cratering record of Iapetus may suggest that craters only larger than ~100 km diameter are dominated by cometary impacts from heliocentric orbits. Given the high similarity between the cratering records of Mimas and Iapetus, that would imply that only Herschel is probably large enough to fall into the size range where comets may play some role. Although Herschel is almost centered on Mimas' leading side, Mimas does not provide the required cratering statistics in order to prove or disprove an apex-/antapex asymmetry for crater sizes > ~100 km. The observed random distribution of Iapetus' basins would argue against a cometary source of even the largest impact structures.

## 7.6 Crater chronology functions and crater production functions for Mimas and Iapetus

The main impactor source in the Saturnian system is not well understood as outlined before. The chronology model of Zahnle et al. (2003) assumes ecliptic comets on heliocentric orbits as the dominant class of projectiles for craters > ~20 km, although the authors admit this assumption is inconsistent with the unobserved apex/-antapex asymmetry. Assuming a nearly constant impact rate their model applies best to younger ages (e.g. Kirchoff and Schenk, 2010). For the highest crater frequencies found for instance on Iapetus the Zahnle et al. (2003) chronology model results in surface ages equal to the age of the solar system which is in disagreement with geophysical based estimates of highest surface ages by Castillo-Rogez et al. (2007). As an alternative we suggest a lunar-like chronology which is adopted from Neukum et al. (2006). Neukum et al. use highest crater frequencies on Iapetus in order to calibrate their lunar-like chronology. Based on Castillo-Rogez et al. (2007) Iapetus' highest crater frequencies are set to 4.4 Ga. Since Neukum et al. (2006) did not base their crater production function on some kind of scaling law and did not publish the coefficients they used for their chronology and production function we will present scaling parameters and coefficients here.

### 7.6.1 Crater production function

Our analysis in Section 5 suggested that the cratering record on Iapetus and Mimas for diameters < ~100 km appears to be caused by a collisionally evolved projectile population similar to the asteroid Main Belt and lunar projectiles. Thus, to zeroth order we assume a lunar-like crater distribution for Iapetus and Mimas as well. Due to good resemblance of observed crater size-frequency distribution and consistency of projectile characteristics, we assume that the primary impact source for Mimas and Iapetus delivers projectiles with a density of 0.6 g/cm³ at an average impact velocity of ~600 m/s. For Iapetus we actually use its slightly lower escape velocity of about 570 m/s (Bierhaus et al., 2012). However, we do not understand the related dynamical processes which may have brought the projectiles into such low eccentricity planetocentric orbits about Saturn. Table 7-4 gives an overview on the scaling parameters we use for scaling the lunar crater production function to Iapetus and Mimas. The values characterizing the projectile density and impact velocity are derived from our analysis in Section 5 the remaining parameters were already given in table 7-3.

Table 7-4: Scaling parameters: Used parameters for conversion of the lunar crater production function to the impact conditions on Iapetus and Mimas. Values in the table are mostly equal to table 7-3. Where values differ we used best estimates based on results in Section 5.

| | Mimas | Iapetus | Moon |
|---|---|---|---|
| **target density [g/cm³]** | 0.9 | 0.9 | 1.8 (Vasavada et al., 2012) |
| **projectile density [g/cm³]** | 0.6 | 0.6 | 2 |
| **impact velocity [km/s]** | 0.6 | 0.57 | 17.5 (Ivanov, 2008) |
| **impact angle [°]** | 45 | 45 | 45 |
| **surface gravity [m/s²]** | 0.0636 | 0.223 | 1.62 |
| **strength to gravity transition [km]** | 1.46 | 0.42 | 0.3 |
| **simple to complex transition [km]** | 52.6 | 15 | 15 (Ivanov, 2001) |

Eq. (7.5) gives the polynomial of 11th degree for crater production functions (Neukum, 1984; Neukum and Ivanov, 1994 and Neukum et al., 2001). In this equation, $N_{cum}$ is the cumulative crater frequency for craters equal or larger than the crater diameter $D$ and $a_x$ are the coefficients of the individual terms.

$$\log N_{cum} = a_0 + a_1 \log(D) + a_2 (\log(D))^2 + \cdots + a_{11} (\log(D))^{11} \quad (7.5)$$

Table 7-5 provides the respective values for the used coefficients for the Moon, the crater production function of which has been used as a reference, for Iapetus and Mimas.
The used scaling parameters lead to crater production functions which closely resemble the measured crater size-frequency distribution in areas that are presumably undisturbed by geologic processes. Fig. 7-6 presents the derived crater production functions of Mimas, Iapetus and the lunar reference function.

Table 7-5: Coefficients of Mimas' and Iapetus' production functions: The coefficients were derived from impact scaling parameters used in Section 5. Projectile densities and impact velocities are assumed based on results from Section 7-5.

| | Moon (Neukum, 1984) | Mimas | Iapetus |
|---|---|---|---|
| $a_0$ | −2.5339 | -4.067 | -4.2777 |
| $a_1$ | −3.6269 | -2.4279 | -2.3623 |
| $a_2$ | 0.43662 | 0.9078 | 1.3293 |
| $a_3$ | 0.79347 | 0.38702 | 0.16438 |
| $a_4$ | 0.086468 | -0.079932 | -0.94324 |
| $a_5$ | −0.26485 | -0.42628 | -0.31414 |
| $a_6$ | −0.066382 | -0.27682 | 0.38191 |
| $a_7$ | 0.037923 | 0.16441 | 0.097819 |
| $a_8$ | 0.010596 | 0.12387 | -0.09531 |
| $a_9$ | −0.0022496 | -0.038037 | -0.00096443 |
| $a_{10}$ | −0.00051797 | -0.016073 | 0.011245 |
| $a_{11}$ | 0.0000397 | 0.0046267 | -0.0022748 |

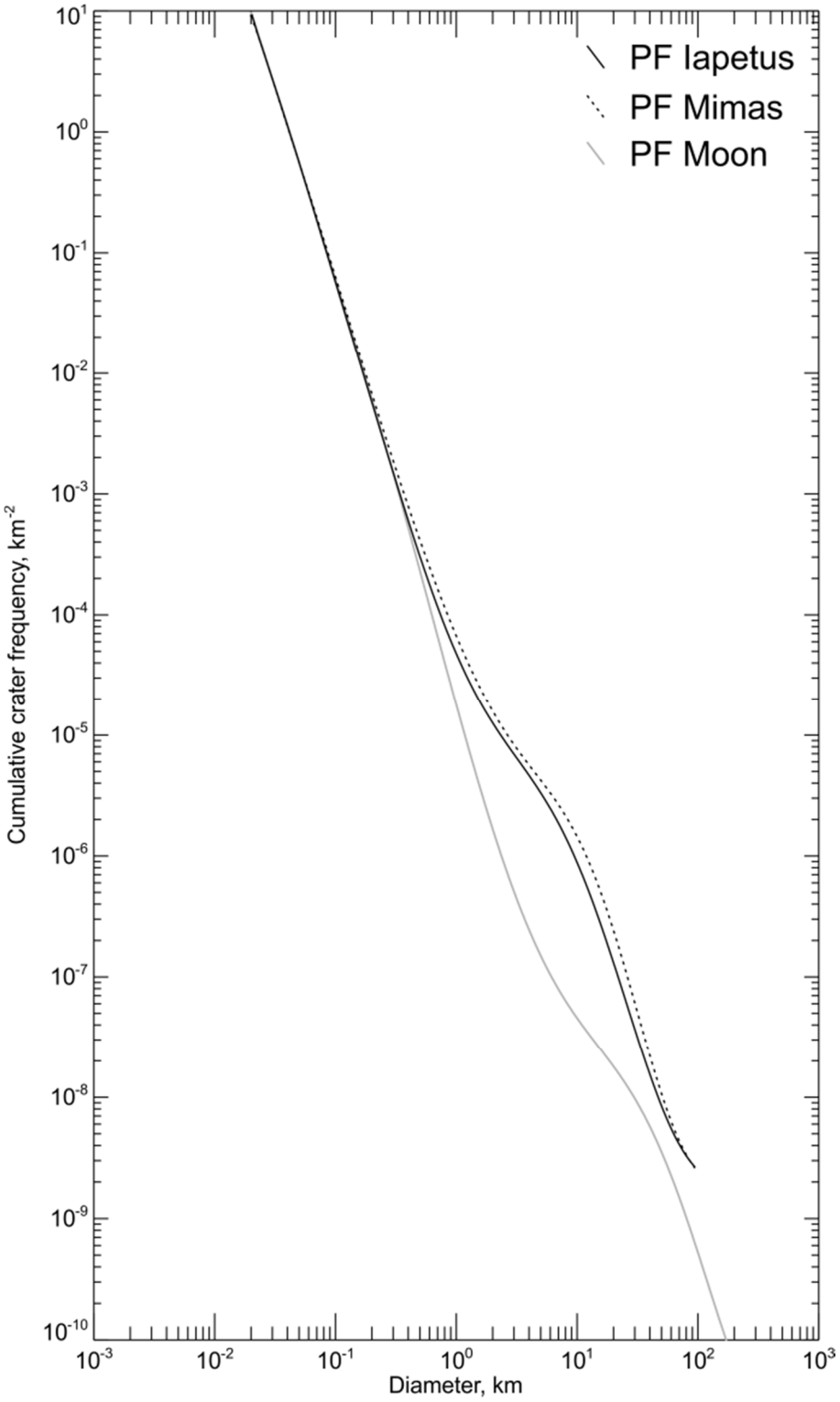


Fig. 7-6: Iapetus', Mimas' and lunar crater production functions: All production functions (PF) are normalized in cumulative crater frequency at 30 m crater diameter and therefore they do not represent the same model ages. The curves for Mimas and Iapetus are truncated at 100 km because it may be possible that larger craters and basins could predominantly be formed by cometary projectiles with likely different flux characteristic. Lunar production function – gray curve, Iapetus production function – black solid curve and Mimas production function – black dashed curve.

### 7.6.2 Crater chronology functions

As mentioned above Neukum et al. (2006) used the maximum surface age of Iapetus estimated by Castillo-Rogez et al. (2007) in order to calibrate a lunar-like chronology for Iapetus. Due to slight differences in crater scaling the crater production functions of Mimas and Iapetus differ from each other slightly. Hence, the projectile flux at 1 km crater diameter also differs and thus the chronology functions are not identical. Fig. 7-7 illustrates the calibration of the lunar-like crater chronology function for Iapetus.

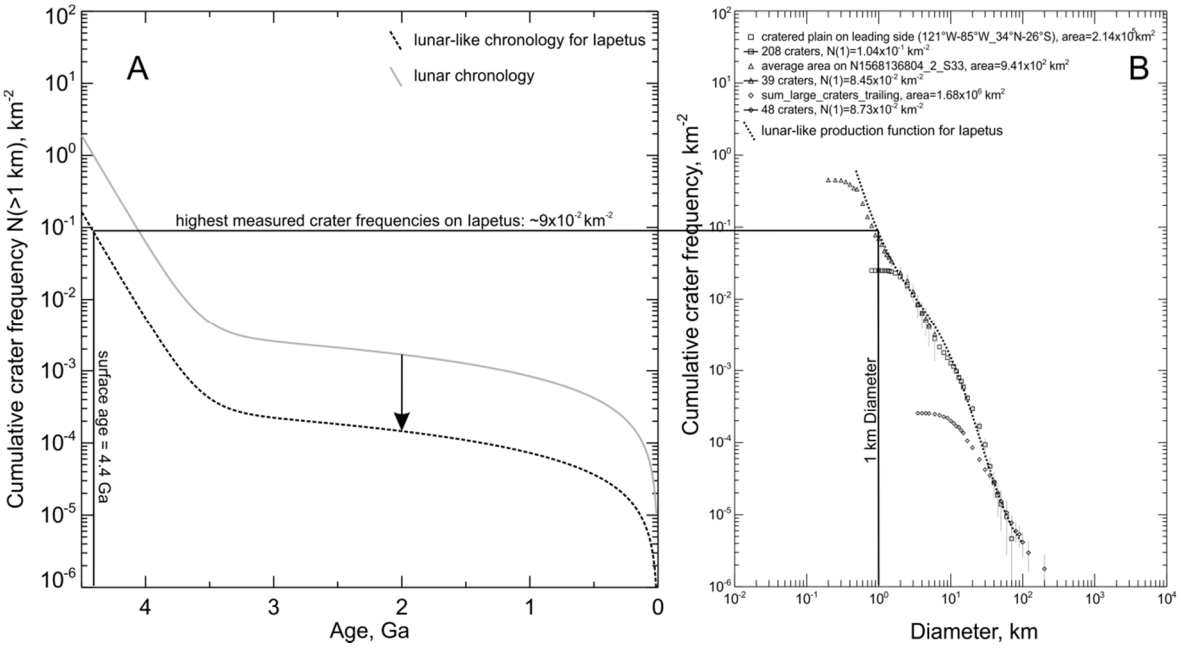


Fig. 7-7: Iapetus chronology calibration: (A) Crater chronology for the Moon (grey curve) and Iapetus (black dashed curve). (B) Measured crater frequencies for three different areas on Iapetus with fitted crater production function for Iapetus. Diagrams in (A) and (B) are equally scaled in vertical axis. In (B) the cumulative crater frequency of the fitted Iapetus production function at 1 km crater diameter gives a value of ~9x10-2km-2 for the highest crater frequencies that can be measured on Iapetus. Castillo-Rogez et al. (2007) estimate the oldest surface of Iapetus to be ~4.4 Ga. In (A) the lunar chronology is vertically shifted downward until it equals the measured crater frequency at a model age of 4.4 Ga.

Derived crater frequencies for the three individual measurements shown in panel (B) of Fig. 7-7 can be averaged. The result of about $9x10^{-2}$ $km^{-2}$ corresponds to the highest crater frequencies that can be measured on Iapetus. Castillo-Rogez et al. (2007) estimate the oldest surface of Iapetus to be about 4.4 Ga old. The cumulative lunar crater frequency at 1 km diameter for 4.4 Ga equals 0.95 $km^{-2}$. Thus, the lunar chronology curve needs to be shifted to lower frequencies by a factor of 10.5. This is accomplished by scaling the k1 and k3 term in the equation of the lunar chronology by the derived factor. Eq. (7.6) defines the lunar-like chronology function following e.g. Neukum (1984), Neukum and Ivanov (1994), Neukum et al. (2001) and Marchi et al. (2009). In this equation $N_{cum}$ is the cumulative crater frequency for craters ≥1 km, $k_{1-3}$ are the used coefficients and t is the surface age in Ga.

$$N_{cum}(D \geq 1\ km) = k_1\left(e^{k_2 t} - 1\right) + k_3 t \qquad (7.6)$$

$k_3$ resembles the linear term in Eq. (7.6), which is equivalent to the current rate of collisions. In Table 7-6 we present the values for the lunar curve as well as those for Iapetus and Mimas.
In order to derive a chronology curve for Mimas we have to analyze the different crater scaling on Iapetus and Mimas. All chronology curves are valid for cumulative crater frequencies at 1 km diameter. Based on our scaling parameters in Table 7-4 on Iapetus a 1 km crater is formed by a 182 m projectile. On Mimas the same crater diameter is formed by a 145 m projectile. On Mimas a 182 m projectile is forming a crater of 1.22 km diameter. From the Mimas production function we find that on Mimas 1 km craters are about 1.6 times more frequent than 1.22 km craters. Hence, for Mimas we have to scale the k1 and k3 values of the lunar-like chronology of Iapetus with the factor 1.6.

Table 7-6: Coefficients for Eq. (7.6) for calculation of cumulative crater frequencies at 1 km crater diameter at a given exposure time for the Moon, Iapetus and Mimas.

| | ***k*1** | ***k*2** | ***k*3** |
|---|---|---|---|
| Moon (Neukum, 1984) | $5.44\times10^{-14}$ | 6.93 | $8.38\times10^{-4}$ |
| Iapetus | $5.181\times10^{-15}$ | 6.93 | $7.981\times10^{-5}$ |
| Mimas | $8.238\times10^{-15}$ | 6.93 | $1.269\times10^{-4}$ |

## 7.7 Surface ages of measured units on Mimas

Fig. 7-8 panel A displays cumulative plots of the merged measurement A235 (filled circles) and its vertically normalized version (open circles) together with the measurements on the heavily cratered plains (A6 - A9). All measurements are given in their differential representation in panel B. Each measurement shows a so-called roll-over at the 3 or 4 smallest crater bins. This is caused by systematic undercounting of craters due to multiple reasons such as issues at resolution or illumination or even human related issues that lead to detection of some but not all such small craters. Except for measurement A7 all measurements show good agreement with the derived (Section 6) crater production function. The measurement A235 shows an offset of a factor of about 6 towards lower crater frequencies with respect to the areas A6 – A9. That suggests a younger surface age of the areas resurfaced by the Herschel impact. These measurements are therefore in agreement with the relative stratigraphic position of Herschel above (or younger than) the heavily cratered plains. Measurement A235 is vertically normalized in order to overlap as well as possible with measurements A6, A7 and A8. The shifted version of A235 is designated as 'A235 (normalized)'. The measurements A235 (normalized) as well as A6 through A9 (lower part of A7) are in good agreement with the 4.3 Ga isochron which is based on the lunar-like crater production function for Mimas.
In the cumulative plot we also fit the individual measurements with the previously derived Mimas production function and calculate a model age based on the lunar-

like chronology function for Mimas. Both functions are explained in Section 7.6. The quoted errors quantify only the statistical error, not that of the model. We also show the Case A and B crater production function for Mimas re-digitized from Zahnle et al. (2003; Fig. 5). The Case B function appears to be in agreement with craters < ~2 km but diverts significantly of up to a factor of 5 for larger craters. The Case A function is in agreement in a diameter range of ~2 to ~10 km. This function is too shallow for smaller and larger crater sizes. Because of these strong inconsistencies between observed crater distribution and Zahnle production functions we used our lunar-like production function in order to derive crater frequencies at 10 km diameter (needed for Zahnle chronologies) from those obtained at 1 km diameter by the craterstats software (Michael and Neukum, 2010; Michael, 2013).

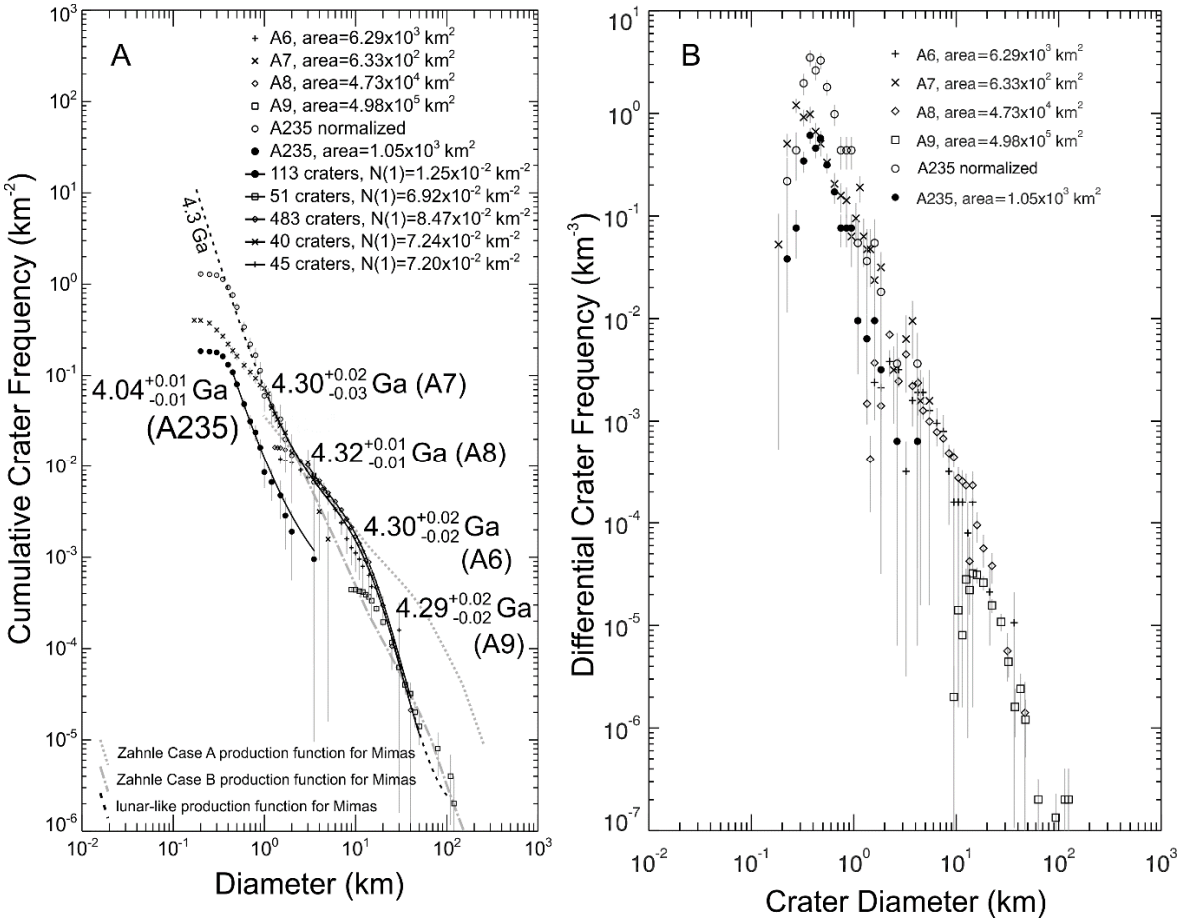


Fig. 7-8: Measurements and Crater SFD: (A) Merged data of areas A2, A3 and A5 (A235; filled circles) plot below the heavily cratered plains (A6 - A9) by a factor of about 6. Open circles represent the vertically normalized measurement "A235 (normalized)". The dashed curve represents the lunar-like crater production function as isochron for an exposure age of 4.3 Ga. Black solid lines indicate the fit ranges used in order to derive surface ages for the individual measurements. The gray dotted and dash-dot curve show the Zahnle Case A and B production functions for Mimas (Zahnle et al., 2003; Fig. 5) aligned to measurements of the heavily cratered plains. (B) Differential plot of the same data with same symbology which is presented in panel (A).

Except for A235 and the upper part of A7 all measurements plot very close to the 4.3 Ga isochron (lunar-like chronology). That indicates that large fractions of Mimas' surface show similar ages over a relatively broad range of crater diameters. Significant ejecta blankets are rarely developed by impact cratering on Mimas.

Because of the very low escape velocity, presumably existing ejecta blankets are widely dispersed over Mimas' surface similar to those on asteroids (e.g. Cintala et al., 1978).
Herschel for instance does show an ejecta blanket with lower crater frequency than the heavily cratered plains. Area A7 is located about one Herschel diameter south west of Herschel and thus it is placed at the outer margin of the classical continuous ejecta blanket (e.g. Melosh, 1989). In fact, measurement A7 shows a resurfacing feature with large craters > ~1 km as frequent as they are on the heavily cratered plains but craters < ~0.5 km are less abundant. This could indicate the destruction of the small craters by Herschel ejecta (Michael, 2013). Given a general depth to diameter ratio of ~0.2 as is also observed on other Solar system bodies (e.g. Vincent et al., 2014) we estimate roughly 200 m of Herschel ejecta in the location of area A7. A detailed plot of measurement A7 in Fig. 7-9 even indicates a model age very close to the model age we find for Herschel from measurement A235 for small craters which are not yet affected by the roll-over.

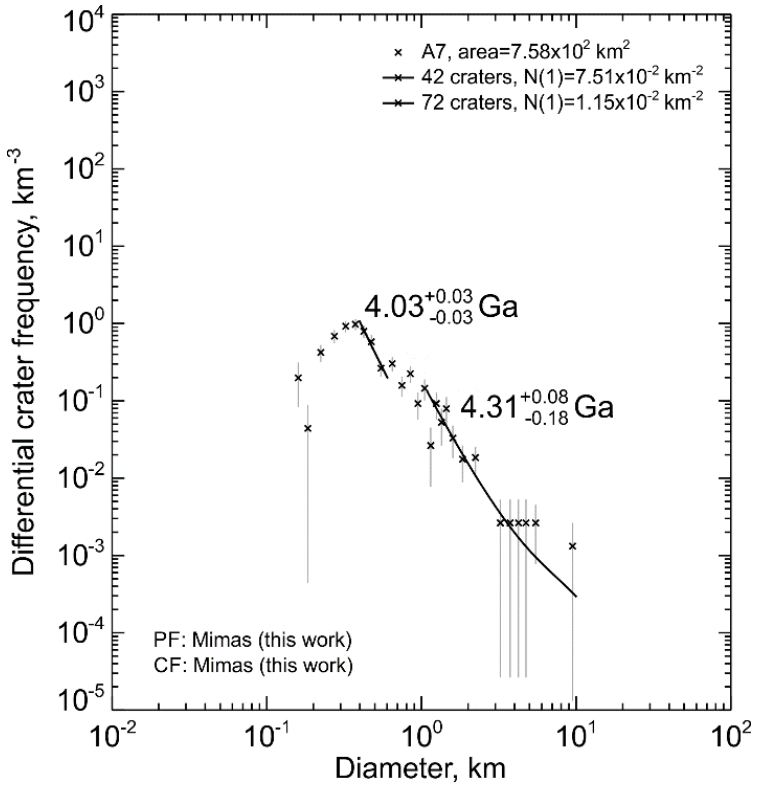


Fig. 7-9: Differential plot and fit of measurement A7: Craters ≤ 500 m show lower crater frequencies than craters > ~1 km. The frequencies of the large craters are consistent with the heavily cratered plains. Small crater frequencies are very similar to those measured at Herschel resurfaced areas. Thus, it appears reasonable to assume that the observed kink in measurement A7 is caused by resurfacing due to Herschel ejecta blanketing.

Table 7-7 gives a summary on the five presented measurements. It shows lunar-like as well as Zahnle model ages for the cases A and B which are described by Zahnle et al. (2003). Zahnle models are calibrated for 10 km crater diameter. We determine crater frequencies at 10 km diameter from the measured frequency at 1 km diameter based on the derived lunar-like crater production function for Mimas. That function indicates 48 times more 1 km craters than 10 km craters on Mimas' surface. We did

not use Zahnle production functions in order to do this conversion because both production functions by Zahnle appear to be relatively inconsistent with the measured data in contrast to our lunar-like solution.

Table 7-7: Lunar-like and Zahnle model ages for measurements A235, A6, A7, A8 and A9 with respective statistical errors. Measured crater frequencies are related to 1 km crater size (N1) and were derived by fitting the lunar-like crater production function for Mimas to the individual measurements (Fig. 7-8; panel (A)). For Zahnle ages crater frequencies are converted to 10 km diameter for which the respective chronologies are calibrated.

| source | Area [km²] | lunar-like Age [Ga] | lunar-like Age '+' Error | lunar-like Age '-' Error | Zahnle Case A Age [Ga] | Zahnle Case A Age '+' Error | Zahnle Case A Age '-' Error | Zahnle Case B Age [Ga] | Zahnle Case B Age '+' Error | Zahnle Case B Age '-' Error | N1 fit | N1 fit Error |
|---|---|---|---|---|---|---|---|---|---|---|---|---|
| A235 | 1049 | 4.04 | 0.013 | 0.015 | 2.01 | 0.13 | -0.14 | 0.29 | 0.03 | -0.03 | 0.0125 | 0.0012 |
| A6 | 6286 | 4.3 | 0.02 | 0.023 | 4.41 | 0.06 | -0.10 | 1.43 | 0.17 | -0.18 | 0.0720 | 0.0105 |
| A7 base | 758 | 4.31 | 0.021 | 0.024 | 4.44 | 0.05 | -0.09 | 1.52 | 0.18 | -0.20 | 0.0776 | 0.0119 |
| A7 resurf | 758 | 4.03 | 0.011 | 0.011 | 1.85 | 0.10 | -0.11 | 0.26 | 0.02 | -0.02 | 0.0112 | 0.0008 |
| A8 | 47300 | 4.32 | 0.0064 | 0.0067 | 4.48 | 0.01 | -0.02 | 1.63 | 0.06 | -0.06 | 0.0847 | 0.0038 |
| A9 | 322500 | 4.29 | 0.015 | 0.017 | 4.37 | 0.06 | -0.08 | 1.35 | 0.12 | -0.13 | 0.0672 | 0.0073 |

For the lowest crater frequencies indicative for the formation age of the Herschel crater model ages differ significantly. The lunar-like model gives about 4 Ga, Zahnle Case A gives roughly 2 Ga and Zahnle Case B points to a relatively recent formation of Herschel only about 300 Ma ago. The situation for measurements of the heavily cratered plains is slightly different. Here the highest model ages are determined from the Zahnle Case A model with about 4.4 Ga, only slightly younger is the result based on our lunar-like chronology with about 4.3 Ga. The Zahnle Case B model again gives clearly the youngest estimate with about 1.5 Ga model age. Thus, the absolute differences in model ages of Herschel with respect to the heavily cratered plains vary between 300 Ma (lunar-like model) and 2.4 Ga (Zahnle Case A model). Fig. 7-10 presents the used chronology models and measured crater frequencies. At points where the horizontal lines of the measured crater frequencies intercept the chronology functions, the x-axis values give the model ages for the respective combination.

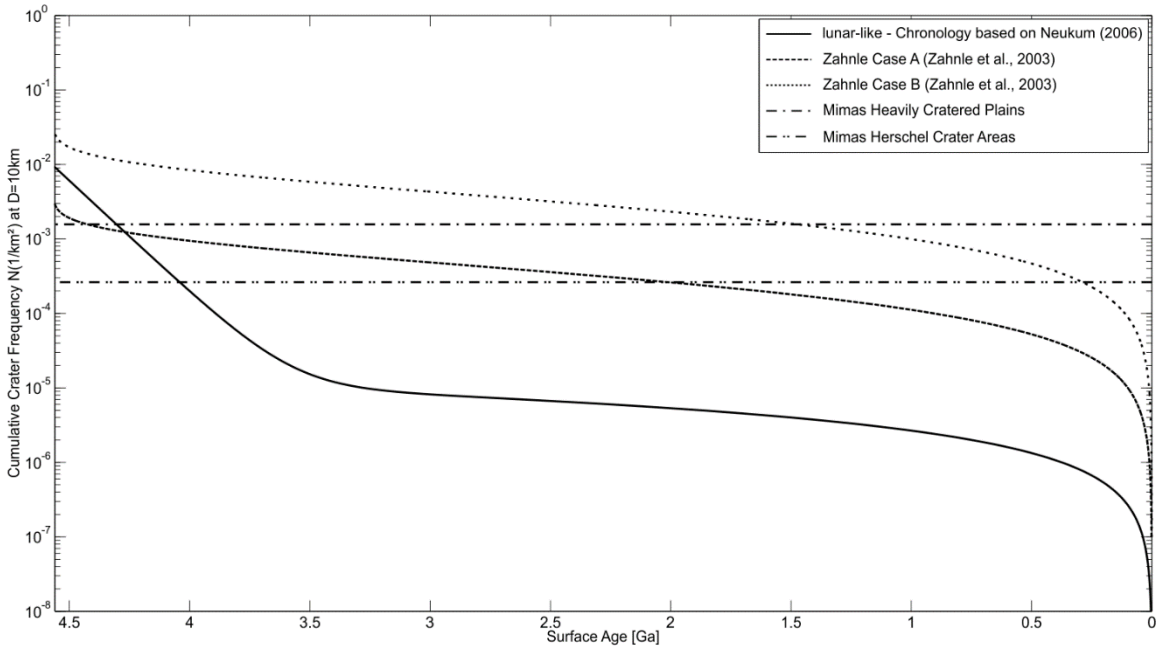


Fig. 7-10: Measured Crater Frequencies and Chronologies: Lunar-like (this work) and Zahnle (Zahnle et al., 2003) chronology models for Mimas, measured cumulative crater frequencies (≥ 1 km crater diameter converted to crater frequencies ≥ 10 km crater diameter) for the heavily cratered plains (A6 - A9) and resurfaced areas at Herschel crater (A235). Crossing points between horizontal lines (measured frequencies) and chronology curves give respective model ages.

## 7.8 Conclusion

We have gathered a reliable data set from the cratering record of Mimas. The data comprise two of the most important surface units; the heavily cratered plains and highly resurfaced areas within or close to Herschel crater. An offset by a factor of 6 towards lower crater frequencies indicates a younger surface age of the Herschel impact-resurfaced areas compared to the surrounding heavily cratered plains.
In order to estimate absolute surface ages we applied the Zahnle chronologies as well as our own alternative chronology to our data. We developed an alternative chronology for Mimas and Iapetus that assumes a collisionally evolved projectile population similar to that which impacted the lunar surface. By comparing projectile SFD, which are derived from the measured crater SFD on Iapetus and Mimas and observed SFD of possible projectile populations such as comets, KBO and Main Belt asteroids we conclude that the predominant projectile distribution visible in the cratering record of the investigated satellites has more similarities with Main Belt asteroids than with comets. We admit that comets and KBO may play some role for crater diameters in excess of roughly 100 km. At smaller sizes a wavy crater distribution is apparent that points to a collisionally evolved projectile distribution similar to that which impacted the lunar surface. This wavy SFD is thought to be a result of intense collisional evolution within the early asteroid Main Belt (e.g. Bottke et al., 2005a). Theoretically a similar process may have developed a collisionally relaxed wavy SFD within the Kuiper Belt as well (e.g. Davis and

Farinella, 1997) but a rather shallow SFD of observed comets may question this hypothesis (Zahnle et al., 2003 and Weiler et al., 2011). Different slopes between asteroidal and cometary SFD would be expected due to different target materials and collision conditions (e.g. Davis and Farinella, 1997 and O'Brien and Greenberg, 2003). Thus, if the Kuiper Belt underwent a collisional evolution its waves most likely differ from those observed in the asteroid Main Belt size distribution.

It has been argued that the steep distribution of small craters is a result of secondary (e.g. Shoemaker, 1965) and sesquinary cratering induced by large cometary impacts (e.g. Zahnle et al., 2003). In fact for Tethys Schmedemann et al. (2014b) may have found indications for significant contribution of sesquinary cratering. The found crater distribution on Tethys has specific similarities with secondary cratering in the northern hemisphere of the asteroid Vesta (Schmedemann et al., 2014a). As discussed with respect to Fig. 7-5 Iapetus as well as Mimas indeed show some excess in crater frequencies in a similar diameter range (0.5 – 5 km) where it is observed on Tethys (<5 km). This might suggest that a small fraction of craters has been formed by sesquinary projectiles on Mimas and Iapetus but it is much less significant than it is on Tethys. Our observation of only a small fraction of sesquinary craters is basically in agreement with (Bierhaus et al., 2012), which did not find indication of extensive sesquinary cratering.

Further analysis of the projectile density and dynamical characteristics in the Saturnian system led to an unsatisfactory result. While the observed crater SFD is very similar but not exactly the same as the SFD of Main Belt asteroids, the projectile densities inferred from crater/projectile scaling point to relatively low densities similar to those of comets. Furthermore, only very low impact velocities are allowed on the order of the escape velocity of the target bodies. These results however heavily depend on the chosen scaling parameters. In Section 5 we argued for a modified 1/g approach (Pike, 1980) in order to determine strength to gravity transitions on Iapetus and Mimas with reasonably good results in terms of similarity between derived production function and observed crater distribution for both cases. However, we did not use the modified surface gravity within the actual scaling between crater and projectile sizes because the modified simple to complex and strength to gravity transitions should already account for the different scaling in icy targets. First results including a modified surface gravity in the crater scaling equation would allow for higher projectile densities as well as higher impact velocities. Thus, this solution appears to be promising for future work but it needs to be investigated whether this approach is valid.

Despite these issues yet to be solved our measurements clearly show a strong inconsistency between the observed crater distribution and the production functions used by Zahnle et al. (2003). Our approach with a lunar-like crater production function for Iapetus as well as Mimas, implying a collisionally evolved projectile distribution, leads to a much higher similarity between model function and measured crater distribution. Such a high degree of similarity is required in order to find unique and narrow ranges for fitting the model production function to a measured crater distribution. In the case of Mimas we find consistent surface ages for the heavily cratered plains over a broad range of crater diameters (~2.5

orders of magnitude). This is not possible with both production functions by Zahnle et al. (2003).
While comets dynamically appear to be the most prominent projectile source in the Saturnian system, they cannot alone be responsible for the observed crater distribution on Mimas and Iapetus. Observations indicate a projectile population that is collisionally evolved similar to the one that impacted the lunar surface. However, it is dynamically difficult to explain how this might have happened. A lot more work is required in order to understand cratering processes and projectile sources in the Saturnian system.

## 7.9 Acknowledgement

This work was supported by the German Space Agency (DLR) on behalf of the Federal Ministry of Economics and Technology, grants 50OH0305 and 50OH1102. We thank the referees for their constructive revisions. We also thank the Cassini imaging team for the supply of the Cassini imaging data. H. Rosenberg also did a great job in mosaicking images and interfacing our image database for simple usage. Finally we express our gratitude to the people who helped to improve this paper.

## 7.10 Appendix – A - data tables

The tables 1 through 9 give the measured crater statistics of the respective areas.

Table A1 – Crater Statistics of A1

| Total Area [km²]: 758.91 | | | | | | |
|---|---|---|---|---|---|---|
| | | | | | | |
| D | F(D) | N_dif | Error | C(D) | N_cum | +/-Error |
| | | | | | | |
| | | | | | | |
| 0.25 | 3 | 7.91E-02 | 4.57E-02 | 42 | 5.53E-02 | 8.54E-03 |
| 0.3 | 3 | 7.91E-02 | 4.57E-02 | 39 | 5.14E-02 | 8.23E-03 |
| 0.35 | 2 | 5.27E-02 | 3.73E-02 | 36 | 4.74E-02 | 7.91E-03 |
| 0.4 | 3 | 7.91E-02 | 4.57E-02 | 34 | 4.48E-02 | 7.68E-03 |
| 0.45 | 5 | 1.32E-01 | 5.89E-02 | 31 | 4.09E-02 | 7.34E-03 |
| 0.5 | 3 | 3.95E-02 | 2.28E-02 | 26 | 3.43E-02 | 6.72E-03 |
| 0.6 | 2 | 2.64E-02 | 1.86E-02 | 23 | 3.03E-02 | 6.32E-03 |
| 0.7 | 2 | 2.64E-02 | 1.86E-02 | 21 | 2.77E-02 | 6.04E-03 |
| 0.8 | 4 | 5.27E-02 | 2.64E-02 | 19 | 2.50E-02 | 5.74E-03 |
| 0.9 | 2 | 2.64E-02 | 1.86E-02 | 15 | 1.98E-02 | 5.10E-03 |
| 1 | 3 | 3.95E-02 | 2.28E-02 | 13 | 1.71E-02 | 4.75E-03 |
| 1.1 | 3 | 3.95E-02 | 2.28E-02 | 10 | 1.32E-02 | 4.17E-03 |
| 1.2 | 1 | 1.32E-02 | 1.32E-02 | 7 | 9.22E-03 | 3.49E-03 |
| 1.3 | 2 | 2.64E-02 | 1.86E-02 | 6 | 7.91E-03 | 3.23E-03 |
| 1.4 | 2 | 2.64E-02 | 1.86E-02 | 4 | 5.27E-03 | 2.64E-03 |
| 1.5 | 2 | 2.64E-02 | 1.86E-02 | 2 | 2.64E-03 | 1.86E-03 |

Table A2 – Crater Statistics of A2

| Total Area [km²]: 354.61 | | | | | | |
|---|---|---|---|---|---|---|
| | | | | | | |
| D | F(D) | N_dif | Error | C(D) | N_cum | +/-Error |
| | | | | | | |
| | | | | | | |
| 0.3 | 2 | 1.13E-01 | 7.98E-02 | 60 | 1.69E-01 | 2.18E-02 |
| 0.35 | 3 | 1.69E-01 | 9.77E-02 | 58 | 1.64E-01 | 2.15E-02 |
| 0.4 | 4 | 2.26E-01 | 1.13E-01 | 55 | 1.55E-01 | 2.09E-02 |
| 0.45 | 12 | 6.77E-01 | 1.95E-01 | 51 | 1.44E-01 | 2.01E-02 |
| 0.5 | 13 | 3.67E-01 | 1.02E-01 | 39 | 1.10E-01 | 1.76E-02 |
| 0.6 | 11 | 3.10E-01 | 9.35E-02 | 26 | 7.33E-02 | 1.44E-02 |
| 0.7 | 5 | 1.41E-01 | 6.31E-02 | 15 | 4.23E-02 | 1.09E-02 |
| 0.8 | 3 | 8.46E-02 | 4.88E-02 | 10 | 2.82E-02 | 8.92E-03 |
| 0.9 | 4 | 1.13E-01 | 5.64E-02 | 7 | 1.97E-02 | 7.46E-03 |
| 1 | 1 | 4.03E-03 | 4.03E-03 | 3 | 8.46E-03 | 4.88E-03 |
| 1.7 | 1 | 1.57E-03 | 1.57E-03 | 2 | 5.64E-03 | 3.99E-03 |
| 3.5 | 1 | 1.57E-03 | 1.57E-03 | 1 | 2.82E-03 | 2.82E-03 |

Table A3 – Crater Statistics of A3

| Total Area [km²]: 150.50 | | | | | | |
|---|---|---|---|---|---|---|
| | | | | | | |
| D | F(D) | N_dif | Error | C(D) | N_cum | +/-Error |
| | | | | | | |
| | | | | | | |
| 0.2 | 1 | 1.33E-01 | 1.33E-01 | 40 | 2.66E-01 | 4.20E-02 |

| | | | | | | |
|---|---|---|---|---|---|---|
| 0.25 | 1 | 1.33E-01 | 1.33E-01 | 39 | 2.59E-01 | 4.15E-02 |
| 0.3 | 5 | 6.65E-01 | 2.97E-01 | 38 | 2.53E-01 | 4.10E-02 |
| 0.35 | 7 | 9.30E-01 | 3.52E-01 | 33 | 2.19E-01 | 3.82E-02 |
| 0.4 | 8 | 1.06E+00 | 3.76E-01 | 26 | 1.73E-01 | 3.39E-02 |
| 0.45 | 6 | 7.97E-01 | 3.26E-01 | 18 | 1.20E-01 | 2.82E-02 |
| 0.5 | 8 | 5.32E-01 | 1.88E-01 | 12 | 7.97E-02 | 2.30E-02 |
| 0.6 | 2 | 6.65E-02 | 4.70E-02 | 4 | 2.66E-02 | 1.33E-02 |
| 0.8 | 1 | 9.49E-03 | 9.49E-03 | 2 | 1.33E-02 | 9.40E-03 |
| 1.5 | 1 | 9.49E-03 | 9.49E-03 | 1 | 6.65E-03 | 6.65E-03 |

Table A4 – Crater Statistics of A4

| Total Area [km²]: 637.46 | | | | | | |
|---|---|---|---|---|---|---|
| | | | | | | |
| D | F(D) | N_dif | Error | C(D) | N_cum | +/-Error |
| | | | | | | |
| | | | | | | |
| 0.35 | 1 | 1.57E-02 | 1.57E-02 | 47 | 7.37E-02 | 1.08E-02 |
| 0.45 | 4 | 1.26E-01 | 6.28E-02 | 46 | 7.22E-02 | 1.06E-02 |
| 0.5 | 4 | 6.28E-02 | 3.14E-02 | 42 | 6.59E-02 | 1.02E-02 |
| 0.6 | 7 | 1.10E-01 | 4.15E-02 | 38 | 5.96E-02 | 9.67E-03 |
| 0.7 | 7 | 1.10E-01 | 4.15E-02 | 31 | 4.86E-02 | 8.73E-03 |
| 0.8 | 4 | 6.28E-02 | 3.14E-02 | 24 | 3.77E-02 | 7.69E-03 |
| 0.9 | 6 | 9.41E-02 | 3.84E-02 | 20 | 3.14E-02 | 7.02E-03 |
| 1 | 1 | 1.57E-02 | 1.57E-02 | 14 | 2.20E-02 | 5.87E-03 |
| 1.1 | 1 | 1.57E-02 | 1.57E-02 | 13 | 2.04E-02 | 5.66E-03 |
| 1.2 | 3 | 4.71E-02 | 2.72E-02 | 12 | 1.88E-02 | 5.43E-03 |
| 1.3 | 2 | 3.14E-02 | 2.22E-02 | 9 | 1.41E-02 | 4.71E-03 |

| | | | | | | |
|---|---|---|---|---|---|---|
| 1.4 | 1 | 1.57E-02 | 1.57E-02 | 7 | 1.10E-02 | 4.15E-03 |
| 1.5 | 1 | 7.84E-03 | 7.84E-03 | 6 | 9.41E-03 | 3.84E-03 |
| 1.7 | 4 | 3.49E-03 | 1.74E-03 | 5 | 7.84E-03 | 3.51E-03 |
| 3.5 | 1 | 8.72E-04 | 8.72E-04 | 1 | 1.57E-03 | 1.57E-03 |

Table A5 – Crater Statistics of A5

| Total Area [km²]: 543.82 | | | | | | |
|---|---|---|---|---|---|---|
| | | | | | | |
| D | F(D) | N_dif | Error | C(D) | N_cum | +/-Error |
| | | | | | | |
| | | | | | | |
| 0.2 | 1 | 3.68E-02 | 3.68E-02 | 94 | 1.73E-01 | 1.78E-02 |
| 0.25 | 3 | 1.10E-01 | 6.37E-02 | 93 | 1.71E-01 | 1.77E-02 |
| 0.3 | 11 | 4.05E-01 | 1.22E-01 | 90 | 1.66E-01 | 1.74E-02 |
| 0.35 | 22 | 8.09E-01 | 1.73E-01 | 79 | 1.45E-01 | 1.63E-02 |
| 0.4 | 12 | 4.41E-01 | 1.27E-01 | 57 | 1.05E-01 | 1.39E-02 |
| 0.45 | 12 | 4.41E-01 | 1.27E-01 | 45 | 8.28E-02 | 1.23E-02 |
| 0.5 | 12 | 2.21E-01 | 6.37E-02 | 33 | 6.07E-02 | 1.06E-02 |
| 0.6 | 5 | 9.19E-02 | 4.11E-02 | 21 | 3.86E-02 | 8.43E-03 |
| 0.7 | 3 | 5.52E-02 | 3.19E-02 | 16 | 2.94E-02 | 7.36E-03 |
| 0.8 | 4 | 7.36E-02 | 3.68E-02 | 13 | 2.39E-02 | 6.63E-03 |
| 0.9 | 4 | 7.36E-02 | 3.68E-02 | 9 | 1.66E-02 | 5.52E-03 |
| 1 | 1 | 9.19E-03 | 9.19E-03 | 5 | 9.19E-03 | 4.11E-03 |
| 1.2 | 2 | 1.23E-02 | 8.67E-03 | 4 | 7.36E-03 | 3.68E-03 |
| 1.5 | 1 | 3.68E-03 | 3.68E-03 | 2 | 3.68E-03 | 2.60E-03 |
| 2 | 1 | 3.68E-03 | 3.68E-03 | 1 | 1.84E-03 | 1.84E-03 |

Table A6 – Crater Statistics of A6

| Total Area [km²]: 6286.39 | | | | | | |
|---|---|---|---|---|---|---|
| | | | | | | |
| D | F(D) | N_dif | Error | C(D) | N_cum | +/-Error |
| | | | | | | |
| | | | | | | |
| 1.5 | 3 | 2.39E-03 | 1.38E-03 | 76 | 1.21E-02 | 1.39E-03 |
| 1.7 | 4 | 2.12E-03 | 1.06E-03 | 73 | 1.16E-02 | 1.36E-03 |
| 2 | 12 | 3.82E-03 | 1.10E-03 | 69 | 1.10E-02 | 1.32E-03 |
| 2.5 | 10 | 3.18E-03 | 1.01E-03 | 57 | 9.07E-03 | 1.20E-03 |
| 3 | 1 | 3.18E-04 | 3.18E-04 | 47 | 7.48E-03 | 1.09E-03 |
| 3.5 | 5 | 1.59E-03 | 7.11E-04 | 46 | 7.32E-03 | 1.08E-03 |
| 4 | 6 | 1.91E-03 | 7.79E-04 | 41 | 6.52E-03 | 1.02E-03 |
| 4.5 | 6 | 1.91E-03 | 7.79E-04 | 35 | 5.57E-03 | 9.41E-04 |
| 5 | 8 | 1.27E-03 | 4.50E-04 | 29 | 4.61E-03 | 8.57E-04 |
| 6 | 6 | 9.54E-04 | 3.90E-04 | 21 | 3.34E-03 | 7.29E-04 |
| 7 | 5 | 7.95E-04 | 3.56E-04 | 15 | 2.39E-03 | 6.16E-04 |
| 8 | 2 | 3.18E-04 | 2.25E-04 | 10 | 1.59E-03 | 5.03E-04 |
| 9 | 1 | 1.59E-04 | 1.59E-04 | 8 | 1.27E-03 | 4.50E-04 |
| 10 | 1 | 1.59E-04 | 1.59E-04 | 7 | 1.11E-03 | 4.21E-04 |
| 11 | 1 | 1.59E-04 | 1.59E-04 | 6 | 9.54E-04 | 3.90E-04 |
| 12 | 1 | 7.95E-05 | 7.95E-05 | 5 | 7.95E-04 | 3.56E-04 |
| 14 | 1 | 1.59E-04 | 1.59E-04 | 4 | 6.36E-04 | 3.18E-04 |
| 15 | 2 | 2.12E-05 | 1.50E-05 | 3 | 4.77E-04 | 2.76E-04 |
| 30 | 1 | 1.06E-05 | 1.06E-05 | 1 | 1.59E-04 | 1.59E-04 |

Table A7 – Crater Statistics of A7

| Total Area [km²] 757.938 | | | | | | |
|---|---|---|---|---|---|---|
| | | | | | | |
| D | F(D) | N_dif | Error | C(D) | N_cum | Error |
| | | | | | | |
| | | | | | | |
| 0.15 | 3 | 3.96E-03 | 2.29E-03 | 302 | 3.98E-01 | 2.29E-02 |
| 0.17 | 1 | 1.32E-03 | 1.32E-03 | 299 | 3.95E-01 | 2.28E-02 |
| 0.2 | 16 | 2.11E-02 | 5.28E-03 | 298 | 3.93E-01 | 2.28E-02 |
| 0.25 | 26 | 3.43E-02 | 6.73E-03 | 282 | 3.72E-01 | 2.22E-02 |
| 0.3 | 35 | 4.62E-02 | 7.81E-03 | 256 | 3.38E-01 | 2.11E-02 |
| 0.35 | 37 | 4.88E-02 | 8.03E-03 | 221 | 2.92E-01 | 1.96E-02 |
| 0.4 | 30 | 3.96E-02 | 7.23E-03 | 184 | 2.43E-01 | 1.79E-02 |
| 0.45 | 22 | 2.90E-02 | 6.19E-03 | 154 | 2.03E-01 | 1.64E-02 |
| 0.5 | 20 | 2.64E-02 | 5.90E-03 | 132 | 1.74E-01 | 1.52E-02 |
| 0.6 | 23 | 3.04E-02 | 6.33E-03 | 112 | 1.48E-01 | 1.40E-02 |
| 0.7 | 12 | 1.58E-02 | 4.57E-03 | 89 | 1.17E-01 | 1.25E-02 |
| 0.8 | 17 | 2.24E-02 | 5.44E-03 | 77 | 1.02E-01 | 1.16E-02 |
| 0.9 | 7 | 9.24E-03 | 3.49E-03 | 60 | 7.92E-02 | 1.02E-02 |
| 1 | 11 | 1.45E-02 | 4.38E-03 | 53 | 6.99E-02 | 9.61E-03 |
| 1.1 | 2 | 2.64E-03 | 1.87E-03 | 42 | 5.54E-02 | 8.55E-03 |
| 1.2 | 7 | 9.24E-03 | 3.49E-03 | 40 | 5.28E-02 | 8.34E-03 |
| 1.3 | 4 | 5.28E-03 | 2.64E-03 | 33 | 4.35E-02 | 7.58E-03 |
| 1.4 | 6 | 7.92E-03 | 3.23E-03 | 29 | 3.83E-02 | 7.11E-03 |
| 1.5 | 5 | 6.60E-03 | 2.95E-03 | 23 | 3.04E-02 | 6.33E-03 |
| 1.7 | 4 | 5.28E-03 | 2.64E-03 | 18 | 2.38E-02 | 5.60E-03 |
| 2 | 7 | 9.24E-03 | 3.49E-03 | 14 | 1.85E-02 | 4.94E-03 |
| 3 | 1 | 1.32E-03 | 1.32E-03 | 7 | 9.24E-03 | 3.49E-03 |
| 3.5 | 1 | 1.32E-03 | 1.32E-03 | 6 | 7.92E-03 | 3.23E-03 |
| 4 | 1 | 1.32E-03 | 1.32E-03 | 5 | 6.60E-03 | 2.95E-03 |
| 4.5 | 1 | 1.32E-03 | 1.32E-03 | 4 | 5.28E-03 | 2.64E-03 |
| 5 | 2 | 2.64E-03 | 1.87E-03 | 3 | 3.96E-03 | 2.29E-03 |
| 9 | 1 | 1.32E-03 | 1.32E-03 | 1 | 1.32E-03 | 1.32E-03 |

Table A8 – Crater Statistics of A8

| Total Area [km²]: 47300.60 | | | | | | |
|---|---|---|---|---|---|---|
| | | | | | | |
| D | F(D) | N_dif | Error | C(D) | N_cum | +/-Error |
| | | | | | | |
| | | | | | | |
| 1.3 | 7 | 1.48E-03 | 5.60E-04 | 771 | 1.63E-02 | 5.87E-04 |
| 1.4 | 2 | 4.23E-04 | 2.99E-04 | 764 | 1.62E-02 | 5.85E-04 |
| 1.5 | 35 | 3.70E-03 | 6.26E-04 | 762 | 1.61E-02 | 5.84E-04 |
| 1.7 | 20 | 1.41E-03 | 3.15E-04 | 727 | 1.54E-02 | 5.70E-04 |
| 2 | 165 | 6.98E-03 | 5.43E-04 | 707 | 1.50E-02 | 5.62E-04 |
| 2.5 | 58 | 2.45E-03 | 3.22E-04 | 542 | 1.15E-02 | 4.92E-04 |
| 3 | 106 | 4.48E-03 | 4.36E-04 | 484 | 1.02E-02 | 4.65E-04 |
| 3.5 | 52 | 2.20E-03 | 3.05E-04 | 378 | 7.99E-03 | 4.11E-04 |
| 4 | 56 | 2.37E-03 | 3.17E-04 | 326 | 6.89E-03 | 3.82E-04 |
| 4.5 | 30 | 1.27E-03 | 2.32E-04 | 270 | 5.71E-03 | 3.48E-04 |
| 5 | 47 | 9.94E-04 | 1.45E-04 | 240 | 5.08E-03 | 3.28E-04 |
| 6 | 37 | 7.83E-04 | 1.29E-04 | 193 | 4.08E-03 | 2.94E-04 |
| 7 | 32 | 6.77E-04 | 1.20E-04 | 156 | 3.30E-03 | 2.64E-04 |
| 8 | 23 | 4.86E-04 | 1.01E-04 | 124 | 2.62E-03 | 2.36E-04 |
| 9 | 21 | 4.44E-04 | 9.69E-05 | 101 | 2.14E-03 | 2.13E-04 |
| 10 | 13 | 2.75E-04 | 7.63E-05 | 80 | 1.69E-03 | 1.89E-04 |
| 11 | 12 | 2.54E-04 | 7.33E-05 | 67 | 1.42E-03 | 1.73E-04 |
| 12 | 11 | 2.33E-04 | 7.01E-05 | 55 | 1.16E-03 | 1.57E-04 |
| 13 | 2 | 4.23E-05 | 2.99E-05 | 44 | 9.31E-04 | 1.40E-04 |
| 14 | 11 | 2.33E-04 | 7.01E-05 | 42 | 8.88E-04 | 1.37E-04 |

| | | | | | | |
|---|---|---|---|---|---|---|
| 15 | 9 | 9.52E-05 | 3.17E-05 | 31 | 6.56E-04 | 1.18E-04 |
| 17 | 8 | 5.64E-05 | 1.99E-05 | 22 | 4.65E-04 | 9.92E-05 |
| 20 | 9 | 3.81E-05 | 1.27E-05 | 14 | 2.96E-04 | 7.91E-05 |
| 25 | 4 | 5.64E-06 | 2.82E-06 | 5 | 1.06E-04 | 4.73E-05 |
| 40 | 1 | 1.41E-06 | 1.41E-06 | 1 | 2.12E-05 | 2.12E-05 |

Table A9 – Crater Statistics of A9

| Total Area [km²]: 322372.15 | | | | | | |
|---|---|---|---|---|---|---|
| | | | | | | |
| D | F(D) | N_dif | Error | C(D) | N_cum | +/-Error |
| | | | | | | |
| | | | | | | |
| 6 | 3 | 9.31E-06 | 5.37E-06 | 338 | 1.05E-03 | 5.70E-05 |
| 7 | 7 | 2.17E-05 | 8.21E-06 | 335 | 1.04E-03 | 5.68E-05 |
| 8 | 27 | 8.38E-05 | 1.61E-05 | 328 | 1.02E-03 | 5.62E-05 |
| 9 | 20 | 6.20E-05 | 1.39E-05 | 301 | 9.34E-04 | 5.38E-05 |
| 10 | 24 | 7.45E-05 | 1.52E-05 | 281 | 8.72E-04 | 5.20E-05 |
| 11 | 25 | 7.76E-05 | 1.55E-05 | 257 | 7.97E-04 | 4.97E-05 |
| 12 | 22 | 6.82E-05 | 1.46E-05 | 232 | 7.20E-04 | 4.73E-05 |
| 13 | 27 | 8.38E-05 | 1.61E-05 | 210 | 6.51E-04 | 4.50E-05 |
| 14 | 35 | 1.09E-04 | 1.84E-05 | 183 | 5.68E-04 | 4.20E-05 |
| 15 | 28 | 4.34E-05 | 8.21E-06 | 148 | 4.59E-04 | 3.77E-05 |
| 17 | 37 | 3.83E-05 | 6.29E-06 | 120 | 3.72E-04 | 3.40E-05 |
| 20 | 41 | 2.54E-05 | 3.97E-06 | 83 | 2.58E-04 | 2.83E-05 |
| 25 | 20 | 1.24E-05 | 2.78E-06 | 42 | 1.30E-04 | 2.01E-05 |

| | | | | | | |
|---|---|---|---|---|---|---|
| 30 | 11 | 6.82E-06 | 2.06E-06 | 22 | 6.82E-05 | 1.46E-05 |
| 35 | 6 | 3.72E-06 | 1.52E-06 | 11 | 3.41E-05 | 1.03E-05 |
| 40 | 1 | 6.20E-07 | 6.20E-07 | 5 | 1.55E-05 | 6.94E-06 |
| 45 | 1 | 6.20E-07 | 6.20E-07 | 4 | 1.24E-05 | 6.20E-06 |
| 50 | 2 | 8.86E-08 | 6.27E-08 | 3 | 9.31E-06 | 5.37E-06 |
| 120 | 1 | 4.43E-08 | 4.43E-08 | 1 | 3.10E-06 | 3.10E-06 |

Table A235 – Crater Statistics of combined measurement A235

| Total Area [km²]: 1048.93 | | | | | | |
|---|---|---|---|---|---|---|
| | | | | | | |
| D | F(D) | N_dif | Error | C(D) | N_cum | +/-Error |
| | | | | | | |
| 0.2 | 2 | 3.81E+01 | 2.70E+01 | 194 | 1.85E+02 | 1.33E+01 |
| 0.25 | 4 | 7.63E+01 | 3.81E+01 | 192 | 1.83E+02 | 1.32E+01 |
| 0.3 | 18 | 3.43E+02 | 8.09E+01 | 188 | 1.79E+02 | 1.31E+01 |
| 0.35 | 32 | 6.10E+02 | 1.08E+02 | 170 | 1.62E+02 | 1.24E+01 |
| 0.4 | 24 | 4.58E+02 | 9.34E+01 | 138 | 1.32E+02 | 1.12E+01 |
| 0.45 | 30 | 5.72E+02 | 1.04E+02 | 114 | 1.09E+02 | 1.02E+01 |
| 0.5 | 33 | 3.15E+02 | 5.48E+01 | 84 | 8.01E+01 | 8.74E+00 |
| 0.6 | 18 | 1.72E+02 | 4.05E+01 | 51 | 4.86E+01 | 6.81E+00 |
| 0.7 | 8 | 7.63E+01 | 2.70E+01 | 33 | 3.15E+01 | 5.48E+00 |
| 0.8 | 8 | 7.63E+01 | 2.70E+01 | 25 | 2.38E+01 | 4.77E+00 |
| 0.9 | 8 | 7.63E+01 | 2.70E+01 | 17 | 1.62E+01 | 3.93E+00 |
| 1 | 2 | 9.53E+00 | 6.74E+00 | 9 | 8.58E+00 | 2.86E+00 |
| 1.2 | 2 | 6.36E+00 | 4.49E+00 | 7 | 6.67E+00 | 2.52E+00 |
| 1.5 | 2 | 9.53E+00 | 6.74E+00 | 5 | 4.77E+00 | 2.13E+00 |

| | | | | | | |
|---|---|---|---|---|---|---|
| 1.7 | 1 | 3.18E+00 | 3.18E+00 | 3 | 2.86E+00 | 1.65E+00 |
| 2 | 1 | 6.36E-01 | 6.36E-01 | 2 | 1.91E+00 | 1.35E+00 |
| 3.5 | 1 | 6.36E-01 | 6.36E-01 | 1 | 9.53E-01 | 9.53E-01 |

Table A1-9 – Crater Statistics of all combined normalized measurements

| Total Area [km²]: 322243.35 (arbitrary due to normalization) | | | | | | |
|---|---|---|---|---|---|---|
| | | | | | | |
| D | F(D) | N_dif | Error | C(D) | N_cum | +/-Error |
| | | | | | | |
| 0.45 | 58125 | 3.61E+03 | 1.50E+01 | 220875 | 6.85E+02 | 1.46E+00 |
| 0.5 | 63937 | 1.98E+03 | 7.85E+00 | 162750 | 5.05E+02 | 1.25E+00 |
| 0.6 | 34875 | 1.08E+03 | 5.80E+00 | 98812 | 3.07E+02 | 9.76E-01 |
| 0.7 | 15500 | 4.81E+02 | 3.86E+00 | 63937 | 1.98E+02 | 7.85E-01 |
| 0.8 | 15500 | 4.81E+02 | 3.86E+00 | 48437 | 1.50E+02 | 6.83E-01 |
| 0.9 | 12514 | 3.88E+02 | 3.47E+00 | 32937 | 1.02E+02 | 5.63E-01 |
| 1.000 | 68 | 2.11E+00 | 2.56E-01 | 20423 | 6.34E+01 | 4.44E-01 |
| 1.100 | 6450 | 2.00E+02 | 2.49E+00 | 20356 | 6.32E+01 | 4.43E-01 |
| 1.200 | 1692 | 5.25E+01 | 1.28E+00 | 13906 | 4.32E+01 | 3.66E-01 |
| 1.300 | 1527 | 4.74E+01 | 1.21E+00 | 12213 | 3.79E+01 | 3.43E-01 |
| 1.400 | 1263 | 3.92E+01 | 1.10E+00 | 10687 | 3.32E+01 | 3.21E-01 |
| 1.500 | 2701 | 4.19E+01 | 8.06E-01 | 9424 | 2.92E+01 | 3.01E-01 |
| 1.700 | 2299 | 2.38E+01 | 4.96E-01 | 6723 | 2.09E+01 | 2.54E-01 |
| 2.000 | 731 | 4.54E+00 | 1.68E-01 | 4424 | 1.37E+01 | 2.06E-01 |
| 2.500 | 263 | 1.63E+00 | 1.01E-01 | 3692 | 1.15E+01 | 1.89E-01 |
| 3.000 | 1155 | 7.17E+00 | 2.11E-01 | 3430 | 1.06E+01 | 1.82E-01 |
| 3.500 | 255 | 1.58E+00 | 9.91E-02 | 2274 | 7.06E+00 | 1.48E-01 |
| 4.000 | 289 | 1.79E+00 | 1.06E-01 | 2020 | 6.27E+00 | 1.40E-01 |

| | | | | | | |
|---|---|---|---|---|---|---|
| 4.500 | 233 | 1.45E+00 | 9.47E-02 | 1731 | 5.37E+00 | 1.29E-01 |
| 5.000 | 345 | 1.07E+00 | 5.76E-02 | 1498 | 4.65E+00 | 1.20E-01 |
| 6.000 | 235 | 7.29E-01 | 4.76E-02 | 1153 | 3.58E+00 | 1.05E-01 |
| 7.000 | 243 | 7.54E-01 | 4.84E-02 | 918 | 2.85E+00 | 9.40E-02 |
| 8.000 | 134 | 4.16E-01 | 3.59E-02 | 675 | 2.10E+00 | 8.06E-02 |
| 9.000 | 93 | 2.89E-01 | 2.99E-02 | 541 | 1.68E+00 | 7.22E-02 |
| 10.000 | 80 | 2.48E-01 | 2.78E-02 | 448 | 1.39E+00 | 6.57E-02 |
| 11.000 | 88 | 2.73E-01 | 2.91E-02 | 368 | 1.14E+00 | 5.95E-02 |
| 12.000 | 33 | 1.02E-01 | 1.78E-02 | 280 | 8.67E-01 | 5.19E-02 |
| 13.000 | 31 | 9.62E-02 | 1.73E-02 | 246 | 7.65E-01 | 4.87E-02 |
| 14.000 | 51 | 1.58E-01 | 2.22E-02 | 215 | 6.68E-01 | 4.55E-02 |
| 15.000 | 35 | 5.43E-02 | 9.18E-03 | 164 | 5.11E-01 | 3.97E-02 |
| 17.000 | 39 | 4.03E-02 | 6.46E-03 | 130 | 4.03E-01 | 3.54E-02 |
| 20.000 | 51 | 3.17E-02 | 4.43E-03 | 91 | 2.82E-01 | 2.96E-02 |
| 25.000 | 20 | 1.24E-02 | 2.78E-03 | 40 | 1.24E-01 | 1.96E-02 |
| 30.000 | 8 | 4.97E-03 | 1.76E-03 | 20 | 6.20E-02 | 1.39E-02 |
| 35.000 | 5 | 3.10E-03 | 1.39E-03 | 12 | 3.72E-02 | 1.08E-02 |
| 40.000 | 2 | 1.24E-03 | 8.78E-04 | 7 | 2.20E-02 | 8.21E-03 |
| 45.000 | 1 | 6.21E-04 | 6.21E-04 | 5 | 1.55E-02 | 6.94E-03 |
| 50.000 | 3 | 9.31E-05 | 5.38E-05 | 4 | 1.24E-02 | 6.21E-03 |
| 150.000 | 1 | 3.10E-05 | 3.10E-05 | 1 | 3.10E-03 | 3.10E-03 |

# 8 Summary and outlook

The published papers and manuscript prepared for publication presented in the previous chapters (3 - 7) contain their own summaries pronouncing the specific topic of the paper with respect to a broader context. Specifically chapters 4, 5 and 6 are related to the first extensive global characterization of asteroid Vesta based on orbital remote sensing data in the frame of the Dawn mission. In this final chapter results from Phobos, Ida, Gaspra, Lutetia, Vesta and Mimas will be summarized with conclusions about the applicability of lunar derived cratering characteristics going from the inner to the outer Solar System.
The goal of this thesis was to convert the lunar crater production and chronology function to asteroids and planetary satellites with significantly different impact conditions than observed on the Moon and at various dynamical environments in the inner and outer Solar System as well as inside the asteroid Main Belt. Furthermore, the derived crater production function was verified against the observed crater size-frequency distribution. The chronology function on the other hand was verified by plausibility tests of derived crater retention ages, respective stratigraphic relationships of the measured geologic units and consistency with independent chronometers. In addition, the crater-derived projectile distributions were compared with observed size-frequency distributions of possible projectile populations. The application of the found crater production and chronology functions to the cratering records of geologic key units on Phobos, Ida, Gaspra, Lutetia, Vesta and Mimas allowed for the determination of time constraints for major events in the geologic histories of these bodies. For this purpose geologic mapping of representative sample areas on each body were carried out in order to apply the technique of age determination of planetary surfaces by measurements of crater size-frequency distributions.

## 8.1 Applicability of lunar-like crater production and chronology functions:

In the scientific community there is a significantly decreasing acceptance concerning the applicability of a lunar-like projectile flux (size distribution and development over time) going from the inner to the outer Solar System. In contrast to that concern it was shown, that a lunar-like crater size-frequency distribution is well applicable on Phobos, the Main Belt asteroids as well as the Saturnian satellites, if correctly scaled to the respective impact conditions. The lunar-like chronology could be compared with an independent chronology only for the case of Vesta. For this case a good agreement was found between crater retention ages on Vesta and radiometric ages of Vesta-derived HED meteorites.

The following sub-chapters detail the results from Phobos, the investigated Main Belt asteroids and Mimas.

### 8.1.1 Phobos (chapter 3):

It was shown that a slightly better fit of the measured crater distribution favored the dynamical case in which Phobos spent most of its existence in orbit about Mars. Although highly controversial, estimates about the groove formation on Phobos by Murray and Heggie (2014) are well in agreement with groove formation ages (>3 Ga) derived for the previously mentioned dynamic case. As well as the groove formation ages, the formation age of the large crater Stickney was also determined at 4 - 4.2 Ga. Thus, from simple principles of superposition, it is possible that Stickney was resurfaced by a groove formation event, which is actually observed. Hence, the absolute dating and observed stratigraphic position of Stickney with respect to the grooves are realistic, although relative stratigraphy alone cannot discriminate between both dynamical cases. In order to find a further constraint on the dynamical history of Phobos its apex-/antapex asymmetry was analyzed. Unfortunately, only large craters could be used for this analysis due to heterogeneous resurfacing of Phobos' surface. Such craters are too sparse to give statistically valid results. Thus, this approach was inconclusive.

### 8.1.2 Main Belt asteroids (chapters 4, 5 and 6):

The primary goal in investigating the crater size-frequency distribution and surface ages on Ida and Gaspra was to compare results with previous publications (Neukum and Ivanov, 1994; Chapman et al., 1996a and Chapman et al., 1996b) in order to show the reproducibility of older results by the taken approach. It is shown that the measured crater distribution on both bodies is well in agreement with previously published data. Improved image restoration techniques and enhanced handling of highly irregular body surfaces allowed for upgraded measurements that pushed the limit of crater identification slightly further out. This allowed for identification of even older underlying stratigraphic layers in both cases. The lunar production function, scaled to the impact conditions on Ida and Gaspra, is also well in agreement with measured crater distributions. For crater diameters below ~10 km these measurements show, that the observed small crater population with a cumulative slope of about -3.5 is clearly steeper than the expected size-frequency distribution of small projectiles inside the Main Belt (e.g. Dohnanyi, 1969 and Gladman et al., 2009). The steep slope in observed crater distributions cannot be explained by secondary craters, because of the very low surface gravity on Ida and Gaspra with respectively low escape velocities, which are far too low for the formation of secondary craters (Bierhaus et al., 2012). On the other hand, the observed size- frequency distribution of small (< ~1 km) Main Belt asteroids indeed appears to show a shallow (~-1.5) cumulative slope (Gladman et al., 2009). A possible solution to this puzzle involving radiation forces such as the Yarkovsky effect (e.g. Farinella et al., 1998) is proposed in chapter 4.2.2. Surface ages derived

from crater counts on Ida and Gaspra are in good agreement with previous publications as well. Thus, the applied conversion of lunar crater functions to the impact conditions on Main Belt asteroids was successful. In addition, the used technique to scale the lunar chronology based on a statistical analysis of orbital elements of orbit-crossing asteroids (Bottke et al., 1994) provided reasonable results, comparable with previous publications.

Lutetia is about twice as large as Ida and thus the cratering record covers a critical part of the lunar-like crater production function for Lutetia around 10 km, where the distribution slope is changing. On Lutetia measured crater distributions follow closely the lunar-like production function derived for Lutetia. However, an earlier publication (Marchi et al., 2012b) shows a different crater production function that incorporates a kink, which has been interpreted as a result of layering in the surface regolith of Lutetia. The measurements presented in chapter 4.7.1.3 of this thesis show that the previously observed kink in the crater distribution is most likely not a result of regolith layering but a resurfacing effect, in which small craters were damaged or destroyed by seismic shaking and/or ejecta blanketing of neighboring impact events. Thus, the found chronostratigraphy for Lutetia is reinterpreted and more detailed than in the publication by Marchi et al. (2012b) although in general, the found model ages are comparable.

As outlined before, techniques for transferring the lunar crater functions to Main Belt asteroids and deriving realistic collision probabilities for correct chronology scaling worked well on Ida, Gaspra and Lutetia. Applying the same techniques to Vesta result in basin formation ages for Rheasilvia and Veneneia of about 3.5 and 3.7 Ga, respectively. These results are in strong disagreement with Marchi et al. (2012c) and Schenk et al. (2012a). These publications find 1 Ga for the formation age of Rheasilvia and at least 2.1 Ga for the formation age of Veneneia. In chapters 4 and 5 reasons for the disagreement are detailed. Three major reasons for disagreement can be identified.

I) *Geologic interpretation of measured areas:* Marchi et al. (2012c) and Schenk et al. (2012a) assume that no significant mass wasting inside the Rheasilvia basin occurred long after its formation. They extract the Rheasilvia formation age from the basin floor. A careful analysis of statements in Schenk et al. (2012a) reveals strong indication that the authors date Rheasilvia ejecta on the floor of the neighboring Veneneia basin with 2.1 Ga in their chronology system (see also next point). Thus, in their chronology system (asteroid-flux system) Rheasilvia ejecta are at least twice as old as the floor of the Rheasilvia basin, implying significant resurfacing processes up to 1 Ga after the basin formation. Hence, results by Marchi et al. (2012c) and Schenk et al. (2012a) are inconsistent.

A second indication that results by Marchi et al. (2012c) are inconsistent due to flawed geologic interpretation of measured counting areas is related to an undescribed crater plot in Fig. 14c by Williams et al. (2014a). A measurement by the co-author S. Marchi (the lead author of Marchi et al. (2012c)) is labeled with "Df" for Divalia Fossae. That is the equatorial trough system that formed as a by-product of the Rheasilvia impact event

(Jaumann et al., 2012b). In the Fig. by Williams et al. the Df measurement is fitted with a 2 Ga isochron of the model production function used by Marchi et al. (2012c) and Schenk et al. (2012a), indicating the formation of the Rheasilvia-connected trough system took place about 2 Ga ago (asteroid-flux system), very similar to the result from the floor of the Veneneia basin.

A third indication that the Rheasilvia formation age is higher than the crater retention age on its floor, can be found in Marchi et al. (2014). In that publication a measurement on Matronalia Rupes at the Rheasilvia basin rim is described. Marchi et al. (2014) fit both the crater distribution of the Rheasilvia floor (Marchi et al., 2012c) and the crater distribution of Matronalia Rupes with a 1 Ga isochron, in order to prove the same formation age of Rheasilvia ejecta at Matronalia Rupes and the floor of the Rheasilvia basin. However, cumulative frequencies of several of the largest crater size bins of the Matronalia measurement plot clearly above the fitted isochron, which point towards a higher formation age of Rheasilvia ejecta at Matronalia Rupes than the floor of Rheasilvia shows.

II) *Shape of the crater production function:* The lunar-like crater production function (chapter 4.2.2) shows a slightly steeper slope than the model production function by Marchi et al. (2014) for small diameters that includes the reference diameter of 1 km (Kneissl et al., 2014; chapter 5 and chapter 2.4). Even with the same chronology function these various slopes result in variable model ages depending on whether a crater distribution is fitted at diameters smaller or larger than 1 km as described in chapter 2.4. For the example of crater measurements on the ejecta blankets of Octavia and Oppia craters presented in chapters 4.3 and 6.4.3 as well as the Rheasilvia floor measurement by Schenk et al. (2012a) it can be demonstrated, that in the framework of the model production function by Marchi et al. Octavia, Oppia and the floor of Rheasilvia are roughly contemporary with ~1 Ga formation age (Fig. 8-1). From principles of superposition Octavia and Oppia clearly formed after Rheasilvia. Octavia and Oppia feature "orange material" ejecta blankets in Clementine color ratios that are interpreted to be most likely related to impact melt from Rheasilvia and/or Veneneia formation that was excavated by the Oppia and Octavia impact events (Le Corre et al., 2013). If that is true, it is not clear why the orange material is not observed in other parts of the Rheasilvia ejecta blanket as prominent as it is seen in the ejecta of Oppia and Octavia.

For the case of the lunar-like crater production function, Oppia and Octavia are about 1.4 Ga younger than the floor of Rheasilvia. As outlined in the previous point I) the floor of Rheasilvia most likely does not show the formation age of the basin. Considering a Rheasilvia formation age of 3.5 Ga (chapter 4) Oppia and Octavia are roughly 3 Ga younger than Rheasilvia. In this case the disappearance of the "orange" characteristic

of large parts of the Rheasilvia ejecta is plausible e.g. due to impact gardening.

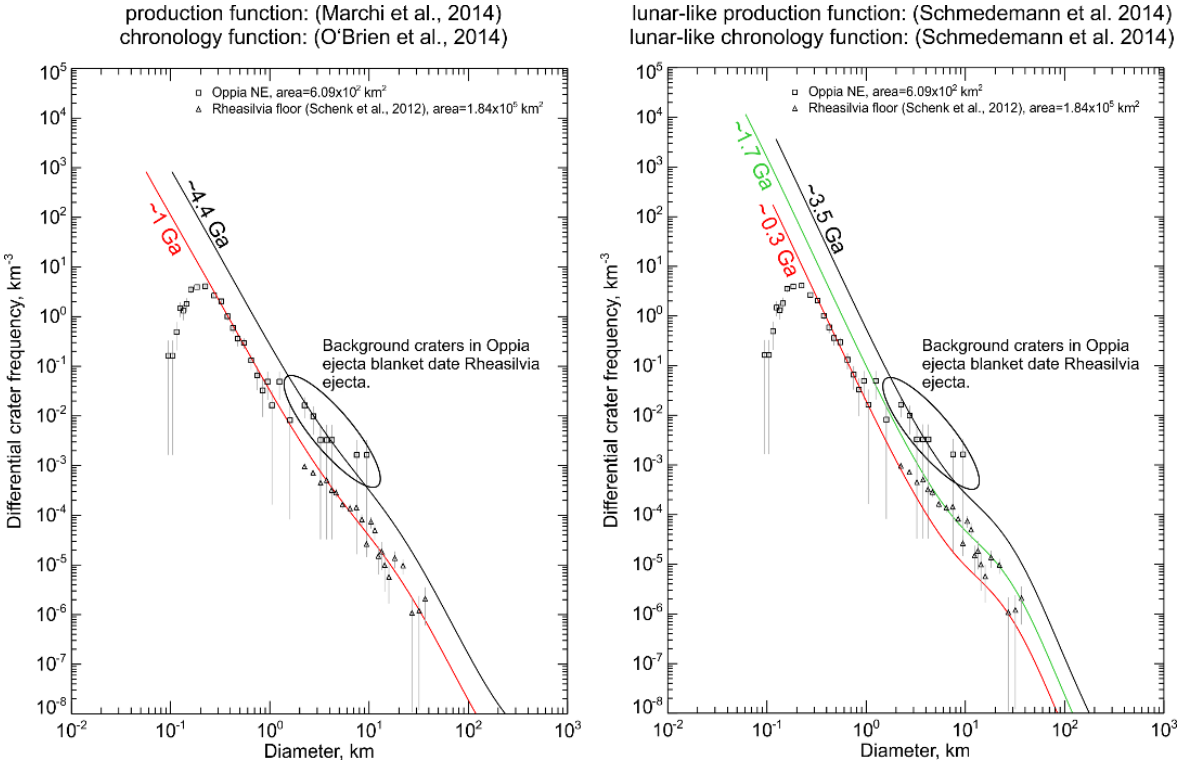


Fig. 8-1: Comparison of crater retention ages for lunar-like (Schmedemann et al., 2014a) and Marchi et al. (2014) production functions: Squares – Oppia NE measurement from chapter 4.3.2.8, triangles – Rheasilvia floor redigitized measurement from Schenk et al. (2012a). The Rheasilvia floor measurement is comparable to the Rheasilvia Ridge and Groove terrain measurement (chapters 4.3.2.3 and 5). Left panel: a single isochron at 1 Ga model age based on the model production function by Marchi et al. (2014) is able to fit both, the cater distribution on the Oppia ejecta blanket and on the floor of Rheasilvia, implying similar formation ages. Observed higher crater frequencies in the ejecta blanket of Rheasilvia are not considered with respect to the Rheasilvia formation age by Schenk et al. (2012a) and Marchi et al. (2014). Right panel: the steeper lunar-like production function result in an Oppia formation age, clearly younger than the floor of Rheasilvia (age difference: ~1.4 Ga). Besides other areas Schmedemann et al. (2014a; chapter 4.3) link crater frequencies on the Rheasilvia ejecta blanket to the basin formation age. Oppia formed on the proximal Rheasilvia ejecta. Thus, background craters that are still showing through the Oppia ejecta date the Rheasilvia formation with about 3.5 Ga in the lunar-like chronology system.

Shape of the crater chronology function: The shape of the chronology functions by O'Brien et al. (2014) and Schmedemann et al. (2014a) in chapter 4.2.3.1 are nearly identical for ages younger than ~3 Ga. For ages higher than that, differences occur up to 1 Ga in a way that the lunar-like chronology Schmedemann et al. (2014a) provides younger ages than the chronology by O'Brien et al. (2014), which is predominantly founded on dynamical models such as the Nice model (e.g. Morbidelli et al., 2012) and the E-Belt model (Bottke et al., 2012). Fig. 8-1 gives an example for background craters in the Oppia ejecta blanket that are used to date the formation of the Rheasilvia ejecta blanket. For respectively measured crater frequencies model ages from both chronologies divert by roughly 1 Ga. This is nearly the largest possible difference between the two chronologies. Going to even higher crater frequencies result in smaller differences again, because the shallow

chronology by O'Brien et al. (2014) quickly approaches the age of the Solar System but then shows a very steep characteristic close to the formation age of the Solar System. Thus, the age difference for the highest measured crater frequencies on Vesta, derived from the global distribution of craters ≥ 200 km is only ~600 Ma (chapter 4.7.3).
Results for the crater retention derived formation ages of the Veneneia basin and the Rheasilvia basin are compared with independent radiometric ages that record high energetic impacts on Vesta. For the lunar-like frame work a reasonably good correlation is found for the two most recent major events recorded in the Ar-Ar chronometer of Vesta derived HED meteorites (chapter 4.4). If crater frequencies presented in chapter 4.3 are used with the alternative chronology by O'Brien et al. (2014) then the formation of Rheasilvia occurred about 4.4 Ga ago (see also Fig. 8-1). That is in disagreement with the comparatively fresh morphology of the Rheasilvia basin and its ejecta blanket that are not superimposed by any of the major impact events recorded in the Ar-Ar chronometer of HED meteorites within the time frame between 3 and 4 Ga.

### 8.1.3 Mimas (chapter 7):

Crater measurements: Measurements of the crater size-frequency distribution on Mimas' heavily cratered plains in several areas that cover the satellites leading and trailing hemisphere revealed very similar crater frequencies in their overlapping sections. This result underlines the well-known non-existence of a clear apex-/antapex asymmetry that would be expected from heliocentric projectiles but is not observed in the Saturnian system (Neukum, 1985; Zahnle et al., 2003 and Dones et al., 2009). Furthermore, these measurements imply a nearly global uniform surface age for Mimas as a result of a geologically dead body. Only one measurement (A7) shows a clear diversion towards smaller crater frequencies. Because this area is located at the outer margin of the continuous ejecta blanket of the large crater Herschel, the measured deficiency in crater frequencies is interpreted as a resurfacing effect caused by the Herschel ejecta. Measurements conducted on the proximal Herschel ejecta and within the crater revealed very similar crater distributions as well. If the crater frequencies from the Herschel resurfaced areas and the heavily cratered plains are compared with each other, a clear offset (factor: ~6) is found with lower frequencies on the Herschel ejecta.
Derivation of the crater production function: The nature of the projectiles in the Saturnian system is still controversial. Mainly dynamicists argue for ecliptic comets or Kuiper Belt Objects that impact the Saturnian satellites from heliocentric orbits at hyper velocity (e.g., Zahnle et al., 2003 and Dones et al., 2009). That view is contradicted by the non-existence of an apex-/antapex asymmetry and an observed crater size-frequency distribution that is much different from the size-frequency distribution of observed cometary nuclei (e.g., Neukum, 1985 and Zahnle et al., 2003). However, the small diameter (< ~50 km) size distribution of Kuiper Belt Objects is still unknown due to observational limits. In the manuscript presented in chapter 7 the crater size frequency distributions that are observed on Mimas and Iapetus are scaled to projectile sizes for various dynamic cases. By assuming the

same projectile population at both bodies, a comparison of the cratering record derived projectile distributions for the chosen dynamic cases were used in order to identify the most likely impact conditions at the two different levels in the gravity well of Saturn where Iapetus and Mimas reside. Crater data from Iapetus were also used for crater scaling purposes and chronology calibration for Mimas. Further comparison of derived projectile distributions with body size-frequency distributions of known small body populations (Kuiper Belt Objects, comets and the Moon impacting Main Belt asteroids) led to the conclusion that the observed crater distributions on Mimas and Iapetus are consistent with a collisionally evolved projectile population similar to the one that impacted the lunar surface but with densities similar to cometary nuclei at very low velocities on the order of ~600 m/s. These boundary conditions provided the parameters for scaling the lunar crater production function to Iapetus and Mimas. The problematic transition in scaling material behavior going from basaltic regolith to cold icy regolith was solved by a modified surface gravity for the icy satellites. The modification was applied based on the observed simple to complex transitions on Iapetus and Vesta. The resulting lunar-like crater production function is purely derived from observed data and simple ratio equations. It fits the observed crater distributions on Iapetus and Mimas reasonably well. However, it diverts significantly from previously published production functions based on a cometary projectile source (Zahnle et al., 2003).

Derivation of the chronology function: Previously published chronologies for the Saturnian satellites are derived from orbital mechanics and observed small body populations (e.g. Zahnle et al., 2003). A different approach is used in the presented manuscript (chapter 7). By geophysical modeling Castillo-Rogez et al. (2007) derived a surface age of roughly 4.4 Ga for the oldest crust rigid enough to retain even large impact basins on Iapetus. This is used in an approach by Neukum et al. (2006) to calibrate the crater chronology function of Iapetus by assuming that the highest crater frequencies found on Iapetus reflect a crater retention age of 4.4 Ga. The shape of the used chronology function equals the lunar chronology but is vertically offset in order to satisfy the mentioned boundary condition. The conversion of the lunar-like chronology from Iapetus to Mimas assumes the same flux characteristic and projectile source for both bodies. Given the lower surface gravity on Mimas the slightly different crater scaling required a respective scaling of the chronology function as well.

Resulting model ages: The application of the derived crater production and chronology functions to the measured crater frequencies on Mimas result in relatively high surface model ages of ~4.3 Ga for the heavily cratered plains and ~4 Ga for the Herschel impact. Previously published chronologies by Zahnle et al. (2003) provide two cases for Mimas. In the case A scenario the measured crater frequencies for the heavily cratered plains, fitted with the lunar-like production function, give a model age of ~4.4 Ga and for the Herschel resurfaced areas only 2 Ga. Case B provides much younger ages of 1.5 Ga and 0.3 Ga for the heavily cratered plains and the Herschel resurfaced areas, respectively. Thus, the presented cratering chronology for Mimas is only in rough agreement with the case A scenario by Zahnle et al. (2003) for the heavily cratered plains. All other ages divert significantly. The lunar-like production function was used for Zahnle model ages,

because it shows higher similarity to the actually measured crater distributions than the production function for Mimas provided by Zahnle et al. (2003). Given the geophysically determined surface age estimate for Iapetus (Castillo-Rogez et al., 2007), it appears rather unlikely that Mimas shows highest surface ages on the order of 1 to 2 Ga. Thus, the lunar-like approach gives reasonable model ages although no independent chronology is available yet. Much wore work is required in order to understand the main projectile source and projectile dynamics in the Saturnian system.

Results in the broader context of Solar System evolution:

Assuming the derived crater production and chronology functions, conducted measurements and respective interpretations result in reasonable surface model ages, the results presented in this thesis add valuable information for understanding the Solar System around an important time of its evolution. That is its dynamical transition from a state of accretion to a quasi-stable configuration around 3.5 Ga ago. The declining impact flux in the lunar chronology during the first billion years of Solar System evolution is direct evidence that the rate of mass accretion was decreasing until about 3.5 Ga ago. Since that time collisions in the asteroid Main Belt have delivered collisional debris at a nearly constant rate. The period of the exponential decay in impact rates appears to be accompanied by basin forming events as well. Thus, this relationship was proposed in order to derive crater retention ages from the Jovian satellites by setting the age of the youngest basin in the Jovian system (Gilgamesh on Ganymede) to the age of the youngest lunar basin (Orientale; e.g. Neukum, 1984). Results from Vesta, Mimas and the possible capture of Phobos around 3.9 Ga are in agreement with this view. Furthermore, the timing of the last major break up events of the Ida and Lutetia precursor bodies around 3.5 Ga may point to the reason why basin formation stopped around that time. Ida and Lutetia are in the right size range in order to form basins for example on the Moon. It appears that around 3.5 Ga ago break up events of larger bodies within the Main Belt that resulted in basin forming debris ceased. Because of the similar timing of youngest basin forming impacts on Vesta and the inner Solar System bodies and generation of basin related projectiles, the dynamical models described in the Nice (e.g. Morbidelli et al., 2012) and E-Belt (Bottke et al., 2012) models appear to be incomplete. These dynamical models predict clearly different ages for the cessation of basin forming events as it is illustrated for instance for the formation age of the Rheasilvia basin (3.5 vs. 4.4 Ga; Table 4-6) in the two chronologies for Vesta. Furthermore, the high correlation between crater retention ages for the Rheasilvia and Veneneia basins on Vesta and radiometric ages of Vesta derived HED meteorites in the lunar-like chronology (Fig. 4-16) that is not found for the Nice-model based chronology is a strong argument against a dynamical evolution of the Solar System as it is described in the Nice and E-Belt models.
In order to understand why a lunar-like crater size-frequency distribution is found even in the outer Solar System, the origin and material as well as dynamical characteristics of possible projectile populations have to be taken into account. Smaller Main Belt asteroids and debris from collisions among the asteroids is driven

by the collisions themselfes and radiation forces such as the Yarkovsky effect into different orbits. On this migration these bodies collide with other asteroids or could even reach a resonant zone in the asteroid Main Belt. Inside the resonant zones they are quickly dynamically excited and thrown onto planet crossing orbits (e.g. O'Brien and Greenberg, 2005). The radiation related migration acts as a size dependent sink for small bodies within the Main Belt and could explain why the observed transient small body distribution is shallower than small crater distributions found on planetary surfaces, where craters accumulate over time (chapter 4.2.2). Gravitational interactions with the major planets enable small bodies to migrate independently of their size between the planets. Thus, asteroidal material impacting the major planets or their satellites is predominantly derived by a roughly fixed ratio from the numerous mean motion resonances in the Main Belt. The ratio relates to the effectiveness of each resonance. The most effective resonances are v6 at the inner Main Belt border, 3:1 at about 2.5 AU and the 5:2 resonance at about 2.825 AU (Gladman et al., 1997). These resonances occupy the inner and middle Main Belt, the body size-frequency distribution of which is slightly different from the average Main Belt. The small body migration between the major planets could explain why even in the outer Solar System the same crater distribution is observed that is also known from the Moon and which corresponds well with the inner and middle Main Belt body distribution. In principle also Kuiper Belt objects do the same migration between the major planets (Levison and Duncan, 1997) but much longer orbital periods in the distant outer Solar System require longer time scales for orbit changing interaction with other bodies. Furthermore, icy Kuiper Belt Objects may simply sublimate on their way into the inner Solar System. Sublimation acts more efficiently on small bodies than on larger ones, because of the higher surface to volume ratio. Hence, there is a chance of Kuiper Belt projectiles impacting the satellites in the outer Solar System, if they hit their target soon after the projectiles left the Kuiper Belt. Therefore, cratering records of Saturnian satellites could show some influence by Kuiper Belt objects but most likely at large projectile sizes (> ~20 km) rather than at smaller diameters.

## 8.2 Outlook:

The Cassini mission will end in 2017. Until then it will provide more valuable imaging data of the Saturnian satellites. Moreover, existing Cassini and Voyager data will be reanalyzed and further in-depth analysis will be conducted in order to continue the investigation of the cratering record of the Saturnian satellites and understand the nature, dynamics and importance of the impacting projectile populations. Built on this foundation crater production and chronology functions can be derived or improved for each of the Saturnian satellites.
With the ongoing Dawn mission to the dwarf planet Ceres respective crater production and chronology functions are currently under development. It is expected that Ceres has an ice-rich layer in excess of 100 km thickness (McCord et al., 2012a) just tens of meters under its dusty surface regolith (pers. com. J. Castillo-Rogez). The ice layer requires an advanced crater scaling technique, because of the

much different material parameters compared with basaltic bodies. However, the experience gained from crater scaling applications on icy bodies in the Saturnian system is very helpful in deriving a reliable set of crater functions for Ceres. A first test of those functions is planned on the early imaging data from the Dawn at Ceres mission in spring 2015.

Following in short order in July 2015 the targeted fly-by of the New Horizons spacecraft at the Pluto-Charon system will provide high resolution imaging data of the planetary surfaces in the Plutonian system. Although not involved in the New Horizons team, publicly available data will allow for analyzing the crater distribution in the Plutonian system. That will certainly provide extremely valuable data for understanding the projectile distributions in the outer Solar system. Following the Pluto fly-by, New Horizons will be aimed at a Kuiper Belt Object even further out in the Solar system. A few candidates are already identified and at least one can definitely serve as target for a fly-by mission in the time frame of 2018-2020 (pers. com. A. Stern).

In July 2016 the Juno mission[3], a NASA spacecraft of the New Frontiers program, will arrive at Jupiter. This mission is dedicated to study the Jovian magnetosphere and atmosphere in great detail and depth. This will possibly allow for the investigation of atmospheric residuals of observed impacts on Jupiter. By chance even a direct observation of small impacts in Jupiter's atmosphere might be possible. The probably most famous of such events was the impact of the fragments of comet Shoemaker-Levy 9 in 1994. But also in recent years amateur astronomers observed smaller impacts that might be caused by asteroids as well. Due to different composition of both classes of small bodies, they may have left behind characteristic traces in the Jovian atmosphere that could help in understanding the nature of the impacting projectiles.

Following the US-led Juno mission in the early 2030s the European JUICE Mission[4] will start to investigate the Jovian satellite system. Besides other tasks one goal of the mission will be the generation of high resolution imaging data of the Galilean satellites surpassing the already high quality imaging data by the Galileo mission that suffered from a low data transmission rate due to an incompletely unfolded high gain antenna. This high quality data from JUICE will further support our understanding of the cratering records on the Jovian satellites and the respective projectile populations.

In the tradition of the Galileo and still active Cassini missions a Uranus and Neptune orbiter mission would be very helpful in order to fill in large gaps of our knowledge about the ice giants and their role in the Solar System in many respects. From the Voyager2 mission we know for instance about the weird processes of nitrogen geysers on the surface of Triton, which is certainly a captured Kuiper Belt Object, because it circles Neptune on a retrograde orbit. It features an extreme apex-/antapex asymmetry (e.g. Dones et al., 2009) that probably implies a substantial population of prograde projectiles in orbit about Neptune. Understanding the Neptunian system, thus could also help in understanding all the other giant planet satellite systems much better.

[3] http://www.nasa.gov/mission_pages/juno/overview/index.html#.VFd_88nwu10
[4] http://sci.esa.int/juice/

Furthermore, ground truth data is needed in order to verify results of earlier investigations that are exclusively based on remote sensing data or just model data. In the case of Vesta HED meteorites give confidence that the lunar-like approach gives reasonable results. Unfortunately, in general the sample sites of meteorites are unknown. Thus, linking crater retention ages and radiometric ages of meteorites is problematic.

Any mission that puts a lander on the surface of any satellite should be considered for the feasibility of a sample return. Unfortunately this attempt with respect to the Russian Phobos Grunt mission failed unexpectedly already in low Earth orbit.

Another interesting development for the aim of understanding the Solar System's small body populations is the planning and construction of a new generation of ground-based telescopes with aperture sizes on the order of 30 m that will help to push the observational limits of small body populations to much smaller diameters. For instance, based on the small body inventory of the JPL Horizon system from the 72 bodies (≥ 15 km) currently (02.11.2014) known, that cross the orbit of Saturn, 10 were discovered only in 2014 and 27 within the last 5 years. These numbers imply that the investigation of our cosmic backyard has just begun and many more discoveries lie ahead of us. A better understanding of the small body populations and impact risk development throughout the Solar System history can also help in understanding how life on planet Earth coped with a changing rate of catastrophic impact events. In mankind's own interest of survival, better knowledge about the orbits and size-frequency distributions of even very small objects in the Solar System will help in predicting impact risks on Earth. The comparatively small bolide of Chelyabinsk in 2013 appeared out of the blue sky and injured more than 1200 people. In the future, such events could possibly be predicted and people could be protected if necessary.

# References

Adams, J.B., Goullaud, L.H., 1978. Plagioclase feldspars - Visible and near infrared diffuse reflectance spectra as applied to remote sensing, Lunar and Planetary Science Conference Proceedings, pp. 2901-2909.

Adams, J.B., Horz, F., Gibbons, R.V., 1979. Effects of Shock-Loading on the Reflectance Spectra of Plagioclase, Pyroxene, and Glass, Lunar and Planetary Science Conference, pp. 1-3.

Alexander, C.M., Bowden, R., Fogel, M.L., Howard, K.T., Herd, C.D., Nittler, L.R., 2012. The provenances of asteroids, and their contributions to the volatile inventories of the terrestrial planets. Science 337, 721-723.

Alvarellos, J.L., Zahnle, K.J., Dobrovolskis, A.R., Hamill, P., 2005. Fates of satellite ejecta in the Saturn system. Icarus 178, 104-123.

Anderson, J.A., Sides, S.C., Soltesz, D.L., Sucharski, T.L., Becker, K.J., Stansbery, E., 2004. Modernization of the Integrated Software for Imagers and Spectrometers, In: Mackwell, S. (Ed.), Lunar and Planetary Science Conference, p. 2039.

Archinal, B.A., A'Hearn, M.F., Bowell, E., Conrad, A., Consolmagno, G.J., Courtin, R., Fukushima, T., Hestroffer, D., Hilton, J.L., Krasinsky, G.A., Neumann, G., Oberst, J., Seidelmann, P.K., Stooke, P., Tholen, D.J., Thomas, P.C., Williams, I.P., 2011. Report of the IAU Working Group on Cartographic Coordinates and Rotational Elements: 2009. Celestial Mechanics and Dynamical Astronomy 109, 101-135.

Arvidson, R., 1979. Crater Analysis Techniques Working Group - Standard techniques for presentation and analysis of crater size-frequency data. Icarus 37, 467-474.

Baldwin, R.B., 1964. Lunar crater counts. The Astronomical Journal 69, 377-392.

Baldwin, R.B., 1974. Was there a "terminal lunar cataclysm" 3.9-4.0×109 years ago? Icarus 23, 157-166.

Baldwin, R.B., 2006. Was there ever a Terminal Lunar Cataclysm?: With lunar viscosity arguments. Icarus 184, 308-318.

Barlow, N.G., Boyce, J.M., Costard, F.M., Craddock, R.A., Garvin, J.B., Sakimoto, S.E.H., Kuzmin, R.O., Roddy, D.J., Soderblom, L.A., 2000. Standardizing the nomenclature of Martian impact crater ejecta morphologies. Journal of Geophysical Research 105, 26733-26738.

Barlow, N.G., Strom, R.G., 1984. Martian crater size distributions and terrain age, NASA Tech. Memo., NASA TM-86246, pp. 85-86.

Barnouin-Jha, O.S., Schultz, P.H., 1998. Lobateness of impact ejecta deposits from atmospheric interactions. Journal of Geophysical Research 103, 25739-25756.

Beck, A.W., McSween, H.Y., Jr., 2010. Diogenites as polymict breccias composed of orthopyroxenite and harzburgite. Meteoritics and Planetary Science 45, 850-872.

Becker, K.J., Anderson, J.A., Barrett, J.M., Sides, S.C., Titus, T.N., 2012. ISIS Support for Dawn Instruments, Lunar and Planetary Institute Science Conference Abstracts, p. 2892.

Becker, K.J., Anderson, J.A., Weller, L.A., Becker, T.L., 2013. ISIS Support for NASA Mission Instrument Ground Data Processing Systems, Lunar and Planetary Science Conference, p. 2829.

Becker, L., Poreda, R.J., Basu, A.R., Pope, K.O., Harrison, T.M., Nicholson, C., Iasky, R., 2004. Bedout: A Possible End-Permian Impact Crater Offshore of Northwestern Australia. Science 304, 1469-1476.

Bell, J.F., McSween, H.Y., Crisp, J.A., Morris, R.V., Murchie, S.L., Bridges, N.T., Johnson, J.R., Britt, D.T., Golombek, M.P., Moore, H.J., Ghosh, A., Bishop, J.L., Anderson, R.C., Brückner, J., Economou, T., Greenwood, J.P., Gunnlaugsson, H.P., Hargraves, R.M., Hviid, S., Knudsen, J.M., Madsen, M.B., Reid, R., Rieder, R., Soderblom, L., 2000. Mineralogic and compositional properties of Martian soil and dust: Results from Mars Pathfinder. Journal of Geophysical Research 105, 1721-1756.

Belton, M.J.S., Chapman, C.R., Klaasen, K.P., Harch, A.P., Thomas, P.C., Veverka, J., McEwen, A.S., Pappalardo, R.T., 1996. Galileo's Encounter with 243 Ida: An Overview of the Imaging Experiment. Icarus 120, 1-19.

Bierhaus, E.B., Chapman, C.R., Merline, W.J., Brooks, S.M., Asphaug, E., 2001. Pwyll Secondaries and Other Small Craters on Europa. Icarus 153, 264-276.

Bierhaus, E.B., Dones, L., Alvarellos, J.L., Zahnle, K., 2012. The role of ejecta in the small crater populations on the mid-sized saturnian satellites. Icarus 218, 602-621.

Bills, B.G., Neumann, G.A., Smith, D.E., Zuber, M.T., 2005. Improved estimate of tidal dissipation within Mars from MOLA observations of the shadow of Phobos. Journal of Geophysical Research: Planets 110, E07004.

Binzel, R.P., Gaffey, M.J., Thomas, P.C., Zellner, B.H., Storrs, A.D., Wells, E.N., 1997. Geologic Mapping of Vesta from 1994 Hubble Space Telescope Images. Icarus 128, 95-103.

Binzel, R.P., Xu, S., 1993. Chips off of Asteroid 4 Vesta: Evidence for the Parent Body of Basaltic Achondrite Meteorites. Science 260, 186-191.

Blanco, C., Catalano, S., 1979. UBV photometry of Vesta. Icarus 40, 359-363.

Bobrovnikoff, N.T., 1929. The spectra of minor planets. Lick Observatory Bulletin 14, 18-27.

Bogard, D.D., 1995. Impact Ages of Meteorites - a Synthesis. Meteoritics 30, 244-268.

Bogard, D.D., 2011. K-Ar ages of meteorites: Clues to parent-body thermal histories. Chemie der Erde - Geochemistry, vol. 71, issue 3, 207-226.

Bogard, D.D., 2013. Analysis of Thermal Conditions Required to Reset Ar-Ar Ages, Lunar and Planetary Institute Science Conference Abstracts, p. 1022.

Bogard, D.D., Garrison, D.H., 2003. 39Ar-40Ar ages of eucrites and thermal history of asteroid 4 Vesta. Meteoritics & Planetary Science 38, 669-710.

Bottke Jr, W.F., Morbidelli, A., Jedicke, R., Petit, J.-M., Levison, H.F., Michel, P., Metcalfe, T.S., 2002. Debiased Orbital and Absolute Magnitude Distribution of the Near-Earth Objects. Icarus 156, 399-433.

Bottke, W.F., Durda, D.D., Nesvorny, D., Jedicke, R., Morbidelli, A., Vokrouhlicky, D., Levison, H., 2005a. The fossilized size distribution of the main asteroid belt. Icarus 175, 111-140.

Bottke, W.F., Durda, D.D., Nesvorný, D., Jedicke, R., Morbidelli, A., Vokrouhlicky, D., Levison, H.F., 2005b. Linking the collisional history of the main asteroid belt to its dynamical excitation and depletion [ Erratum: 2006Icar..183..235B ]. Icarus 179, 63-94.

Bottke, W.F., Jr., Vokrouhlický, D., Rubincam, D.P., Nesvorný, D., 2006. The Yarkovsky and Yorp Effects: Implications for Asteroid Dynamics. Annual Review of Earth and Planetary Sciences 34, 157-191.

Bottke, W.F., Nolan, M.C., Greenberg, R., Kolvoord, R.A., 1994. Velocity Distributions among Colliding Asteroids. Icarus 107, 255-268.

Bottke, W.F., Vokrouhlicky, D., Chapman, C.R., Nesvorny, D., 2007. Gaspra's Steep Crater Population Was Produced by a Large Recent Breakup in the Main Asteroid Belt, Lunar and Planetary Science Conference, 1338 ed, League City, Texas, p. 2165.

Bottke, W.F., Vokrouhlický, D., Minton, D., Nesvorny, D., Morbidelli, A., Brasser, R., Simonson, B., Levison, H.F., 2012. An Archaean heavy bombardment from a destabilized extension of the asteroid belt. Nature 485, 78-81.

Bowling, T.J., Johnson, B.C., Melosh, H.J., Ivanov, B.A., O'Brien, D.P., Gaskell, R., Marchi, S., 2013. Antipodal terrains created by the Rheasilvia basin forming impact on asteroid 4 Vesta. Journal of Geophysical Research (Planets) 118, 1821-1834.

Britt, D.T., Pieters, C.M., 1994. Darkening in black and gas-rich ordinary chondrites: The spectral effects of opaque morphology and distribution. Geochimica et Cosmochimica Acta 58, 3905-3919.

Britt, D.T., Yeomans, D., Housen, K., Consolmagno, G., 2002. Asteroid Density, Porosity, and Structure. Asteroids III, W. F. Bottke Jr., A. Cellino, P. Paolicchi, and R. P. Binzel (eds), University of Arizona Press, Tucson, 485-500.

Brown, P.G., Assink, J.D., Astiz, L., Blaauw, R., Boslough, M.B., Borovicka, J., Brachet, N., Brown, D., Campbell-Brown, M., Ceranna, L., Cooke, W., de Groot-Hedlin, C., Drob, D.P., Edwards, W., Evers, L.G., Garces, M., Gill, J., Hedlin, M., Kingery, A., Laske, G., Le Pichon, A., Mialle, P., Moser, D.E., Saffer, A., Silber, E., Smets, P., Spalding, R.E., Spurný, P., Tagliaferri, E., Uren, D., Weryk, R.J., Whitaker, R., Krzeminski, Z., 2013. A 500-kiloton airburst over Chelyabinsk and an enhanced hazard from small impactors. Nature 503, 238-241.

Buchanan, P.C., Lindstrom, D.J., Mittlefehldt, D.W., Koeberl, C., Reimold, W.U., 2000. The South African polymict eucrite Macibini. Meteoritics and Planetary Science 35, 1321-1331.

Buchanan, P.C., Zolensky, M.E., Reid, A.M., 1993. Carbonaceous chondrite clasts in the howardites Bholghati and EET87513. Meteoritics 28, 659-669.

Buczkowski, D.L., Barnouin-Jha, O.S., Prockter, L.M., 2008. 433 Eros lineaments: Global mapping and analysis. Icarus 193, 39-52.

Buczkowski, D.L., Wyrick, D.Y., Iyer, K.A., Kahn, E.G., Scully, J.E.C., Nathues, A., Gaskell, R.W., Roatsch, T., Preusker, F., Schenk, P.M., Le Corre, L., Reddy, V., Yingst, R.A., Mest, S., Williams, D.A., Garry, W.B., Barnouin, O.S., Jaumann, R., Raymond, C.A., Russell, C.T., 2012. Large-scale troughs on Vesta: A signature of planetary tectonics. Geophysical Research Letters 39, 18205.

Buczkowski, D.L., Wyrick, D.Y., Toplis, M., Yingst, R.A., Williams, D.A., Garry, W.B., Mest, S., Kneissl, T., Scully, J.E.C., Nathues, A., De Sanctis, M.C., LeCorre, L., Reddy, V., Hoffmann, M., Ammannito, E., Frigeri, A., Tosi, F., Preusker, F., Roatsch, T., Raymond, C.A., Jaumann, R., Pieters, C.M., Russell, C.T., 2014. The unique geomorphology and physical properties of the Vestalia Terra plateau. Icarus 244, 89-103.

Burbine, T.H., Buchanan, P.C., 2010. Determining Constraints on Crustal Formation Processes on Vesta Using Data from the Dawn Mission, Lunar and Planetary Science Conference, p. 1843.

Burbine, T.H., Buchanan, P.C., Binzel, R.P., Bus, S.J., Hiroi, T., Hinrichs, J.L., Meibom, A., McCoy, T.J., 2001. Vesta, Vestoids, and the howardite, eucrite, diogenite group: Relationships and the origin of spectral differences. Meteoritics and Planetary Science 36, 761-781.

Burns, J.A., 1978. The dynamical evolution and origin of the Martian moons. Vistas in Astronomy 22, Part 2, 193-210.

Capria, M.T., Tosi, F., Capaccioni, F., de Sanctis, M.C., Palomba, E., Ammannito, E., Titus, T.N., Combe, J.P., Toplis, M., Sunshine, J., Russell, C.T., Raymond, C.A., 2012. Thermal Inertia Variations on the Surface of Vesta from the Dawn Data, Publication: 43rd Lunar and Planetary Science Conference, held March 19--23, 2012 at The Woodlands, Texas. LPI Contribution No. 1659, id.1863.

Carr, M.H., Crumpler, L.S., Cutts, J.A., Greeley, R., Guest, J.E., Masursky, H., 1977. Martian impact craters and emplacement of ejecta by surface flow. Journal of Geophysical Research 82, 4055-4065.

Carr, M.H., Kirk, R.L., McEwen, A., Veverka, J., Thomas, P., Head, J.W., Murchie, S., 1994. The Geology of Gaspra. Icarus 107, 61-71.

Castillo-Rogez, J.C., Matson, D.L., Sotin, C., Johnson, T.V., Lunine, J.I., Thomas, P.C., 2007. Iapetus' geophysics: Rotation rate, shape, and equatorial ridge. Icarus 190, 179-202.

Chapman, C.R., Cohen, B.A., Grinspoon, D.H., 2007. What are the real constraints on the existence and magnitude of the late heavy bombardment? Icarus 189, 233-245.

Chapman, C.R., McKinnon, W.B., 1986. Cratering of planetary satellites, In: Burns, J.A., Matthews, M.S. (Eds.), Satellites. University of Arizona Press, Tucson, pp. 492-580.

Chapman, C.R., Ryan, E.V., Merline, W.J., Neukum, G., Wagner, R., Thomas, P.C., Veverka, J., Sullivan, R.J., 1996a. Cratering on Ida. Icarus 120, 77-86.

Chapman, C.R., Veverka, J., Belton, M.J.S., Neukum, G., Morrison, D., 1996b. Cratering on Gaspra. Icarus 120, 231-245.

Chesley, S.R., Ostro, S.J., Vokrouhlický, D., Čapek, D., Giorgini, J.D., Nolan, M.C., Margot, J.-L., Hine, A.A., Benner, L.A.M., Chamberlin, A.B., 2003. Direct Detection of the Yarkovsky Effect by Radar Ranging to Asteroid 6489 Golevka. Science 302, 1739-1742.

Chou, C.-L., Boynton, W.V., Kimberlin, J., Wasson, J.T., Bild, R.W., 1976. Trace element evidence regarding a chondritic component in howardite meteorites, In: Merrill, R.B. (Ed.), Lunar and Planetary Science Conference Proceedings, pp. 3501-3518.

Cintala, M.J., Head, J.W., Veverka, J., 1978. Characteristics of the cratering process on small satellites and asteroids, Lunar and Planetary Science Conference, 1575 ed. Pergamon Press, Houston, Texas, pp. 3803-3830.

Cloutis, E.A., Gaffey, M.J., 1991. Pyroxene Spectroscopy Revisited - Spectral-Compositional Correlations and Relationship to Geothermometry. J Geophys Res-Planet 96, 22809-22826.

Cloutis, E.A., Gaffey, M.J., Jackowski, T.L., Reed, K.L., 1986. Calibrations of phase abundance, composition, and particle size distribution for olivine-orthopyroxene mixtures from reflectance spectra. Journal of Geophysical Research 91, 11641.

Cloutis, E.A., Gaffey, M.J., Smith, D.G.W., Lambert, R.S.J., 1990. Reflectance spectra of mafic silicate-opaque assemblages with applications to meteorite spectra. Icarus 84, 315-333.

Cloutis, E.A., Hudon, P., Romanek, C.S., Bishop, J.L., Reddy, V., Gaffey, M.J., Hardersen, P.S., 2010. Spectral reflectance properties of ureilites. Meteoritics and Planetary Science 45, 1668-1694.

Crater Analysis Techniques Working Group, Arvidson, R.E., Boyce, J., Chapman, C., Cintala, M., Fulchignoni, M., Moore, H., Neukum, G., Schultz, P., Soderblom, L., Strom, R., Woronow, A., Young, R., 1979. Standard techniques for presentation and analysis of crater size-frequency data. Icarus, vol. 37, Feb. 1979, 467-474.

Cuk, M., Gladman, B.J., Stewart, S.T., 2010. Constraints on the source of lunar cataclysm impactors. Icarus 207, 590-594.

Daubar, I.J., McEwen, A.S., Byrne, S., Kennedy, M.R., Ivanov, B., 2013. The current martian cratering rate. Icarus 225, 506-516.

Davies, M.E., Colvin, T.R., Belton, M.J.S., Veverka, J., Thomas, P.C., 1996. The Direction of the North Pole and the Control Network of Asteroid 243 Ida. Icarus 120, 33-37.

Davis, D.R., Farinella, P., 1997. Collisional Evolution of Edgeworth–Kuiper Belt Objects. Icarus 125, 50-60.

Davis, D.R., Housen, K.R., Greenberg, R., 1981. The unusual dynamical environment of PHOBOS and Deimos. Icarus 47, 220-233.

Davison, T.M., Collins, G.S., Ciesla, F.J., 2010. Numerical modelling of heating in porous planetesimal collisions. Icarus 208, 468-481.

de Elía, G.C., Brunini, A., 2007. Collisional and dynamical evolution of the main belt and NEA population. Astronomy and Astrophysics 466, 1159-1177.

de Sanctis, M.C., Coradini, A., Ammannito, E., Filacchione, G., Capria, M.T., Fonte, S., Magni, G., Barbis, A., Bini, A., Dami, M., Ficai-Veltroni, I., Preti, G., 2011. The VIR Spectrometer. Space Science Reviews 163, 329-369.

Denevi, B.W., Blewett, D.T., Buczkowski, D.L., Capaccioni, F., Capria, M.T., De Sanctis, M.C., Garry, W.B., Gaskell, R.W., Le Corre, L., Li, J.Y., Marchi, S., McCoy, T.J., Nathues, A., O'Brien, D.P., Petro, N.E., Pieters, C.M., Preusker, F., Raymond, C.A., Reddy, V., Russell, C.T., Schenk, P., Scully, J.E., Sunshine, J.M., Tosi, F., Williams, D.A., Wyrick, D., 2012a. Pitted terrain on Vesta and implications for the presence of volatiles. Science 338, 246-249.

Denevi, B.W., Koeber, S.D., Robinson, M.S., Garry, W.B., Hawke, B.R., Tran, T.N., Lawrence, S.J., Keszthelyi, L.P., Barnouin, O.S., Ernst, C.M., Tornabene, L.L., 2012b. Physical constraints on impact melt properties from Lunar Reconnaissance Orbiter Camera images. Icarus 219, 665-675.

Denk, T., Neukum, G., Roatsch, T., Porco, C.C., Burns, J.A., Galuba, G.G., Schmedemann, N., Helfenstein, P., Thomas, P.C., Wagner, R.J., West, R.A., 2010. Iapetus: Unique Surface Properties and a Global Color Dichotomy from Cassini Imaging. Science 327, 435-439.

Desnoyers, C., Jerome, D.Y., 1977. The Malvern howardite - A petrological and chemical discussion. Geochimica et Cosmochimica Acta 41, 81-86.

Dohnanyi, J.S., 1969. Collisional model of asteroids and their debris. Journal of Geophysical Research 74, 2531-2554.

Dohnanyi, J.S., 1971. Fragmentation and Distribution of Asteroids. NASA Special Publication 267, 263.

Dones, L., Chapman, C.R., McKinnon, W.B., Melosh, H.J., Kirchoff, M.R., Neukum, G., Zahnle, K.J., 2009. Icy Satellites of Saturn: Impact Cratering and Age Determination, In: Dougherty, M.K., Esposito, L.W., Krimigis, S.M. (Eds.), Saturn from Cassini-Huygens. Springer Netherlands, pp. 613-635.

Farinella, P., Vokrouhlický, D., Hartmann, W.K., 1998. Meteorite Delivery via Yarkovsky Orbital Drift. Icarus 132, 378-387.

Fassett, C.I., Head, J.W., Kadish, S.J., Mazarico, E., Neumann, G.A., Smith, D.E., Zuber, M.T., 2012. Lunar impact basins: Stratigraphy, sequence and ages from superposed impact crater populations measured from Lunar Orbiter Laser Altimeter (LOLA) data. J Geophys Res-Planet 117.

Feierberg, M.A., Drake, M.J., 1980. The meteorite-asteroid connection - The infrared spectra of eucrites, shergottites, and Vesta. Science 209, 805-807.

Fernandes, V., Artemieva, N., 2012. Impact Ejecta Temperature Profile on the Moon --- What are the Effects on the Ar-Ar Dating Method? Publication: 43rd Lunar and Planetary Science Conference, held March 19--23, 2012 at The Woodlands, Texas. LPI Contribution No. 1659, id.1367.

Fernandes, V.A., Fritz, J., Weiss, B.P., Garrick-Bethell, I., Shuster, D.L., 2013. The bombardment history of the Moon as recorded by $^{40}$Ar-$^{39}$Ar chronology. Meteoritics & Planetary Science 48, 241–269.

Festou, M.C., Stern, S.A., Tozzi, G.P., 1991. Asteroid 4 Vesta - Simultaneous visible and ultraviolet IUE observations. Icarus 94, 218-231.

Filacchione, G., Capaccioni, F., Clark, R.N., Cuzzi, J.N., Cruikshank, D.P., Coradini, A., Cerroni, P., Nicholson, P.D., McCord, T.B., Brown, R.H., Buratti, B.J., Tosi, F., Nelson, R.M., Jaumann, R., Stephan, K., 2010. Saturn's icy satellites investigated by Cassini-VIMS II. Results at the end of nominal mission. Icarus 206, 507-523.

Fischer-Gödde, M., Becker, H., 2012. Osmium isotope and highly siderophile element constraints on ages and nature of meteoritic components in ancient lunar impact rocks. Geochimica et Cosmochimica Acta 77, 135-156.

Fraser, W.C., Kavelaars, J.J., Holman, M.J., Pritchet, C.J., Gladman, B.J., Grav, T., Jones, R.L., MacWilliams, J., Petit, J.M., 2008. The Kuiper belt luminosity function from $m_R$=21 to 26. Icarus 195, 827-843.

Gaffey, M.J., 1976. Spectral reflectance characteristics of the meteorite classes. Journal of Geophysical Research 81, 905-920.

Gaffey, M.J., 1997. Surface Lithologic Heterogeneity of Asteroid 4 Vesta. Icarus 127, 130-157.

Gaffey, M.J., Bell, J.F., Brown, R.H., Burbine, T.H., Piatek, J.L., Reed, K.L., Chaky, D.A., 1993. Mineralogical Variations within the S-Type Asteroid Class. Icarus 106, 573-602.

Gaffey, M.J., Cloutis, E.A., Kelley, M.S., Reed, K.L., 2002. Mineralogy of Asteroids. Asteroids III, 183-204.

Gaskell, R.W., 2012. SPC Shape and Topography of Vesta from DAWN Imaging Data, AAS/Division for Planetary Sciences Meeting Abstracts.

Gault, D.E., Greeley, R., 1978. Exploratory experiments of impact craters formed in viscous-liquid targets - Analogs for Martian rampart craters. Icarus 34, 486-495.

Gehrels, T., 1995. Hazards Due to Comets and Asteroids. Hazards Due to Comets and Asteroids by T. Gehrels. University of Arizona Press, 1995. ISBN: 978-0-8165-1505-9

Gilbert, G.K., 1893. The moon's face. A study of the origin of its features. Publication: Washington, The Society, 1893.

Giorgini, J.D., Yeomans, D.K., Chamberlin, A.B., Chodas, P.W., Jacobson, R.A., Keesey, M.S., Lieske, J.H., Ostro, S.J., Standish, E.M., Wimberly, R.N., 1996. JPL's On-Line Solar System Data Service, American Astronomical Society, DPS meeting #28, #25.04; Bulletin of the American Astronomical Society, Vol. 28, p. 1158.

Giuranna, M., Roush, T.L., Duxbury, T., Hogan, R.C., Carli, C., Geminale, A., Formisano, V., 2011. Compositional interpretation of PFS/MEx and TES/MGS thermal infrared spectra of Phobos. Planetary and Space Science 59, 1308-1325.

Gladman, B.J., Davis, D.R., Neese, C., Jedicke, R., Williams, G., Kavelaars, J.J., Petit, J.-M., Scholl, H., Holman, M., Warrington, B., Esquerdo, G., Tricarico, P., 2009. On the asteroid belt's orbital and size distribution. Icarus 202, 104-118.

Gladman, B.J., Migliorini, F., Morbidelli, A., Zappalà, V., Michel, P., Cellino, A., Froeschlé, C., Levison, H.F., Bailey, M., Duncan, M., 1997. Dynamical Lifetimes of Objects Injected into Asteroid Belt Resonances. Science 277, 197-201.

Gomes, R., Levison, H.F., Tsiganis, K., Morbidelli, A., 2005. Origin of the cataclysmic Late Heavy Bombardment period of the terrestrial planets. Nature 435, 466-469.

Greeley, R., Gault, D.E., 1970. Precision Size-Frequency Distributions of Craters for 12 Selected Areas of the Lunar Surface. Moon 2, 10.

Greenberg, R., Bottke, W.F., Nolan, M., Geissler, P., Petit, J.-M., Durda, D.D., Asphaug, E., Head, J., 1996. Collisional and Dynamical History of Ida. Icarus 120, 106-118.

Greenberg, R., Nolan, M.C., Bottke, W.F., Kolvoord, R.A., Veverka, J., 1994. Collisional History of Gaspra. Icarus 107, 84-97.

Guillot, T., Gautier, D., 2007. 10.13 - Giant Planets, In: Schubert, G. (Ed.), Treatise on Geophysics. Elsevier, Amsterdam, pp. 439-464.

Hamelin, M., 2011. Motion of blocks on the surface of Phobos: New constraints for the formation of grooves. Planetary and Space Science 59, 1293-1307.

Hapke, B., 2001. Space weathering from Mercury to the asteroid belt. Journal of Geophysical Research 106, 10039-10074.

Hartmann, W.K., 1965a. Secular Changes in Meteoritic Flux through the History of the Solar System. Icarus 4, 207-213.

Hartmann, W.K., 1965b. Terrestrial and Lunar Flux of Large Meteorites in the Last Two Billion Years. Icarus 4, 157-165.

Hartmann, W.K., 1966. Early lunar cratering. Icarus 5, 406-418.

Hartmann, W.K., 1970. Note: Preliminary Note on Lunar Cratering Rates and Absolute Time-Scales. Icarus 12, 131-133.

Hartmann, W.K., 1971. Martian Cratering III: Theory of Crater Obliteration. Icarus 15, 410.

Hartmann, W.K., 1972. Paleocratering of the Moon: Review of Post-Apollo Data. Astrophysics and Space Science 17, 48-64.

Hartmann, W.K., 1975. Lunar "cataclysm": A misconception? Icarus 24, 181-187.

Hartmann, W.K., 1984. Does crater “saturation equilibrium” occur in the solar system? Icarus 60, 56-74.

Hartmann, W.K., 2003. Megaregolith evolution and cratering cataclysm models - Lunar cataclysm as a misconception (28 years later). Meteoritics and Planetary Science 38, 579-593.

Hartmann, W.K., Gaskell, R.W., 1997. Planetary cratering 2: Studies of saturation equilibrium. Meteoritics & Planetary Science 32, 109-121.

Hartmann, W.K., Neukum, G., 2001. Cratering chronology and the evolution of Mars. Space Science Reviews 96, 165-194.

Hartmann, W.K., Werner, S.C., 2010. Martian Cratering 10. Progress in use of crater counts to interpret geological processes: Examples from two debris aprons. Earth and Planetary Science Letters 294, 230-237.

Haskin, L.A., Korotev, R.L., Rockow, K.M., Jolliff, B.L., 1998. The case for an Imbrium origin of the Apollo Th-rich impact-melt breccias. Meteoritics & Planetary Science, vol. 33, no. 5, 959-975.

Head, J.W., 3rd, Fassett, C.I., Kadish, S.J., Smith, D.E., Zuber, M.T., Neumann, G.A., Mazarico, E., 2010. Global distribution of large lunar craters: implications for resurfacing and impactor populations. Science 329, 1504-1507.

Hendrix, A.R., Vilas, F., Festou, M.C., 2003. Vesta's UV lightcurve: hemispheric variation in brightness and spectral reversal. Icarus 162, 1-9.

Hiesinger, H., Head, J.W., Wolf, U., Jaumann, R., Neukum, G., 2002. Lunar mare basalt flow units: Thicknesses determined from crater size-frequency distributions. Geophysical Research Letters 29, 1248.

Hiesinger, H., Head, J.W., Wolf, U., Jaumann, R., Neukum, G., 2010. Ages and stratigraphy of lunar mare basalts in Mare Frigoris and other nearside maria based on crater size-frequency distribution measurements. Journal of Geophysical Research: Planets 115, E03003.

Hiesinger, H., Ruesch, O., Blewett, D.T., Buczkowski, D.L., Scully, J.E.C., Williams, D.A., Yingst, R.A., Russell, C.T., Raymond, C.A., 2013. Geologic Map of the Northern Hemisphere of Vesta Based on Dawn FC Images. LPI Contributions 1719, 2582.

Hildebrand, A.R., Penfield, G.T., Kring, D.A., Pilkington, M., Camargo Z., A., Jacobsen, S.B., Boynton, W.V., 1991. Chicxulub Crater: A possible Cretaceous/Tertiary boundary impact crater on the Yucatán Peninsula, Mexico. Geology 19, 867-871.

Hinrichs, J.L., Lucey, P.G., 2002. Temperature-Dependent Near-Infrared Spectral Properties of Minerals, Meteorites, and Lunar Soil. Icarus 155, 169-180.

Hinrichs, J.L., Lucey, P.G., Robinson, M.S., Meibom, A., Krot, A.N., 1999. Implications of temperature-dependent near-IR spectral properties of common minerals and meteorites for remote sensing of asteroids. Geophysical Research Letters 26, 1661-1664.

Hiroi, T., Binzel, R.P., Sunshine, J.M., Pieters, C.M., Takeda, H., 1995. Grain sizes and mineral compositions of surface regoliths of Vesta-like asteroids. Icarus 115, 374-386.

Holsapple, K., Giblin, I., Housen, K., Nakamura, A., Ryan, E., 2002. Asteroid Impacts: Laboratory Experiments and Scaling Laws. Asteroids III, W. F. Bottke Jr., A. Cellino, P. Paolicchi, and R. P. Binzel (eds), University of Arizona Press, Tucson, 443-462.

Horedt, G.P., Neukum, G., 1984. Cratering rate over the surface of a synchronous satellite. Icarus 60, 710-717.

Horner, V.M., Greeley, R., 1982. Pedestal craters on Ganymede. Icarus 51, 549-562.

Housen, K.R., Holsapple, K.A., 2011. Ejecta from impact craters. Icarus 211, 856-875.

Housen, K.R., Holsapple, K.A., 2012. Craters without ejecta. Icarus 219, 297-306.

Howett, C.J.A., Spencer, J.R., Schenk, P., Johnson, R.E., Paranicas, C., Hurford, T.A., Verbiscer, A., Segura, M., 2011. A high-amplitude thermal inertia anomaly of probable magnetospheric origin on Saturn's moon Mimas. Icarus 216, 221-226.

Inaba, S., Wetherill, G.W., Ikoma, M., 2003. Formation of gas giant planets: core accretion models with fragmentation and planetary envelope. Icarus 166, 46-62.

Irving, A., 2012. Jiddat al Harasis 626. Meteoritical, Bulletin.

Isaacson, P.J., Pieters, C.M., 2009. Northern Imbrium Noritic Anomaly. J Geophys Res-Planet 114, 9007.

Ivanov, B., 2008. Size-Frequency Distribution of Asteroids and Impact Craters: Estimates of Impact Rate, Catastrophic Events Caused by Cosmic Objects, Edited by V.V. Adushkin and I.V. Nemchinov. ISBN 978-1-4020-6451-7. Berlin: Springer, 2008, p.91.

Ivanov, B.A., 2001. Mars/Moon Cratering Rate Ratio Estimates. Space Science Reviews 96, 87-104.

Ivanov, B.A., 2006. Earth/Moon impact rate comparison: Searching constraints for lunar secondary/primary cratering proportion. Icarus 183, 504-507.

Ivanov, B.A., Hartmann, W.K., 2007. 10.06 - Exogenic Dynamics, Cratering and Surface Ages, In: Schubert, G. (Ed.), Treatise on Geophysics. Elsevier, Amsterdam, pp. 207-242.

Ivanov, B.A., Melosh, H.J., 2013. Two-dimensional numerical modeling of the Rheasilvia impact formation. Journal of Geophysical Research (Planets) 118, 1545-1557.

Ivanov, B.A., Neukum, G., Bottke, W.F., Jr., Hartmann, W.K., 2002. The Comparison of Size-Frequency Distributions of Impact Craters and Asteroids and the Planetary Cratering Rate. Asteroids III, W. F. Bottke Jr., A. Cellino, P. Paolicchi, and R. P. Binzel (eds), University of Arizona Press, Tucson, 89-101.

Ivanov, B.A., Neukum, G., Wagner, R., 2001. Size-frequency distributions of planetary impact craters and asteroids In: Collisional processes in the solar system, ed. by: Mikhail Ya. Marov and Hans Rickman, Astrophysics and space science library, Volume 261, Dordrecht: Kluwer Academic Publishers.

Jaumann, R., Neukum, G., Behnke, T., Duxbury, T.C., Eichentopf, K., Flohrer, J., van Gasselt, S., Giese, B., Gwinner, K., Hauber, E., Hoffmann, H., Hoffmeister, A., Köhler, U., Matz, K.D., McCord, T.B., Mertens, V., Oberst, J., Pischel, R., Reiss, D., Ress, E., Roatsch, T., Saiger, P., Scholten, F., Schwarz, G., Stephan, K., Wählisch, M., the Hrsc Co-Investigator Team, 2007. The high-resolution stereo camera (HRSC) experiment on Mars Express: Instrument aspects and experiment conduct from interplanetary cruise through the nominal mission. Planetary and Space Science 55, 928-952.

Jaumann, R., Otto, K., Krohn, K., McCord, T.B., Williams, D.A., Yingst, R.A., Stephan, K., Combe, J.P., Palomba, E., Tosi, F., Hiesinger, H., Blewett, D.T., Raymond, C.A., Russel, C.T., 2012a. The Geological Context of Vesta's Dark Material. AGU Fall Meeting Abstracts 24, 1477775.

Jaumann, R., Williams, D.A., Buczkowski, D.L., Yingst, R.A., Preusker, F., Hiesinger, H., Schmedemann, N., Kneissl, T., Vincent, J.B., Blewett, D.T., Buratti, B.J., Carsenty, U., Denevi, B.W., De Sanctis, M.C., Garry, W.B., Keller, H.U., Kersten, E., Krohn, K., Li, J.Y., Marchi, S., Matz, K.D., McCord, T.B., McSween, H.Y., Mest, S.C., Mittlefehldt, D.W., Mottola, S., Nathues, A., Neukum, G., O'Brien, D.P., Pieters, C.M., Prettyman, T.H., Raymond, C.A., Roatsch, T., Russell, C.T., Schenk, P., Schmidt, B.E., Scholten, F., Stephan, K., Sykes, M.V., Tricarico, P., Wagner, R., Zuber, M.T., Sierks, H., 2012b. Vesta's shape and morphology. Science 336, 687-690.

Jewitt, D., Luu, J., 1993. Discovery of the candidate Kuiper belt object 1992 QB1. Nature 362, 730-732.

Jones, T.D., Lebofsky, L.A., Lewis, J.S., Marley, M.S., 1990. The composition and origin of the C, P, and D asteroids: Water as a tracer of thermal evolution in the outer belt. Icarus 88, 172-192.

Keil, K., Stoeffler, D., Love, S.G., Scott, E.R.D., 1997. Constraints on the role of impact heating and melting in asteroids. Meteoritics and Planetary Science 32, 349-363.

Kirchoff, M.R., Chapman, C.R., Marchi, S., Curtis, K.M., Enke, B., Bottke, W.F., 2013. Ages of large lunar impact craters and implications for bombardment during the Moon's middle age. Icarus 225, 325-341.

Kirchoff, M.R., Schenk, P., 2010. Impact cratering records of the mid-sized, icy saturnian satellites. Icarus 206, 485-497.

Klima, R.L., Pieters, C.M., Dyar:, M.D., 2008. Characterization of the 1.2 μm M1 pyroxene band: Extracting cooling history from near-IR spectra of pyroxenes and pyroxene-dominated rocks. Meteoritics and Planetary Science 43, 1591-1604.

Kneissl, T., Schmedemann, N., Reddy, V., Williams, D.A., Walter, S.H.G., Neesemann, A., Michael, G.G., Jaumann, R., Krohn, K., Preusker, F., Roatsch, T., Le Corre, L., Nathues, A., Hoffmann, M., Schäfer, M., Buczkowski, D., Garry, W.B., Yingst, R.A., Mest, S.C., Russell, C.T., Raymond, C.A., 2014. Morphology and formation ages of mid-sized post-Rheasilvia craters – Geology of quadrangle Tuccia, Vesta. Icarus 244, 133-157.

Kneissl, T., Schmedemann, N., Walter, S., Williams, D., Garry, W.B., Yingst, R.A., Reddy, V., Jaumann, R., Krohn, K., Preusker, F., Roatsch, T., Buczkowski, D.L., Raymond, C.A., Russell, C.T., 2013. Prominent Impact Craters in the AV-13 Quadrangle Tuccia on Vesta — Morphology, Degradation, and Ages of Tuccia, Eusebia, Vibidia, Galeria, and Antonia. LPI Contributions 1719, 1078.

Kneissl, T., van Gasselt, S., Neukum, G., 2011. Map-projection-independent crater size-frequency determination in GIS environments—New software tool for ArcGIS. Planetary and Space Science 59, 1243-1254.

König, B., 1977. Investigations of primary and secondary impact structures on the moon and laboratory experiments to study the ejecta of secondary particles. Ruprecht Karl Universität ,SCITRAN, Inc., p. 88.

Kreslavsky, M.A., 2007. Statistical Characterization of Spatial Distribution of Impact Craters: Implications to Present-Day Cratering Rate on Mars. LPI Contributions 1353, 3325.

Krohn, K., Jaumann, R., Elbeshausen, D., Kneissl, T., Wagner, R., Stephan, K., Otto, K., Matz, K.D., Preusker, F., Roatsch, T., Schmedemann, N., Raymond, C.A., Russell, C.T., 2013. Bimodal Craters on Vesta: Impacts on Slopes Studied by Geological Investigations. LPI Contributions 1719, 1949.

Krohn, K., Jaumann, R., Otto, K., Hoogenboom, T., Wagner, R., Buczkowski, D.L., Garry, B., Williams, D.A., Yingst, R.A., Scully, J., De Sanctis, M.C., Kneissl, T., Schmedemann, N., Kersten, E., Stephan, K., Matz, K.D., Pieters, C.M., Preusker, F., Roatsch, T., Schenk, P., Russell, C.T., Raymond, C.A., 2014. Mass movement on Vesta at steep scarps and crater rims. Icarus 244, 120-132.

Krohn, K., Jaumann, R., Stephan, K., Pieters, C.M., Wagner, R., Yingst, R.A., Williams, D.A., Schenk, P., Neukum, G., Schmedemann, N., Kneissl, T., de Sanctis, M.C., Nathues, A., Buczkowski, D.L., Roatsch, T., Preusker, F., Kersten, E., Russell, C.T., Raymond, C.A., 2012. Geologic Mapping of the Av-12 Sextlia Quadrangle of Asteroid 4 Vesta, Lunar and Planetary Institute Science Conference Abstracts, p. 1901.

Larson, H.P., Fink, U., 1975. Infrared spectral observations of asteroid 4 Vesta. Icarus 26, 420-427.

Lawrence, D.J., Peplowski, P.N., Prettyman, T.H., Feldman, W.C., Bazell, D., Mittlefehldt, D.W., Reedy, R.C., Yamashita, N., 2013. Constraints on Vesta's elemental composition: Fast neutron measurements by Dawn's gamma ray and neutron detector. Meteoritics and Planetary Science 48, 2271-2288.

Le Corre, L., Reddy, V., Becker, K.J., O'Brien, D.P., Palmer, E., Li, J., Gaskell, R., Denevi, B.W., Nathues, A., Sierks, H., Russel, C.T., 2012a. Nature of Orange Ejecta Around Oppia and Octavia Craters on Vesta from Dawn Framing Camera, AAS/Division for Planetary Sciences Meeting Abstracts.

Le Corre, L., Reddy, V., Nathues, A., Cloutis, E.A., 2011. How to characterize terrains on 4 Vesta using Dawn Framing Camera color bands? Icarus 216, 376-386.

Le Corre, L., Reddy, V., Nathues, A., Li, J.-Y., Denevi, B.W., Buratti, B.J., Sierks, H., Schröder, S.E., Pieters, C.M., Gaskell, R., Becker, K.J., Gutiérrez Marqués, P., Russell, C.T., Raymond, C.A., 2012b. Vesta Terrains Seen by the Dawn Framing Camera Color Filters, Lunar and Planetary Institute Science Conference Abstracts, p. 1624.

Le Corre, L., Reddy, V., Schmedemann, N., Becker, K.J., O'Brien, D.P., Yamashita, N., Peplowski, P.N., Prettyman, T.H., Li, J.-Y., Cloutis, E.A., Denevi, B.W., Kneissl, T., Palmer, E., Gaskell, R.W., Nathues, A., Gaffey, M.J., Mittlefehldt, D.W., Garry, W.B., Sierks, H., Russell, C.T., Raymond, C.A., De Sanctis, M.C., Ammanito, E., 2013. Olivine or impact melt: Nature of the "Orange" material on Vesta from Dawn. Icarus 226, 1568-1594.

Le Feuvre, M., Wieczorek, M.A., 2011. Nonuniform cratering of the Moon and a revised crater chronology of the inner Solar System. Icarus 214, 1-20.

Leliwa-Kopystynski, J., Burchell, M.J., Lowen, D., 2008. Impact cratering and break up of the small bodies of the Solar System. Icarus 195, 817-826.

Levison, H.F., Duncan, M.J., 1997. From the Kuiper Belt to Jupiter-Family Comets: The Spatial Distribution of Ecliptic Comets. Icarus 127, 13-32.

Li, J.-Y., Combe, J.-P., Longobardo, A., Capaccioni, F., De Sanctis, M.C., Ammannito, E., Capria, M.T., Palomba, E., Tosi, F., Zambon, F., Schröder, S.E., Denevi, B.W., Reddy, V., Russell, C.T., Raymond, C.A., 2013a. The Photometric Properties of Vesta in Visible and Near-Infrared from Dawn VIR Instrument. LPI Contributions 1719, 2343.

Li, J.-Y., Le Corre, L., Schröder, S.E., Reddy, V., Denevi, B.W., Buratti, B.J., Mottola, S., Hoffmann, M., Gutierrez-Marques, P., Nathues, A., Russell, C.T., Raymond, C.A., 2013b. Global photometric properties of Asteroid (4) Vesta observed with Dawn Framing Camera. Icarus 226, 1252-1274.

Li, J.-Y., McFadden, L.A., Thomas, P.C., Mutchler, M.J., Parker, J.W., Young, E.F., Russell, C.T., Sykes, M.V., Schmidt, B.E., 2010. Photometric mapping of Asteroid (4) Vesta's southern hemisphere with Hubble Space Telescope. Icarus 208, 238-251.

Li, J.-Y., Thomas, P.C., Carcich, B., Mutchler, M.J., McFadden, L.A., Russell, C.T., Weinstein-Weiss, S.S., Rayman, M.D., Raymond, C.A., 2011. Improved measurement of Asteroid (4) Vesta's rotational axis orientation. Icarus 211, 528-534.

Li, J.Y., 2012. Body-Fixed Coordinate Systems for Asteroid (4) Vesta, (http://sbn.psi.edu/archive/dawn/fc/DWNVFC2_1A/DOCUMENT/VESTA_COORDINATES/VESTA_COORDINATES_131018.PDF).

Lowry, S.C., Fitzsimmons, A., Pravec, P., Vokrouhlicky, D., Boehnhardt, H., Taylor, P.A., Margot, J.L., Galad, A., Irwin, M., Irwin, J., Kusnirak, P., 2007. Direct detection of the asteroidal YORP effect. Science 316, 272-274.

Mahaney, W.C., Kalm, V., Kapran, B., Hewitt, K., 2009. Clast fabric and mass wasting on Asteroid 25143-Itokawa: Correlation with talus and other periglacial features on Earth. Sedimentary Geology 219, 44-57.

Malhotra, R., Strom, R.G., 2011. Comment on "Constraints on the source of lunar cataclysm impactors" (Cuk et al., 2010, Icarus 207, 590-594). Icarus 216, 359-362.

Malin, M.C., Edgett, K.S., Posiolova, L.V., McColley, S.M., Dobrea, E.Z.N., 2006. Present-Day Impact Cratering Rate and Contemporary Gully Activity on Mars. Science 314, 1573-1577.

Marchi, S., Bottke, W.F., Kring, D.A., Morbidelli, A., 2012a. The onset of the lunar cataclysm as recorded in its ancient crater populations. Earth and Planetary Science Letters 325, 27-38.

Marchi, S., Bottke, W.F., O'Brien, D.P., Schenk, P., Mottola, S., De Sanctis, M.C., Kring, D.A., Williams, D.A., Raymond, C.A., Russell, C.T., 2014. Small crater populations on Vesta. Planetary and Space Science 103, 96-103.

Marchi, S., Massironi, M., Vincent, J.B., Morbidelli, A., Mottola, S., Marzari, F., Küppers, M., Besse, S., Thomas, N., Barbieri, C., Naletto, G., Sierks, H., 2012b. The cratering history of asteroid (21) Lutetia. Planetary and Space Science 66, 87-95.

Marchi, S., McSween, H.Y., O'Brien, D.P., Schenk, P., De Sanctis, M.C., Gaskell, R., Jaumann, R., Mottola, S., Preusker, F., Raymond, C.A., Roatsch, T., Russell, C.T., 2012c. The violent collisional history of asteroid 4 Vesta. Science 336, 690-694.

Marchi, S., Mottola, S., Cremonese, G., Massironi, M., Martellato, E., 2009. A New Chronology for the Moon and Mercury. The Astronomical Journal 137, 4936-4948 (2009).

Marzari, F., Cellino, A., Davis, D.R., Farinella, P., Zappala, V., Vanzani, V., 1996. Origin and evolution of the Vesta asteroid family. Astronomy & Astrophysics 316, 248-262.

Massironi, M., Cremonese, G., Marchi, S., Martellato, E., Mottola, S., Wagner, R.J., 2009. Mercury's geochronology revised by applying Model Production Function to Mariner 10 data: Geological implications. Geophysical Research Letters 36, L21204.

Massironi, M., Marchi, S., Pajola, M., Snodgrass, C., Thomas, N., Tubiana, C., Baptiste Vincent, J., Cremonese, G., Da Deppo, V., Ferri, F., Magrin, S., Sierks, H., Barbieri, C., Lamy, P., Rickman, H., Rodrigo, R., Koschny, D., Team, O., 2012. Geological map and stratigraphy of asteroid 21 Lutetia. Planetary and Space Science 66, 125-136.

Mayne, R.G., Sunshine, J.M., McSween, H.Y., Bus, S.J., McCoy, T.J., 2011. The origin of Vesta's crust: Insights from spectroscopy of the Vestoids. Icarus 214, 147-160.

McCord, T., Castillo-Rogez, J., Rivkin, A., 2012a. Ceres: Its Origin, Evolution and Structure and Dawn's Potential Contribution, In: Russell, C., Raymond, C. (Eds.), The Dawn Mission to Minor Planets 4 Vesta and 1 Ceres. Springer New York, pp. 63-76.

McCord, T.B., Adams, J.B., Johnson, T.V., 1970. Asteroid Vesta: Spectral Reflectivity and Compositional Implications. Science 168, 1445-1447.

McCord, T.B., Li, J.-Y., Combe, J.-P., McSween, H.Y., Jaumann, R., Reddy, V., Tosi, F., Williams, D.A., Blewett, D.T., Turrini, D., Palomba, E., Pieters, C.M., de Sanctis, M.C., Ammannito, E., Capria, M.T., Le Corre, L., Longobardo, A., Nathues, A., Mittlefehldt, D.W., Schröder, S.E., Hiesinger, H., Beck, A.W., Capaccioni, F., Carsenty, U., Keller, H.U., Denevi, B.W., Sunshine, J.M., Raymond, C.A., Russell, C.T., 2012b. Dark material on Vesta from the infall of carbonaceous volatile-rich material. Nature 491, 83-86.

McEwen, A.S., Banks, M.E., Baugh, N., Becker, K., Boyd, A., Bergstrom, J.W., Beyer, R.A., Bortolini, E., Bridges, N.T., Byrne, S., Castalia, B., Chuang, F.C., Crumpler, L.S., Daubar, I., Davatzes, A.K., Deardorff, D.G., Dejong, A., Delamere, W.A., Dobrea, E.N., Dundas, C.M., Eliason, E.M., Espinoza, Y., Fennema, A., Fishbaugh, K.E., Forrester, T., Geissler, P.E., Grant, J.A., Griffes, J.L., Grotzinger, J.P., Gulick, V.C., Hansen, C.J., Herkenhoff, K.E., Heyd, R., Jaeger, W.L., Jones, D., Kanefsky, B., Keszthelyi, L., King, R., Kirk, R.L., Kolb, K.J., Lasco, J., Lefort, A., Leis, R., Lewis, K.W., Martinez-Alonso, S., Mattson, S., McArthur, G., Mellon, M.T., Metz, J.M., Milazzo, M.P., Milliken, R.E., Motazedian, T., Okubo, C.H., Ortiz, A., Philippoff, A.J., Plassmann, J., Polit, A., Russell, P.S., Schaller, C., Searls, M.L., Spriggs, T., Squyres, S.W., Tarr, S., Thomas, N., Thomson, B.J., Tornabene, L.L., van Houten, C., Verba, C., Weitz, C.M., Wray, J.J., 2010. The High Resolution Imaging Science Experiment (HiRISE) during MRO's Primary Science Phase (PSP). Icarus 205, 2-37.

McEwen, A.S., Bierhaus, E.B., 2006. The Importance of Secondary Cratering to Age Constraints on Planetary Surfaces. Annual Review of Earth and Planetary Sciences, vol. 34, 535-567.

McEwen, A.S., Gaddis, L.R., Neukum, G., Hoffmann, H., Pieters, C.M., Head, J.W., 1993. Galileo observations of post-imbrium lunar craters during the first Earth-Moon flyby. Journal of Geophysical Research: Planets 98, 17207-17234.

McFadden, L.A., Pieters, C., McCord, T.B., 1977. Vesta - The first pyroxene band from new spectroscopic measurements. Icarus 31, 439-446.

McGetchin, T.R., Settle, M., Head, J.W., 1973. Radial thickness variation in impact crater ejecta: Implications for lunar basin deposits. Earth and Planetary Science Letters 20, 226-236.

McMahon, S.K., 1996. Overview of the Planetary Data System. Planetary and Space Science 44, 3-12.

McSween, H., Mittlefehldt, D., Beck, A., Mayne, R., McCoy, T., 2011. HED Meteorites and Their Relationship to the Geology of Vesta and the Dawn Mission. Space Science Reviews 163, 141-174.

McSween, H.Y., Ammannito, E., Reddy, V., Prettyman, T.H., Beck, A.W., Cristina de Sanctis, M., Nathues, A., Corre, L.L., O'Brien, D.P., Yamashita, N., McCoy, T.J., Mittlefehldt, D.W., Toplis, M.J., Schenk, P., Palomba, E., Turrini, D., Tosi, F., Zambon, F., Longobardo, A., Capaccioni, F., Raymond, C.A., Russell, C.T., 2013. Composition of the Rheasilvia basin, a window into Vesta's interior. Journal of Geophysical Research (Planets) 118, 335-346.

Melosh, H.J., 1989. Impact cratering: A geologic process, Research supported by NASA. New York, Oxford University Press (Oxford Monographs on Geology and Geophysics, No. 11), 1989, 253 p.

Mest, S.C., Yingst, R.A., Williams, D.A., Garry, W.B., Pieters, C.M., Jaumann, R., Buczkowski, D.L., Sykes, M.V., Tricarico, P., Wyrick, D.Y., Schenk, P.M., Russell, C.T., Raymond, C.A., Neukum, G., Schmedemann, N., Roatsch, T., Preusker, F., Ammannito, E., Team, D., 2012. Geologic Mapping of the Av-14 Urbinia Quadrangle of Asteroid 4 Vesta, Lunar and Planetary Institute Science Conference Abstracts, p. 2375.

Michael, G.G., 2013. Planetary surface dating from crater size–frequency distribution measurements: Multiple resurfacing episodes and differential isochron fitting. Icarus 226, 885-890.

Michael, G.G., Neukum, G., 2010. Planetary surface dating from crater size-frequency distribution measurements: Partial resurfacing events and statistical age uncertainty. Earth and Planetary Science Letters 294, 223-229.

Michael, G.G., Platz, T., Kneissl, T., Schmedemann, N., 2012. Planetary surface dating from crater size-frequency distribution measurements: Spatial randomness and clustering. Icarus 218, 169-177.

Mittlefehldt, D.W., 2008. Meteorite Dunite Breccia MIL 03443: A Probable Crustal Cumulate Closely Related to Diogenites from the HED Parent Asteroid, Lunar and Planetary Science Conference, p. 1919.

Mittlefehldt, D.W., McCoy, T.J., Goodrich, C.A., Kracher, A., 1998. Non-chondritic meteorites from asteroidal bodies. Reviews in Mineralogy and Geochemistry 36, 4.1-4.195.

Morbidelli, A., Brasser, R., Gomes, R., Levison, H.F., Tsiganis, K., 2010. Evidence from the Asteroid Belt for a Violent Past Evolution of Jupiter's Orbit. The Astronomical Journal 140, 1391-1401 (2010).

Morbidelli, A., Levison, H.F., Tsiganis, K., Gomes, R., 2005. Chaotic capture of Jupiter's Trojan asteroids in the early Solar System. Nature 435, 462-465.

Morbidelli, A., Marchi, S., Bottke, W.F., Kring, D.A., 2012. A sawtooth-like timeline for the first billion years of lunar bombardment. Earth and Planetary Science Letters 355, 144-151.

Morbidelli, A., Vokrouhlický, D., 2003. The Yarkovsky-driven origin of near-Earth asteroids. Icarus 163, 120-134.

Morota, T., Haruyama, J.i., Honda, C., Yokota, Y., Ohtake, M., Furumoto, M., 2008. Lunar apex-antapex cratering asymmetry as an impactor recorder in the Earth-Moon system. Advances in Space Research 42, 285-288.

Moroz, L., Schade, U., Wäsch, R., 2000. Reflectance Spectra of Olivine-Orthopyroxene-Bearing Assemblages at Decreased Temperatures: Implications for Remote Sensing of Asteroids. Icarus 147, 79-93.

Moskovitz, N.A., Jedicke, R., Gaidos, E., Willman, M., Nesvorný, D., Fevig, R., Ivezić, Ž., 2008. The distribution of basaltic asteroids in the Main Belt. Icarus 198, 77-90.

Moskovitz, N.A., Willman, M., Burbine, T.H., Binzel, R.P., Bus, S.J., 2010. A spectroscopic comparison of HED meteorites and V-type asteroids in the inner Main Belt. Icarus 208, 773-788.

Murray, J.B., Heggie, D.C., 2014. Character and origin of Phobos' grooves. Planetary and Space Science 102, 119-143.

Murray, J.B., Rothery, D.A., Thornhill, G.D., Muller, J.-P., Iliffe, J.C., Day, T., Cook, A.C., 1994. The origin of Phobos' grooves and crater chains. Planetary and Space Science 42, 519-526.

Mutch, P., Woronow, A., 1980. Martian rampart and pedestal craters' ejecta-emplacement: Coprates quadrangle. Icarus 41, 259-268.

Nass, A., van Gasselt, S., Jaumann, R., Asche, H., 2011. Implementation of cartographic symbols for planetary mapping in geographic information systems. Planetary and Space Science 59, 1255-1264.

Nathues, A., Le Corre, L., Reddy, V., Hoffmann, M., Team, D.S., 2012. Identification of Vesta Surface Units with Principal Component Analysis by Using Dawn Framing Camera Imagery, Lunar and Planetary Institute Science Conference Abstracts, p. 1779.

Nesvorný, D., Bottke, W.F., Vokrouhlický, D., Morbidelli, A., Jedicke, R., 2005. Asteroid families. Proceedings of the International Astronomical Union 1, 289-299.

Nesvorný, D., Roig, F., Gladman, B., Lazzaro, D., Carruba, V., Mothé-Diniz, T., 2008. Fugitives from the Vesta family. Icarus 193, 85-95.

Neukum, G., 1984. Meteorite bombardment and dating of planetary surfaces, Publication: Thesis - Feb. 1983 National Aeronautics and Space Administration, Washington, DC. Transl. into ENGLISH of "Meteoritenbombardement und Datierung Planetarer Oberflaechen" Munich, Feb. 1983 p 1-186.

Neukum, G., 1985. Cratering records of the satellites of Jupiter and Saturn. Advances in Space Research 5, 107-116.

Neukum, G., 1997. Bombardment History of the Jovian System, The Three Galileos: the Man, the Spacecraft, the Telescope, Proceedings of the conference held in Padova, Italy on January 7-10, 1997 Publisher: Dordrecht Kluwer Academic Publishers, 1997 Astrophysics and space science library (ASSL) Series vol no 220.

Neukum, G., Basilevsky, A.T., Kneissl, T., Chapmam, M.G., van Gasselt, S., Michael, G., Jaumann, R., Hoffmann, H., Lanz, J.K., 2010. The geologic evolution of Mars: Episodicity of resurfacing events and ages from cratering analysis of image data and correlation with radiometric ages of Martian meteorites. Earth and Planetary Science Letters 294, 204-222.

Neukum, G., Basilevsky, A.T., Kneissl, T., Michael, G.G., Ivanov, B.A., 2012. On the History of Early Meteoritic Bombardment of the Moon: Did the Lunar Terminal Cataclysm Occur? Workshop on the Early Solar System Bombardment II, held 1-3 February 2012, in Houston, Texas. LPI Contribution No. 1649, 55-56.

Neukum, G., Dietzel, H., 1971. On the development of the crater population on the moon with time under meteoroid and solar wind bombardment. Earth and Planetary Science Letters 12, 59-66.

Neukum, G., Hiller, K., 1981. Martian ages. Journal of Geophysical Research: Solid Earth 86, 3097-3121.

Neukum, G., Horn, P., 1976. Effects of lava flows on lunar crater populations. Moon 15, 205-222.

Neukum, G., Ivanov, B.A., 1994. Crater Size Distributions and Impact Probabilities on Earth from Lunar, Terrestrial-planet, and Asteroid Cratering Data. Hazards due to comets and asteroids, Space Science Series, Tucson, AZ: Edited by Tom Gehrels, M. S. Matthews. and A. Schumann. Published by University of Arizona Press, 1994., 359.

Neukum, G., Ivanov, B.A., Hartmann, W.K., 2001. Cratering records in the inner solar system in relation to the lunar reference system. Space Science Reviews 96, 55-86.

Neukum, G., Jaumann, R., Hoffmann, H., Hauber, E., Head, J.W., Basilevsky, A.T., Ivanov, B.A., Werner, S.C., van Gasselt, S., Murray, J.B., McCord, T., Team, H.C.-I., 2004. Recent and episodic volcanic and glacial activity on Mars revealed by the High Resolution Stereo Camera. Nature 432, 971-979.

Neukum, G., Koenig, B., Arkani-Hamed, J., 1975. A study of lunar impact crater size-distributions. The Moon, vol. 12, Feb. 1975, 201-229.

Neukum, G., Schenk, P., Schmedemann, N., Michael, G., Jaumann, R., Scully, J., Russell, C.T., O'Brien, D.P., Hiesinger, H., Nathues, A., Wagner, R., Marchi, S., 2011. Chronology and Cratering at Vesta: First Results from Dawn's Survey Orbit, European Planetary Science Congress - DPS Joint Meeting 2011, Nantes, France, p. 501.

Neukum, G., Wagner, R., Wolf, U., Denk, T., 2006. The Cratering Record and Cratering Chronologies of the Saturnian Satellites and the Origin of Impactors: Results from Cassini ISS Data, European Planetary Science Congress 2006, Berlin, Germany, p. 610.

Neukum, G., Wagner, R., Wolf, U., Head, J.W., Pappalardo, R., Chapman, C.R., Merline, W.J., Greeley, R., Belton, M.J.S., 1998. Bombardment history and ages of the Galilean satellites. Ann. Geophys. 16, C-993-C-993.

Neukum, G., Wagner, R.J., Denk, T., Porco, C.C., Cassini Iss, T., 2005. The Cratering Record of the Saturnian Satellites Phoebe, Tethys, Dione and Iapetus in Comparison: First Results from Analysis of the Cassini ISS Imaging Data, Publication: 36th Annual Lunar and Planetary Science Conference, March 14-18, 2005, in League City, Texas, abstract no.2034.

Neukum, G., Wise, D.U., 1976. Mars: A Standard Crater Curve and Possible New Time Scale. Science 194, 1381-1387.

Nimmo, F., Korycansky, D.G., 2012. Impact-driven ice loss in outer Solar System satellites: Consequences for the Late Heavy Bombardment. Icarus 219, 508-510.

O'Brien, D.P., Greenberg, R., 2003. Steady-state size distributions for collisional populations:analytical solution with size-dependent strength. Icarus 164, 334-345.

O'Brien, D.P., Greenberg, R., 2005. The collisional and dynamical evolution of the main-belt and NEA size distributions. Icarus 178, 179-212.

O'Brien, D.P., Marchi, S., Morbidelli, A., Bottke, W.F., Schenk, P.M., Russell, C.T., Raymond, C.A., 2014. Constraining the cratering chronology of Vesta. Planetary and Space Science 103, 131-142.

O'Brien, D.P., Marchi, S., Schenk, P., Russell, C.T., Raymond, C.A., 2012. The Impact History of Vesta: Developing and Testing an Absolute Cratering Chronology, Lunar and Planetary Institute Science Conference Abstracts, p. 2688.

O'Brien, D.P., Morbidelli, A., Levison, H.F., 2006. Terrestrial planet formation with strong dynamical friction. Icarus 184, 39-58.

O'Brien, D.P., Sykes, M.V., 2011. The Origin and Evolution of the Asteroid Belt---Implications for Vesta and Ceres. Space Science Reviews 163, 41-61.

Öhman, T., Kring, D.A., 2012. Photogeologic analysis of impact melt-rich lithologies in Kepler crater that could be sampled by future missions. Journal of Geophysical Research (Planets) 117.

Öpik, E.J., 1960. The lunar surface as an impact counter. Mon. Not. R. Astron. Soc. 120, 404-411.

Osinski, G.R., Tornabene, L.L., Grieve, R.A.F., 2011. Impact ejecta emplacement on terrestrial planets. Earth and Planetary Science Letters 310, 167-181.

Otto, K.A., Jaumann, R., Krohn, K., Matz, K.-D., Preusker, F., Roatsch, T., Schenk, P., Scholten, F., Stephan, K., Raymond, C.A., Russell, C.T., 2013. Mass-wasting features and processes in Vesta's south polar basin Rheasilvia. Journal of Geophysical Research (Planets) 118, 2279-2294.

Pätzold, M., Andert, T.P., Asmar, S.W., Anderson, J.D., Barriot, J.-P., Bird, M.K., Häusler, B., Hahn, M., Tellmann, S., Sierks, H., Lamy, P., Weiss, B.P., 2011. Asteroid 21 Lutetia: Low Mass, High Density. Science 334, 491-492.

Peplowski, P.N., Lawrence, D.J., Prettyman, T.H., Yamashita, N., Bazell, D., Feldman, W.C., Le Corre, L., McCoy, T.J., Reddy, V., Reedy, R.C., Russell, C.T., Toplis, M.J., 2013. Compositional variability on the surface of 4 Vesta revealed through GRaND measurements of high-energy gamma rays. Meteoritics and Planetary Science 48, 2252-2270.

Pieters, C.M., Ammannito, E., Blewett, D.T., Denevi, B.W., de Sanctis, M.C., Gaffey, M.J., Le Corre, L., Li, J.-Y., Marchi, S., McCord, T.B., McFadden, L.A., Mittlefehldt, D.W., Nathues, A., Palmer, E., Reddy, V., Raymond, C.A., Russell, C.T., 2012. Distinctive space weathering on Vesta from regolith mixing processes. Nature 491, 79-82.

Pieters, C.M., Fischer, E.M., Rode, O., Basu, A., 1993. Optical Effects of Space Weathering - the Role of the Finest Fraction. J Geophys Res-Planet 98, 20817-20824.

Pieters, C.M., Murchie, S., Thomas, N., Britt, D., 2014. Composition of Surface Materials on the Moons of Mars. Planetary and Space Science 102, 144-151.

Pieters, C.M., Staid, M.I., Fischer, E.M., Tompkins, S., He, G., 1994. A Sharper View of Impact Craters from Clementine Data. Science 266, 1844-1848.

Pieters, C.M., Taylor, L.A., Noble, S.K., Keller, L.P., Hapke, B., Morris, R.V., Allen, C.C., McKay, D.S., Wentworth, S., 2000. Space weathering on airless bodies: Resolving a mystery with lunar samples. Meteoritics and Planetary Science 35, 1101-1107.

Pike, R.J., 1980. Formation of complex impact craters: Evidence from Mars and other planets. Icarus 43, 1-19.

Platz, T., Michael, G., Tanaka, K.L., Skinner, J.A., Fortezzo, C.M., 2013. Crater-based dating of geological units on Mars: Methods and application for the new global geological map. Icarus 225, 806-827.

Plescia, J.B., 2012. Impacts on Sloping Surfaces: Lunar Examples. Meteoritics and Planetary Science Supplement 75, 5318.

Pollack, J.B., Burns, J.A., 1977. An Origin by Capture for the Martian Satellites?, Bulletin of the American Astronomical Society, p. 518.

Porco, C.C., Baker, E., Barbara, J., Beurle, K., Brahic, A., Burns, J.A., Charnoz, S., Cooper, N., Dawson, D.D., Del Genio, A.D., Denk, T., Dones, L., Dyudina, U., Evans, M.W., Giese, B., Grazier, K., Helfenstein, P., Ingersoll, A.P., Jacobson, R.A., Johnson, T.V., McEwen, A., Murray, C.D., Neukum, G., Owen, W.M., Perry, J., Roatsch, T., Spitale, J., Squyres, S., Thomas, P.C., Tiscareno, H., Turtle, E., Vasavada, A.R., Veverka, J., Wagner, R., West, R., 2005. Cassini Imaging Science: Initial results on Phoebe and Iapetus. Science 307, 1237-1242.

Porco, C.C., West, R.A., Squyres, S., McEwen, A., Thomas, P., Murray, C.D., Del Genio, A., Ingersoll, A.P., Johnson, T.V., Neukum, G., Veverka, J., Dones, L., Brahic, A., Burns, J.A., Haemmerle, V., Knowles, B., Dawson, D., Roatsch, T., Beurle, K., Owen, W., 2004. Cassini Imaging Science: Instrument Characteristics And Anticipated Scientific Investigations At Saturn. Space Science Reviews 115, 363-497.

Prettyman, T.H., Feldman, W.C., McSween, H.Y., Dingler, R.D., Enemark, D.C., Patrick, D.E., Storms, S.A., Hendricks, J.S., Morgenthaler, J.P., Pitman, K.M., Reedy, R.C., 2011. Dawn's Gamma Ray and Neutron Detector. Space Science Reviews 163, 371-459.

Prettyman, T.H., Mittlefehldt, D.W., Yamashita, N., Beck, A.W., Feldman, W.C., Hendricks, J.S., Lawrence, D.J., McCoy, T.J., McSween, H.Y., Peplowski, P.N., Reedy, R.C., Toplis, M.J., Corre, L., Mizzon, H., Reddy, V., Titus, T.N., Raymond, C.A., Russell, C.T., 2013. Neutron absorption constraints on the composition of 4 Vesta. Meteoritics and Planetary Science 48, 2211-2236.

Prettyman, T.H., Mittlefehldt, D.W., Yamashita, N., Lawrence, D.J., Beck, A.W., Feldman, W.C., McCoy, T.J., McSween, H.Y., Toplis, M.J., Titus, T.N., Tricarico, P., Reedy, R.C., Hendricks, J.S., Forni, O., Le Corre, L., Li, J.Y., Mizzon, H., Reddy, V., Raymond, C.A., Russell, C.T., 2012. Elemental mapping by Dawn reveals exogenic H in Vesta's regolith. Science 338, 242-246.

Preusker, F., Scholten, F., Knollenberg, J., Kührt, E., Matz, K.-D., Mottola, S., Roatsch, T., Thomas, N., 2012a. The northern hemisphere of asteroid (21) Lutetia—topography and orthoimages from Rosetta OSIRIS NAC image data. Planetary and Space Science 66, 54-63.

Preusker, F., Scholten, F., Matz, K.-D., Jaumann, R., Roatsch, T., Raymond, C.A., Russell, C.T., 2012b. Topography of Vesta from Dawn FC Stereo Images, Lunar and Planetary Science Conference 1659 ed, The Woodlands, Texas, p. 2012.

Preusker, F., Scholten, F., Matz, K.-D., Roatsch, T., Jaumann, R., Raymond, C.A., Russell, C.T., 2012c. Topography of Vesta from Dawn FC stereo images, European Planetary Science Congress 2012, p. 428.

Preusker, F., Scholten, F., Matz, K.-D., Roatsch, T., Jaumann, R., Raymond, C.A., Russell, C.T., Giesen, N., 2012d. Topography of asteroid (4) Vesta from Dawn FC HAMO stereo images, In: Abbasi, A. (Ed.), EGU General Assembly Conference Abstracts, p. 11805.

Ramsley, K.R., Head III, J.W., 2013. The origin of Phobos grooves from ejecta launched from impact craters on Mars: Tests of the hypothesis. Planetary and Space Science 75, 69-95.

Raymond, C.A., Park, R.S., Asmar, S.W., Konopliv, A.S., Buczkowski, D.L., De Sanctis, M.C., McSween, H.Y., Russell, C.T., Jaumann, R., Preusker, F., 2013. Vestalia Terra: An Ancient Mascon in the Southern Hemisphere of Vesta. LPI Contributions 1719, 2882.

Raymond, S.N., O'Brien, D.P., Morbidelli, A., Kaib, N.A., 2009. Building the terrestrial planets: Constrained accretion in the inner Solar System. Icarus 203, 644-662.

Reddy, V., Gaffey, M.J., Kelley, M.S., Nathues, A., Li, J.-Y., Yarbrough, R., 2010. Compositional heterogeneity of Asteroid 4 Vesta's southern hemisphere: Implications for the Dawn mission. Icarus 210, 693-706.

Reddy, V., Le Corre, L., McCoy, T.J., Nathues, A., Mayne, R.G., Sunshine, J., Gaffey, M.J., Becker, K.J., Cloutis, E.A., 2012a. Testing the Magma Ocean Model Using Distribution of Chromium on Vesta's Surface from Dawn Framing Camera Color Images, Lunar and Planetary Institute Science Conference Abstracts, p. 1588.

Reddy, V., Le Corre, L., O'Brien, D.P., Nathues, A., Cloutis, E.A., Durda, D.D., Bottke, W.F., Bhatt, M.U., Nesvorný, D., Buczkowski, D., Scully, J.E.C., Palmer, E.M., Sierks, H., Mann, P.J., Becker, K.J., Beck, A.W., Mittlefehldt, D., Li, J.-Y., Gaskell, R., Russell, C.T., Gaffey, M.J., McSween, H.Y., McCord, T.B., Combe, J.-P., Blewett, D., 2012b. Delivery of dark material to Vesta via carbonaceous chondritic impacts. Icarus 221, 544-559.

Reddy, V., Li, J.-Y., Le Corre, L., Scully, J.E.C., Gaskell, R., Russell, C.T., Park, R.S., Nathues, A., Raymond, C., Gaffey, M.J., Sierks, H., Becker, K.J., McFadden, L.A., 2013. Comparing Dawn, Hubble Space Telescope, and ground-based interpretations of (4) Vesta. Icarus 226, 1103-1114.

Reddy, V., Nathues, A., Gaffey, M.J., 2011a. First fragment of Asteroid 4 Vesta's mantle detected. Icarus 212, 175-179.

Reddy, V., Nathues, A., Gaffey, M.J., Schaeff, S., 2011b. Mineralogical characterization of potential targets for the ASTEX mission scenario. Planetary and Space Science 59, 772-778.

Reddy, V., Nathues, A., Le Corre, L., Sierks, H., Li, J.Y., Gaskell, R., McCoy, T., Beck, A.W., Schroder, S.E., Pieters, C.M., Becker, K.J., Buratti, B.J., Denevi, B., Blewett, D.T., Christensen, U., Gaffey, M.J., Gutierrez-Marques, P., Hicks, M., Keller, H.U., Maue, T., Mottola, S., McFadden, L.A., McSween, H.Y., Mittlefehldt, D., O'Brien, D.P., Raymond, C., Russell, C., 2012c. Color and albedo heterogeneity of Vesta from Dawn. Science 336, 700-704.

Reddy, V., Sanchez, J.A., Nathues, A., Moskovitz, N.A., Li, J.-Y., Cloutis, E.A., Archer, K., Tucker, R.A., Gaffey, M.J., Paul Mann, J., Sierks, H., Schade, U., 2012d. Photometric, spectral phase and temperature effects on 4 Vesta and HED meteorites: Implications for the Dawn mission. Icarus 217, 153-168.

Richardson, J.E., 2009. Cratering saturation and equilibrium: A new model looks at an old problem. Icarus 204, 697-715.

Richardson, J.E., 2013. Three-Dimensional Modeling of Crater Degradation via the Effects of Impact Induced Seismic Shaking, with Comparison to Crater Count Data. LPI Contributions 1719, 2397.

Richardson, J.E., Melosh, H.J., Greenberg, R., 2004. Impact-Induced Seismic Activity on Asteroid 433 Eros: A Surface Modification Process. Science 306, 1526-1529.

Richardson, J.E., Melosh, H.J., Greenberg, R.J., O'Brien, D.P., 2005. The global effects of impact-induced seismic activity on fractured asteroid surface morphology. Icarus 179, 325-349.

Richardson, J.E., Minton, D.A., Thomas, P.C., 2012. Exploring the Bombardment History of the Outer Solar System via Saturnian Satellite Cratering Records, Workshop on the Early Solar System Bombardment II, held 1-3 February 2012, in Houston, Texas. LPI Contribution No. 1649, pp. 65-66.

Rivkin, A.S., McFadden, L.A., Binzel, R.P., Sykes, M., 2006. Rotationally-resolved spectroscopy of Vesta I: 2 4 mum region. Icarus 180, 464-472.

Roatsch, T., Kersten, E., Hoffmeister, A., Wählisch, M., Matz, K.D., Porco, C.C., 2013a. Recent improvements of the Saturnian satellites atlases: Mimas, Enceladus, and Dione. Planetary and Space Science 77, 118-125.

Roatsch, T., Kersten, E., Matz, K.-D., Preusker, F., Scholten, F., Elgner, S., Jaumann, R., Raymond, C.A., Russell, C.T., 2013b. High-resolution Vesta Low Altitude Mapping Orbit Atlas derived from Dawn Framing Camera images. Planetary and Space Science 85, 293-298.

Roatsch, T., Kersten, E., Matz, K.D., Preusker, F., Scholten, F., Jaumann, R., Raymond, C.A., Russell, C.T., 2012. High resolution Vesta High Altitude Mapping Orbit (HAMO) Atlas derived from Dawn framing camera images. Planetary and Space Science 73, 283-286.

Roatsch, T., Wählisch, M., Hoffmeister, A., Kersten, E., Matz, K.D., Scholten, F., Wagner, R., Denk, T., Neukum, G., Helfenstein, P., Porco, C., 2009. High-resolution Atlases of Mimas, Tethys, and Iapetus derived from Cassini-ISS images. Planetary and Space Science 57, 83-92.

Roig, F., Nesvorný, D., Gil-Hutton, R., Lazzaro, D., 2008. V-type asteroids in the middle main belt. Icarus 194, 125-136.

Ruesch, O., Hiesinger, H., Blewett, D.T., Williams, D.A., Buczkowski, D., Scully, J., Yingst, R.A., Roatsch, T., Preusker, F., Jaumann, R., Russell, C.T., Raymond, C.A., 2014. Geologic map of the northern hemisphere of Vesta based on Dawn Framing Camera (FC) images. Icarus 244, 41-59.

Russell, C.T., Barucci, M.A., Binzel, R.P., Capria, M.T., Christensen, U., Coradini, A., De Sanctis, M.C., Feldman, W.C., Jaumann, R., Keller, H.U., Konopliv, A.S., McCord, T.B., McFadden, L.A., McKeegan, K.D., McSween, H.Y., Mottola, S., Nathues, A., Neukum, G., Pieters, C.M., Prettyman, T.H., Raymond, C.A., Sierks, H., Smith, D.E., Spohn, T., Sykes, M.V., Vilas, F., Zuber, M.T., 2007. Exploring the asteroid belt with ion propulsion: Dawn mission history, status and plans. Advances in Space Research 40, 193-201.

Russell, C.T., Raymond, C.A., 2011. The Dawn Mission to Vesta and Ceres. Space Science Reviews 163, 3-23.

Russell, C.T., Raymond, C.A., Coradini, A., McSween, H.Y., Zuber, M.T., Nathues, A., De Sanctis, M.C., Jaumann, R., Konopliv, A.S., Preusker, F., Asmar, S.W., Park, R.S., Gaskell, R., Keller, H.U., Mottola, S., Roatsch, T., Scully, J.E.C., Smith, D.E., Tricarico, P., Toplis, M.J., Christensen, U.R., Feldman, W.C., Lawrence, D.J., McCoy, T.J., Prettyman, T.H., Reedy, R.C., Sykes, M.E., Titus, T.N., 2012. Dawn at Vesta: Testing the Protoplanetary Paradigm. Science 336, 684-686.

Schade, U., Wäsch, R., 1999. NIR reflectance spectroscopy of mafic minerals in the temperature range between 80 and 473 K. Advances in Space Research 23, 1253-1256.

Schenk, P., O'Brien, D.P., Marchi, S., Gaskell, R., Preusker, F., Roatsch, T., Jaumann, R., Buczkowski, D., McCord, T., McSween, H.Y., Williams, D., Yingst, A., Raymond, C., Russell, C., 2012a. The geologically recent giant impact basins at Vesta's south pole. Science 336, 694-697.

Schenk, P., Vincent, J.-B., O'Brien, D.P., Jaumann, R., Williams, D., 2012b. Impact crater morphologies on Vesta, European Planetary Science Congress 2012, p. 700.

Schenk, P.M., Murphy, S.W., 2011. The Rayed Craters of Saturn's Icy Satellites (Including Iapetus): Current Impactor Populations and Origins, Lunar and Planetary Science Conference, 1608 ed, The Woodlands, Texas, p. 2098.

Schmedemann, N., Denk, T., Wagner, R., Neukum, G., 2007. Stratigraphy and Surface Ages on Iapetus. Bulletin of the American Astronomical Society 39, 418.

Schmedemann, N., Galuba, G., Neukum, G., Denk, T., Wagner, R., Hartmann, O., 2010. Size-Frequency Distributions (SFD) of Impact Craters on Saturnian Satellites and of the Body Diameters of Possible Impactors, Lunar and Planetary Science Conference, 1533 ed, The Woodlands, Texas, p. 1989.

Schmedemann, N., Kneissl, T., Ivanov, B.A., Michael, G.G., Wagner, R.J., Neukum, G., Ruesch, O., Hiesinger, H., Krohn, K., Roatsch, T., Preusker, F., Sierks, H., Jaumann, R., Reddy, V., Nathues, A., Walter, S.H.G., Neesemann, A., Raymond, C.A., Russell, C.T., 2014a. The cratering record, chronology and surface ages of (4) Vesta in comparison to smaller asteroids and the ages of HED meteorites. Planetary and Space Science 103, 104-130.

Schmedemann, N., Kneissl, T., Michael, G., Neukum, G., Nathues, A., Sierks, H., Wagner, R., Krohn, K., Reddy, V., Hiesinger, H., Jaumann, R., Raymond, C.A., Russell, C.T., 2012a. Crater Size-Frequency Distribution (CSFD) and Chronology of Vesta --- Crater Counts Matching HED Ages. Publication: 43rd Lunar and Planetary Science Conference, held March 19--23, 2012 at The Woodlands, Texas. LPI Contribution No. 1659, id.2544.

Schmedemann, N., Kneissl, T., Michael, G., Neukum, G., Nathues, A., Sierks, H., Wagner, R., Krohn, K., Reddy, V., Hiesinger, H., Jaumann, R., Raymond, C.A., Russell, C.T., 2012b. Cratering on 4 Vesta - Comparison of Crater Retention Ages and Ar-Ar Ages of HED Meteorites. EGU General Assembly 2012, held 22-27 April, 2012 in Vienna, Austria., 9055.

Schmedemann, N., Kneissl, T., Neesemann, A., Michael, G., Wagner, R.J., Raymond, C.A., Russell, C.T., 2014b. The Signature of Secondary Cratering on 4 Vesta and Tethys, Lunar and Planetary Science Conference, p. 1960.

Schmedemann, N., Michael, G.G., Ivanov, B.A., Murray, J.B., Neukum, G., 2014c. The age of Phobos and its largest crater, Stickney. Planetary and Space Science 102, 152-163.

Schmedemann, N., Neukum, G., Denk, T., Wagner, R., 2009. Impact Crater Size-Frequency Distribution (SFD) on Saturnian Satellites and Comparison with Other Solar-System Bodies, Publication: 40th Lunar and Planetary Science Conference, (Lunar and Planetary Science XL), held March 23-27, 2009 in The Woodlands, Texas, id.1941.

Schultz, P.H., Gault, D.E., 1979. Atmospheric effects on Martian ejecta emplacement. Journal of Geophysical Research 84, 7669-7687.

Scott, E.R.D., Greenwood, R.C., Franchi, I.A., Sanders, I.S., 2009. Oxygen isotopic constraints on the origin and parent bodies of eucrites, diogenites, and howardites. Geochimica et Cosmochimica Acta 73, 5835-5853.

Shoemaker, E.M., 1965. Preliminary Analysis of the Fine Structure of the Lunar Surface in Mare Cognitum. The Nature of the Lunar Surface: proceedings of the 1965 IAU-NASA symposium held at Goddard Space Flight Center, April 15-16, 1965. Sponsored by IAU Commission 17 (the Moon) and NASA. Edited by Wilmot N. Hess, Donald H. Menz and John A. O'Keefe. Library of Congress Catalog Card Number 65-27671; QB591.C748 1965 c.2. Published by the Johns Hopkins Press, Baltimore, MD USA, 1965, 23.

Shoemaker, E.M., Hackman, R.J., 1962. Stratigraphic Basis for a Lunar Time Scale, In: amp, Z. K. Mikhailov, Z.K. (Eds.), The Moon. Academic Press, London and New York, pp. 289-300.

Sierks, H., Keller, H.U., Jaumann, R., Michalik, H., Behnke, T., Bubenhagen, F., Büttner, I., Carsenty, U., Christensen, U., Enge, R., Fiethe, B., Gutiérrez Marqués, P., Hartwig, H., Krüger, H., Kühne, W., Maue, T., Mottola, S., Nathues, A., Reiche, K.-U., Richards, M.L., Roatsch, T., Schröder, S.E., Szemerey, I., Tschentscher, M., 2011a. The Dawn Framing Camera. Space Science Reviews 163, 263-327.

Sierks, H., Lamy, P., Barbieri, C., Koschny, D., Rickman, H., Rodrigo, R., A'Hearn, M.F., Angrilli, F., Barucci, M.A., Bertaux, J.L., Bertini, I., Besse, S., Carry, B., Cremonese, G., Da Deppo, V., Davidsson, B., Debei, S., De Cecco, M., De Leon, J., Ferri, F., Fornasier, S., Fulle, M., Hviid, S.F., Gaskell, R.W., Groussin, O., Gutierrez, P., Ip, W., Jorda, L., Kaasalainen, M., Keller, H.U., Knollenberg, J., Kramm, R., Kührt, E., Küppers, M., Lara, L., Lazzarin, M., Leyrat, C., Lopez Moreno, J.J., Magrin, S., Marchi, S., Marzari, F., Massironi, M., Michalik, H., Moissl, R., Naletto, G., Preusker, F., Sabau, L., Sabolo, W., Scholten, F., Snodgrass, C., Thomas, N., Tubiana, C., Vernazza, P., Vincent, J.B., Wenzel, K.P., Andert, T., Patzold, M., Weiss, B.P., 2011b. Images of asteroid 21 Lutetia: a remnant planetesimal from the early Solar System. Science 334, 487-490.

Singer, R.B., Roush, T.L., 1985. Effects of Temperature on Remotely Sensed Mineral Absorption Features. J Geophys Res-Solid 90, 2434-2444.

Soter, S., Harris, A., 1977. Are Striations on Phobos Evidence for Tidal Stress. Nature 268, 421-422.

Spaute, D., Weidenschilling, S.J., Davis, D.R., Marzari, F., 1991. Accretional evolution of a planetesimal swarm: 1. A new simulation. Icarus 92, 147-164.

Spencer, J.R., Denk, T., 2010. Formation of Iapetus' Extreme Albedo Dichotomy by Exogenically Triggered Thermal Ice Migration. Science 327, 432-435.

Stooke, P., 2012. Stooke Small Bodies Maps V2.0. NASA Planetary Data System 183.

Strom, R.G., 1977. Origin and relative age of lunar and Mercurian intercrater plains. Physics of the Earth and Planetary Interiors 15, 156-172.

Strom, R.G., Malhotra, R., Ito, T., Yoshida, F., Kring, D.A., 2005. The Origin of Planetary Impactors in the Inner Solar System. Science 309, 1847-1850 (2005).

Tagle, R., Hecht, L., 2006. Geochemical identification of projectiles in impact rocks. Meteoritics and Planetary Science 41, 1721-1735.

Tanaka, H., Inaba, S., Nakazawa, K., 1996. Steady-State Size Distribution for the Self-Similar Collision Cascade. Icarus 123, 450-455.

Taylor, R.C., Tapia, S., Tedesco, E.F., 1985. The rotation period and pole orientation of asteroid 4 Vesta. Icarus 62, 298-304.

Taylor, S.R., 1975. Lunar science - a post-Apollo view. Scientific results and insights from the lunar samples, Lunar science - a post-Apollo view. Scientific results and insights from the lunar samples., by Taylor, S. R.. New York, NY (USA): Pergamon Press, 19 + 372 p.

Tedesco, E.F., Cellino, A., Zappalá, V., 2005. The Statistical Asteroid Model. I. The Main-Belt Population for Diameters Greater than 1 Kilometer. The Astronomical Journal 129, 2869-2886.

Tedesco, E.F., Veeder, G.J., Fowler, J.W., Chillemi, J.R., 1992. The IRAS Minor Planet Survey. Publication: The IRAS Minor Planet Survey, Final Report by E.R. Tedesco, G.J. Veeder, J.W. Fowler, and J.R. Chillemi. Phillips Laboratory, Hanscom Air Force Base, MA, December 1992. PL-TR-92-2049.

Tera, F., Papanastassiou, D.A., Wasserburg, G.J., 1974. Isotopic evidence for a terminal lunar cataclysm. Earth and Planetary Science Letters 22, 1-21.

Thomas, N., Barbieri, C., Keller, H.U., Lamy, P., Rickman, H., Rodrigo, R., Sierks, H., Wenzel, K.P., Cremonese, G., Jorda, L., Küppers, M., Marchi, S., Marzari, F., Massironi, M., Preusker, F., Scholten, F., Stephan, K., Barucci, M.A., Besse, S., El-Maarry, M.R., Fornasier, S., Groussin, O., Hviid, S.F., Koschny, D., Kührt, E., Martellato, E., Moissl, R., Snodgrass, C., Tubiana, C., Vincent, J.B., 2012. The geomorphology of (21) Lutetia: Results from the OSIRIS imaging system onboard ESA's Rosetta spacecraft. Planetary and Space Science 66, 96-124.

Thomas, N., Stelter, R., Ivanov, A., Bridges, N.T., Herkenhoff, K.E., McEwen, A.S., 2011. Spectral heterogeneity on Phobos and Deimos: HiRISE observations and comparisons to Mars Pathfinder results. Planetary and Space Science 59, 1281-1292.

Thomas, P., A'Hearn, M., Belton, M.J.S., Brownlee, D., Carcich, B., Hermalyn, B., Klaasen, K., Sackett, S., Schultz, P.H., Veverka, J., Bhaskaran, S., Bodewits, D., Chesley, S., Clark, B., Farnham, T., Groussin, O., Harris, A., Kissel, J., Li, J.Y., Meech, K., Melosh, J., Quick, A., Richardson, J., Sunshine, J., Wellnitz, D., 2013. The nucleus of Comet 9P/Tempel 1: Shape and geology from two flybys. Icarus 222, 453-466.

Thomas, P., Veverka, J., 1977. Phobos: Surface density of impact craters. Icarus 30, 595-597.

Thomas, P., Veverka, J., 1980. Crater densities on the satellites of Mars. Icarus 41, 365-380.

Thomas, P.C., 2010. Sizes, shapes, and derived properties of the saturnian satellites after the Cassini nominal mission. Icarus 208, 395-401.

Thomas, P.C., Belton, M.J.S., Carcich, B., Chapman, C.R., Davies, M.E., Sullivan, R., Veverka, J., 1996. The Shape of Ida. Icarus 120, 20-32.

Thomas, P.C., Binzel, R.P., Gaffey, M.J., Storrs, A.D., Wells, E.N., Zellner, B.H., 1997a. Impact Excavation on Asteroid 4 Vesta: Hubble Space Telescope Results. Science 277, 1492-1495.

Thomas, P.C., Binzel, R.P., Gaffey, M.J., Zellner, B.H., Storrs, A.D., Wells, E., 1997b. Vesta: Spin Pole, Size, and Shape from HST Images. Icarus 128, 88-94.

Thomas, P.C., Burns, J.A., Helfenstein, R., Squyres, S., Veverka, J., Porco, C., Turtle, E.P., McEwen, A., Denk, T., Giese, B., Roatsch, T., Johnson, T.V., Jacobson, R.A., 2007. Shapes of the saturnian icy satellites and their significance. Icarus 190, 573-584.

Thomas, P.C., Robinson, M.S., 2005. Seismic resurfacing by a single impact on the asteroid 433 Eros. Nature 436, 366-369.

Thomas, P.C., Veverka, J., Simonelli, D., Helfenstein, P., Carcich, B., Belton, M.J.S., Davies, M.E., Chapman, C., 1994. The Shape of Gaspra. Icarus 107, 23-36.

Titley, S.R., 1966. Seismic energy as an agent of morphologic modification on the Moon. Tech. Rep. United States Geological Survey, Flagstaff, AZ.

Tompkins, S., Pieters, C.M., 1999. Mineralogy of the lunar crust: Results from Clementine. Meteoritics and Planetary Science 34, 25-41.

Tompkins, S., Pieters, C.M., 2010. Spectral characteristics of lunar impact melts and inferred mineralogy. Meteoritics and Planetary Science 45, 1152-1169.

Tsiganis, K., Gomes, R., Morbidelli, A., Levison, H.F., 2005. Origin of the orbital architecture of the giant planets of the Solar System. Nature 435, 459-461.

U.S.G.S., 2006. FGDC Digital Cartographic Standard for Geologic Map Symbolization (PostScript Implementation):U.S. Geological Survey Techniques and Methods 11-A2.

Usui, T., McSween, H.Y., 2007. Geochemistry of 4 Vesta based on HED meteorites: Prospective study for interpretation of gamma ray and neutron spectra for the Dawn mission. Meteoritics and Planetary Science 42, 255-269.

Usui, T., McSween, H.Y.j., Jr., Mittlefehldt, D.W., Prettyman, T.H., 2010. K-Th-Ti systematics and new three-component mixing model of HED meteorites: Prospective study for interpretation of gamma-ray and neutron spectra for the Dawn mission. Meteoritics and Planetary Science 45, 1170-1190.

van der Bogert, C.H., Hiesinger, H., McEwen, A.S., Dundas, C., Bray, V., Robinson, M.S., Plescia, J.B., Reiss, D., Klemm, K., Lroc, T., 2010. Discrepancies Between Crater Size-Frequency Distributions on Ejecta and Impact Melt Pools at Lunar Craters: An Effect of Differing Target Properties? 41st Lunar and Planetary Science Conference, held March 1-5, 2010 in The Woodlands, Texas. LPI Contribution No. 1533, 2165.

Vasavada, A.R., Bandfield, J.L., Greenhagen, B.T., Hayne, P.O., Siegler, M.A., Williams, J.-P., Paige, D.A., 2012. Lunar equatorial surface temperatures and regolith properties from the Diviner Lunar Radiometer Experiment. Journal of Geophysical Research: Planets 117, E00H18.

Veverka, J., Belton, M., Klaasen, K., Chapman, C., 1994. Galileo's Encounter with 951 Gaspra: Overview. Icarus 107, 2-17.

Veverka, J., Helfenstein, P., Lee, P., Thomas, P., McEwen, A., Belton, M., Klaasen, K., Johnson, T.V., Granahan, J., Fanale, F., Geissler, P., Head, J.W., III, 1996. Ida and Dactyl: Spectral Reflectance and Color Variations. Icarus 120, 66-76.

Veverka, J., Thomas, P., Duxbury, T., 1978. The puzzling moons of Mars. Sky and Telescope 56, 186-189.

Vincent, J.-B., Besse, S., Marchi, S., Sierks, H., Massironi, M., The OSIRIS Team, 2012a. Physical properties of craters on asteroid (21) Lutetia. Planetary and Space Science 66, 79-86.

Vincent, J.-B., Hoffman, M., Nathues, A., Sierks, H., Gaskell, R.W., Marchi, S., O'Brien, D., Schenk, P., Fulchignoni, M., Keller, H.U., Raymond, C., Sykes, M., 2012b. Crater Depth-to-Diameter Ratio and Surface Properties of (4) Vesta, Lunar and Planetary Science Conference, p. 1415.

Vincent, J.B., Schenk, P., Nathues, A., Sierks, H., Hoffmann, M., Gaskell, R.W., Marchi, S., O'Brien, D.P., Sykes, M., Russell, C.T., Fulchignoni, M., Kellerg, H.U., Raymond, C., Palmer, E., Preusker, F., 2014. Crater depth-to-diameter distribution and surface properties of (4) vesta. Planetary and Space Science 103, 57-65.

Wagner, R., Neukum, G., Giese, B., Roatsch, T., Wolf, U., Denk, T., Cassini Iss, T., 2006. Geology, Ages and Topography of Saturn's Satellite Dione Observed by the Cassini ISS Camera, Publication: 37th Annual Lunar and Planetary Science Conference, March 13-17, 2006, League City, Texas, abstract no.1805.

Wagner, R.J., Neukum, G., Wolf, U., Schmedemann, N., Denk, T., Stephan, K., Roatsch, T., Porco, C.C., 2011. Bright Ray Craters on Rhea and Dione, Lunar and Planetary Science Conference, 1608 ed, The Woodlands, Texas, p. 2249.

Wählisch, M., Stooke, P.J., Karachevtseva, I.P., Kirk, R., Oberst, J., Willner, K., Nadejdina, I.A., Zubarev, A.E., Konopikhin, A.A., Shingareva, K.B., 2014. Phobos and Deimos cartography. Planetary and Space Science 102, 60-73.

Wählisch, M., Willner, K., Oberst, J., Matz, K.D., Scholten, F., Roatsch, T., Hoffmann, H., Semm, S., Neukum, G., 2010. A new topographic image atlas of Phobos. Earth and Planetary Science Letters 294, 547-553.

Wee, B.S., Yamaguchi, A., Ebihara, M., 2010. Platinum Group Elements in Howardites and Polymict Eucrites: Implications for Impactors on the HED Parent Body, Lunar and Planetary Science Conference, p. 1886.

Weidenschilling, S.J., 1974. A model for accretion of the terrestrial planets. Icarus 22, 426-435.

Weidenschilling, S.J., 1976. Accretion of the terrestrial planets. II. Icarus 27, 161-170.

Weidenschilling, S.J., 1977. The distribution of mass in the planetary system and solar nebula. Astrophysics and Space Science 51, 153-158.

Weidenschilling, S.J., 2011. Initial sizes of planetesimals and accretion of the asteroids. Icarus 214, 671-684.

Weiler, M., Rauer, H., Sterken, C., 2011. Cometary nuclear magnitudes from sky survey observations. Icarus 212, 351-366.

Weiss, B.P., Elkins-Tanton, L.T., Antonietta Barucci, M., Sierks, H., Snodgrass, C., Vincent, J.-B., Marchi, S., Weissman, P.R., Pätzold, M., Richter, I., Fulchignoni, M., Binzel, R.P., Schulz, R., 2012. Possible evidence for partial differentiation of asteroid Lutetia from Rosetta. Planetary and Space Science 66, 137-146.

Werner, S.C., 2005. Major Aspects of the Chronostratigraphy and Geologic Evolutionary History of Mars. Freie Universität Berlin, Fachbereich Geowissenschaften, p. 160.

Werner, S.C., 2008. The early martian evolution - Constraints from basin formation ages. Icarus 195, 45-60.

Werner, S.C., Harris, A.W., Neukum, G., Ivanov, B.A., 2002. The Near-Earth Asteroid Size-Frequency Distribution: A Snapshot of the Lunar Impactor Size-Frequency Distribution. Icarus 156, 287-290.

Werner, S.C., Ivanov, B.A., Neukum, G., 2009. Theoretical analysis of secondary cratering on Mars and an image-based study on the Cerberus Plains. Icarus 200, 406-417.

Werner, S.C., Ody, A., Poulet, F., 2014. The Source Crater of Martian Shergottite Meteorites. Science 343, 1343-1346.

Wetherill, G.W., 1975. Late heavy bombardment of the moon and terrestrial planets, Lunar and Planetary Science Conference Proceedings, pp. 1539-1561.

Wilhelms, D.E., McCauley, J.F., Trask, N.J., 1987. The geologic history of the moon, Washington : U.S. G.P.O. ; Denver, CO (Federal Center, Box 25425, Denver 80225) : For sale by the Books and Open-file Reports Section, U.S. Geological Survey, 1987.

Williams, D.A., Denevi, B.W., Mittlefehldt, D.W., Mest, S.C., Schenk, P.M., Yingst, R.A., Buczkowski, D.L., Scully, J.E.C., Garry, W.B., McCord, T.B., Combe, J.-P., Jaumann, R., Pieters, C.M., Nathues, A., Le Corre, L., Hoffmann, M., Reddy, V., Schäfer, M., Roatsch, T., Preusker, F., Marchi, S., Kneissl, T., Schmedemann, N., Neukum, G., Hiesinger, H., De Sanctis, M.C., Ammannito, E., Frigeri, A., Prettyman, T.H., Russell, C.T., Raymond, C.A., 2014a. The geology of the Marcia quadrangle of asteroid Vesta: Assessing the effects of large, young craters. Icarus 244, 74-88.

Williams, D.A., Jaumann, R., McSween, H.Y., Marchi, S., Schmedemann, N., Raymond, C.A., Russell, C.T., 2014b. The chronostratigraphy of protoplanet Vesta. Icarus 244, 158-165.

Williams, D.A., O'Brien, D.P., Schenk, P.M., Denevi, B.W., Carsenty, U., Marchi, S., Scully, J.E.C., Jaumann, R., De Sanctis, M.C., Palomba, E., Ammannito, E., Longobardo, A., Magni, G., Frigeri, A., Russell, C.T., Raymond, C.A., Davison, T.M., 2014c. Lobate and flow-like features on asteroid Vesta. Planetary and Space Science 103, 24-35.

Williams, D.A., Yingst, R.A., Garry, W.B., 2014d. Introduction: The geologic mapping of Vesta. Icarus 244, 1-12.

Williams, D.R., Wetherill, G.W., 1994. Size Distribution of Collisionally Evolved Asteroidal Populations: Analytical Solution for Self-Similar Collision Cascades. Icarus 107, 117-128.

Willner, K., Oberst, J., Hussmann, H., Giese, B., Hoffmann, H., Matz, K.-D., Roatsch, T., Duxbury, T., 2010. Phobos control point network, rotation, and shape. Earth and Planetary Science Letters 294, 541-546.

Willner, K., Shi, X., Oberst, J., 2014. Phobos' shape and topography models. Planetary and Space Science 102, 51-59.

Wohletz, K.H., Sheridan, M.F., 1983. Martian rampart crater ejecta - Experiments and analysis of melt-water interaction. Icarus 56, 15-37.

Wünnemann, K., Collins, G.S., Osinski, G.R., 2008. Numerical modelling of impact melt production in porous rocks. Earth and Planetary Science Letters 269, 530-539.

Yamashita, N., Prettyman, T.H., Mittlefehldt, D.W., Toplis, M.J., McCoy, T.J., Beck, A.W., Reedy, R.C., Feldman, W.C., Lawrence, D.J., Peplowski, P.N., Forni, O., Mizzon, H., Raymond, C.A., Russell, C.T., 2013. Distribution of iron on Vesta. Meteoritics and Planetary Science 48, 2237-2251.

Yingst, R.A., Mest, S.C., Berman, D.C., Garry, W.B., Williams, D.A., Buczkowski, D., Jaumann, R., Pieters, C.M., De Sanctis, M.C., Frigeri, A., Le Corre, L., Preusker, F., Raymond, C.A., Reddy, V., Russell, C.T., Roatsch, T., Schenk, P.M., 2014. Geologic mapping of Vesta. Planetary and Space Science 103, 2-23.

Zahnle, K., Dones, L., Levison, H.F., 1998. Cratering Rates on the Galilean Satellites. Icarus 136, 202-222.

Zahnle, K., Schenk, P., Levison, H., Dones, L., 2003. Cratering rates in the outer Solar System. Icarus 163, 263-289.

Zahnle, K., Schenk, P., Sobieszczyk, S., Dones, L., Levison, H.F., 2001. Differential Cratering of Synchronously Rotating Satellites by Ecliptic Comets. Icarus 153, 111-129.

Zellner, N.E.B., Gibbard, S., de Pater, I., Marchis, F., Gaffey, M.J., 2005. Near-IR imaging of Asteroid 4 Vesta. Icarus 177, 190-195.

Zolensky, M., Ivanov, A., 2003. The Kaidun Microbreccia Meteorite: A Harvest from the Inner and Outer Asteroid Belt. Chemie der Erde - Geochemistry 63, 185-246.

Zolensky, M.E., Weisberg, M.K., Buchanan, P.C., Mittlefehldt, D.W., 1996. Mineralogy of carbonaceous chondrite clasts in HED achondrites and the Moon. Meteoritics and Planetary Science 31, 518-537.

# Curriculum Vitae

The CV is removed from the online version of this document for data security reasons.

Der Lebenslauf ist in der Online-Version aus Gründen des Datenschutzes nicht enthalten.

# Publications

*Peer-Reviewed Papers (published papers)*

Denk, T., Neukum, G., Roatsch, T., Porco, C.C., Burns, J.A., Galuba, G.G., Schmedemann, N., Helfenstein, P., Thomas, P.C., Wagner, R.J., West, R.A., 2010. Iapetus: Unique Surface Properties and a Global Color Dichotomy from Cassini Imaging. Science 327, 435-439.

Hoffmann, G., Schmedemann, N., Schafmeister, M.T., 2009. Relative sea-level curve for SE Rügen and Usedom Island (SW Baltic Sea coast, Germany) using decompacted profiles. Zeitschrift der Deutschen Gesellschaft fur Geowissenschaften 160, 69-78.

Jaumann, R., Williams, D.A., Buczkowski, D.L., Yingst, R.A., Preusker, F., Hiesinger, H., Schmedemann, N., Kneissl, T., Vincent, J.B., Blewett, D.T., Buratti, B.J., Carsenty, U., Denevi, B.W., De Sanctis, M.C., Garry, W.B., Keller, H.U., Kersten, E., Krohn, K., Li, J.Y., Marchi, S., Matz, K.D., McCord, T.B., McSween, H.Y., Mest, S.C., Mittlefehldt, D.W., Mottola, S., Nathues, A., Neukum, G., O'Brien, D.P., Pieters, C.M., Prettyman, T.H., Raymond, C.A., Roatsch, T., Russell, C.T., Schenk, P., Schmidt, B.E., Scholten, F., Stephan, K., Sykes, M.V., Tricarico, P., Wagner, R., Zuber, M.T., Sierks, H., 2012b. Vesta's shape and morphology. Science 336, 687-690.

Kneissl, T., Schmedemann, N., Reddy, V., Williams, D.A., Walter, S.H.G., Neesemann, A., Michael, G.G., Jaumann, R., Krohn, K., Preusker, F., Roatsch, T., Le Corre, L., Nathues, A., Hoffmann, M., Schäfer, M., Buczkowski, D., Garry, W.B., Yingst, R.A., Mest, S.C., Russell, C.T., Raymond, C.A., 2014. Morphology and formation ages of mid-sized post-Rheasilvia craters – Geology of quadrangle Tuccia, Vesta. Icarus 244, 133-157.

Krohn, K., Jaumann, R., Elbeshausen, D., Kneissl, T., Schmedemann, N., Wagner, R., Voigt, J., Otto, K., Matz, K.D., Preusker, F., Roatsch, T., Stephan, K., Raymond, C.A., Russell, C.T., 2014. Asymmetric craters on Vesta: Impact on sloping surfaces. Planetary and Space Science 103, 36-56.

Krohn, K., Jaumann, R., Otto, K., Hoogenboom, T., Wagner, R., Buczkowski, D.L., Garry, B., Williams, D.A., Yingst, R.A., Scully, J., De Sanctis, M.C., Kneissl, T., Schmedemann, N., Kersten, E., Stephan, K., Matz, K.D., Pieters, C.M., Preusker, F., Roatsch, T., Schenk, P., Russell, C.T., Raymond, C.A., 2014. Mass movement on Vesta at steep scarps and crater rims. Icarus 244, 120-132.

Le Corre, L., Reddy, V., Schmedemann, N., Becker, K.J., O'Brien, D.P., Yamashita, N., Peplowski, P.N., Prettyman, T.H., Li, J.-Y., Cloutis, E.A., Denevi, B.W., Kneissl, T., Palmer, E., Gaskell, R.W., Nathues, A., Gaffey, M.J., Mittlefehldt, D.W., Garry, W.B., Sierks, H., Russell, C.T., Raymond, C.A., De Sanctis, M.C., Ammanito, E., 2013. Olivine or impact melt: Nature of the "Orange" material on Vesta from Dawn. Icarus 226, 1568-1594.

Michael, G.G., Platz, T., Kneissl, T., Schmedemann, N., 2012. Planetary surface dating from crater size-frequency distribution measurements: Spatial randomness and clustering. Icarus 218, 169-177.

Nathues, A., Hoffmann, M., Cloutis, E.A., Schäfer, M., Reddy, V., Christensen, U., Sierks, H., Thangjam, G.S., Le Corre, L., Mengel, K., Vincent, J.-B., Russell, C.T., Prettyman, T., Schmedemann, N., Kneissl, T., Raymond, C., Gutierrez-Marques, P., Hall, I., Büttner, I., 2014. Detection of serpentine in exogenic carbonaceous chondrite material on Vesta from Dawn FC data. Icarus 239, 222-237.

Schäfer, M., Nathues, A., Williams, D.A., Mittlefehldt, D.W., Le Corre, L., Buczkowski, D.L., Kneissl, T., Thangjam, G.S., Hoffmann, M., Schmedemann, N., Schäfer, T., Scully, J.E.C., Li, J.-Y., Reddy, V., Garry, W.B., Krohn, K., Yingst, R.A., Gaskell, R.W., Russell, C.T., 2014. Imprint of the Rheasilvia impact on Vesta – Geologic mapping of quadrangles Gegania and Lucaria. Icarus 244, 60-73.

Schmedemann, N., Kneissl, T., Ivanov, B.A., Michael, G.G., Wagner, R.J., Neukum, G., Ruesch, O., Hiesinger, H., Krohn, K., Roatsch, T., Preusker, F., Sierks, H., Jaumann, R., Reddy, V., Nathues, A., Walter, S.H.G., Neesemann, A., Raymond, C.A., Russell, C.T., 2014. The cratering record, chronology and surface ages of (4) Vesta in comparison to smaller asteroids and the ages of HED meteorites. Planetary and Space Science 103, 104-130.

Schmedemann, N., Michael, G.G., Ivanov, B.A., Murray, J.B., Neukum, G., 2014. The age of Phobos and its largest crater, Stickney. Planetary and Space Science 102, 152-163.

Schmedemann, N., Schafmeister, M.T., Hoffman, G., 2008. Numeric de-compaction of Holocene sediments. Polish Geological Institute Special Papers 23, 87-94.

Schmedemann, N., Schafmeister, M.T., Hoffmann, G., 2006. Impact of near surface compaction on layer geometry within unconsolidated sediments, south western Baltic Sea. Baltica 19, 64-71.

Williams, D.A., Denevi, B.W., Mittlefehldt, D.W., Mest, S.C., Schenk, P.M., Yingst, R.A., Buczkowski, D.L., Scully, J.E.C., Garry, W.B., McCord, T.B., Combe, J.-P., Jaumann, R., Pieters, C.M., Nathues, A., Le Corre, L., Hoffmann, M., Reddy, V., Schäfer, M., Roatsch, T., Preusker, F., Marchi, S., Kneissl, T., Schmedemann, N., Neukum, G., Hiesinger, H., De Sanctis, M.C., Ammannito, E., Frigeri, A., Prettyman, T.H., Russell, C.T., Raymond, C.A., 2014. The geology of the Marcia quadrangle of asteroid Vesta: Assessing the effects of large, young craters. Icarus 244, 74-88.

Williams, D.A., Jaumann, R., McSween, H.Y., Marchi, S., Schmedemann, N., Raymond, C.A., Russell, C.T., 2014. The chronostratigraphy of protoplanet Vesta. Icarus 244, 158-165.

Witasse, O., Duxbury, T., Chicarro, A., Altobelli, N., Andert, T., Aronica, A., Barabash, S., Bertaux, J.L., Bibring, J.P., Cardesin-Moinelo, A., Cichetti, A., Companys, V., Dehant, V., Denis, M., Formisano, V., Futaana, Y., Giuranna, M., Gondet, B., Heather, D., Hoffmann, H., Holmström, M., Manaud, N., Martin, P., Matz, K.D., Montmessin, F., Morley, T., Mueller, M., Neukum, G., Oberst, J., Orosei, R., Pätzold, M., Picardi, G., Pischel, R., Plaut, J.J., Reberac, A., Pardo Voss, P., Roatsch, T., Rosenblatt, P., Remus, S., Schmedemann, N., Willner, K., Zegers, T., 2014. Mars Express investigations of Phobos and Deimos. Planetary and Space Science 102, 18-34.

### *Manuscripts in review*

Schmedemann, N., Michael, G., Wagner, R.J., Denk, T., in review for Icarus. Impact Crater Size – Frequency Distribution on Mimas and the Age of Herschel.

### *Extended Abstracts*

Schmedemann, N., Dietrich, H., Hoffmann, G., Schafmeister, M.T., 2005. Computerized de-compaction of holocene sediments, GIS and Spatial Analysis - 2005 Annual Conference of the International Association for Mathematical Geology, IAMG 2005, pp. 422-427.

### *Conference Abstracts (excluding abstracts from less important meetings)*

Buczkowski, D., Kahn, E., Barnouin, O.S., Wyrick, D.Y., Gaskell, R.W., Yingst, R., Williams, D.A., Garry, W.B., LeCorre, L., Nathues, A., Scully, J.E., Blewett, D.T., Hiesinger, H., Schenk, P., Mest, S.C., Schmedemann, N., Krohn, K., Jaumann, R., Raymond, C.A., Roatsch, T., Preusker, F., Reddy, V., Denevi, B.W., Filacchione, G., Pieters, C.M., Russell, C.T., 2011. Structural features on 4Vesta: Observations and analysis. AGU Fall Meeting Abstracts 21, 05.

Buczkowski, D.L., Kahn, E., Barnouin, O., Wyrick, D.Y., Gaskell, R.W., Yingst, R.A., Williams, D.A., Garry, W.B., Le Corre, L., Nathues, A., Scully, J.E.C., Blewett, D., Hiesinger, H., Mest, S., Schenk, P.M., Schmedemann, N., Krohn, K., Jaumann, R., Raymond, C.A., Pieters, C.M., Roatsch, T., Preusker, F., Russell, C.T., 2012. Large-Scale Troughs on 4 Vesta: Observations and Analysis, Asteroids, Comets, Meteors 2012, 1667 ed, Niigata, Japan, p. 6432.

Denevi, B.W., Coman, E.I., Blewett, D.T., Mittlefehldt, D.W., Buczkowski, D.L., Combe, J.P., de Sanctis, M.C., Jaumann, R., Li, J.Y., Marchi, S., Nathues, A., Petro, N.E., Pieters, C.M., Schenk, P., Schmedemann, N., Schröder, S., Sunshine, J.M., Williams, D.A., Raymond, C.A., Russell, C.T., 2012. Regolith Depth, Mobility, and Variability on Vesta from Dawn's Low Altitude Mapping Orbit, Publication: 43rd Lunar and Planetary Science Conference, held March 19--23, 2012 at The Woodlands, Texas. LPI Contribution No. 1659, id.1943.

Denk, T., Neukum, G., Schmedemann, N., Roatsch, T., Thomas, P.C., Helfenstein, P., Turtle, E.P., Porco, C.C., 2008. Iapetus: Major discoveries from the Cassini imaging experiment, European Planetary Science Congress 2008, Proceedings of the conference held 21-25 September, 2008 in Münster, Germany. Muenster, Germany, p. 850.

Denk, T., Neukum, G., Schmedemann, N., Roatsch, T., Wagner, R.J., Giese, B., Perry, J.E., Helfenstein, P., Turtle, E.P., Porco, C.C., 2008. Iapetus Imaging During the Targeted Flyby of the Cassini Spacecraft, Lunar and Planetary Science Conference, 1391 ed, League City, Texas, p. 2533.

Denk, T., Roatsch, T., Giese, B., Wagner, R., Schmedemann, N., Neukum, G., 2007. The Saturnian Moon Iapetus and the Cassini Targeted Flyby on September 10, 2007, European Planetary Science Congress 2007, Proceedings of a conference held 20-24 August, 2007 in Potsdam, Germany. Potsdam, Germany, p. 670.

Denk, T., Schmedemann, N., Wagner, R., Giese, B., Perry, J., Helfenstein, P., Turtle, E., Neukum, G., Roatsch, T., Porco, C., 2008. Cassini ISS observations of Iapetus: Results from the primary mission, COSPAR Scientific Assembly, Montreal, Canada, p. 700.

Hiesinger, H., van der Bogert, C.H., Pasckert, J.H., Schmedemann, N., Robinson, M.S., Jolliff, B., Petro, N., 2012. New Crater Counts of the South Pole-Aitken Basin. EGU General Assembly 2012, held 22-27 April, 2012 in Vienna, Austria., 8410.

Hiesinger, H., van der Bogert, C.H., Pasckert, J.H., Schmedemann, N., Robinson, M.S., Jolliff, B., Petro, N., 2012. New Crater Size-Frequency Distribution Measurements of the South Pole-Aitken Basin, Publication: 43rd Lunar and Planetary Science Conference, held March 19--23, 2012 at The Woodlands, Texas. LPI Contribution No. 1659, id.2863.

Hoogenboom, T., Schenk, P., White, O.L., Williams, D., Heisinger, H., Garry, W.B., Yingst, R.A., Buczkowski, D.L., McCord, T.B., Jaumann, R., Pieters, C.M., Gaskell, R.W., Neukum, G., Schmedemann, N., Marchi, S., Nathues, A., Lecorre, L., Roatsch, T., Preusker, F., de Sanctis, M.C., Fillacchione, G., Raymond, C.A., Russell, C.T., 2012. Geologic Mapping of the Av-11 Pinaria Quadrangle of Asteroid 4 Vesta, Publication: 43rd Lunar and Planetary Science Conference, held March 19--23, 2012 at The Woodlands, Texas. LPI Contribution No. 1659, id.2179.

Hoogenboom, T., Schenk, P., Williams, D.A., Hiesinger, H., Garry, W.B., Yingst, R., Buczkowski, D., McCord, T.B., Jaumann, R., Pieters, C.M., Gaskell, R.W., Neukum, G., Schmedemann, N., Marchi, S., Nathues, A., Le Corre, L., Roatsch, T., Preusker, F., White, O.L., DeSanctis, C., Filacchione, G., Raymond, C.A., Russell, C.T., 2011. Mapping Vesta Mid-Latitude Quadrangle V-12EW: Mapping the Edge of the South Polar Structure. AGU Fall Meeting Abstracts 31, 0020.

Jaumann, R., Mottola, S., Pieters, C.M., Russell, C.T., Raymond, C.A., Yingst, R.A., Williams, D.A., Schenk, P., Buczkowski, D.L., Denevi, B., Neukum, G., O'Brien, D.P., Garry, W.G., Blewett, D., Roatsch, T., Preusker, F., Krohn, K., Stephan, K., Carsenty, U., Nathues, A., Sykes, M.V., De Sanctis, M.C., McSween, H.Y., Keller, H.U., Schmedemann, N., Hiesinger, H., Marchi, S., McCord, T.B., Zuber, M.T., Sierks, H., 2012. Mapping Vesta: A Geological Overview. Publication: Asteroids, Comets, Meteors 2012, Proceedings of the conference held May 16-20, 2012 in Niigata, Japan. LPI Contribution No. 1667, id.6124.

Jaumann, R., Pieters, C.M., Raymond, C.A., Yingst, R.A., Williams, D.A., Schenk, P., Buczkowski, D.L., Denevi, B.W., Neukum, G., Mottola, S., O'Brien, D.P., Garry, W.B., Blewett, D.T., Roatsch, T., Preusker, F., Krohn, K., Stephan, K., Nathues, A., Sykes, M.V., de Sanctis, M.C., McSween, H.Y., Keller, H.U., Schmedemann, N., Hiesinger, H., Marchi, S., McCord, T.B., Zuber, M.T., 2012. Mapping Vesta: A Geological Overview, Publication: 43rd Lunar and Planetary Science Conference, held March 19--23, 2012 at The Woodlands, Texas. LPI Contribution No. 1659, id.1788.

Jaumann, R., Russell, C.T., Raymond, C.A., Pieters, C.M., Yingst, R.A., Williams, D.A., Buczkowski, D.L., Schenk, P., Denevi, B., Krohn, K., Stephan, K., Roatsch, T., Preusker, F., Otto, K., Mest, S.C., Ammannito, E., Blewett, D., Carsenty, U., DeSanctis, C.M., Garry, W., Hiesinger, H., Keller, H.U., Kersten, E., Marchi, S., Matz, K.D., McCord, T.B., McSween, H.Y., Mottola, S., Nathues, A., Neukum, G., O'Brien, D.P., Schmedemann, N., Scully, J.E.C., Sykes, M.V., Zuber, M.T., 2012. Vesta: A Geological Overview, AAS/Division for Planetary Sciences Meeting Abstracts.

Jaumann, R., Yingst, R., Schenk, P., Schmedemann, N., Williams, D.A., Pieters, C.M., Buczkowski, D., Stephan, K., Roatsch, T., Preusker, F., Scholten, F., Neukum, G., O'Brien, D.P., Mest, S.C., Krohn, K., Marchi, S., Filacchione, G., Russell, C.T., Raymond, C.A., De Sanctis, M.C., 2011. Mapping Vesta South Polar Quadrangle V-15SP: A Complex Geological Structure Dominates Vesta. AGU Fall Meeting Abstracts 31, 0023.

Jaumann, R., Yingst, R.A., Pieters, C.M., Russell, C.T., Raymond, C.A., Neukum, G., Mottola, S., Keller, H.U., Nathues, A., Sierks, H., Coradini, A., Desanctis, M.C., McSween, H.Y., Ammannito, E., Berman, D., Blewett, D., Buczkowski, D.L., Capria, M.T., Combe, J.P., Denevi, B., Filacchione, G., Frigeri, A., Garry, W.B., Gutierrez Marquš, P., Hiesinger, H., Kneissl, T., Krohn, K., Kührt, E., Le Corre, L., Li, J.Y., Marchi, S., McFadden, L., Mest, S., Mittlefehldt, D., O'Brien, D.P., Petro, N., Prettyman, T.H., Preusker, F., Rayman, M.D., Roatsch, T., Schenk, P., Scholten, F., Schmedemann, N., Schröder, S., Scully, J., Stephan, K., Sunshine, J., Sykes, M.V., Turrini, D., Wagner, R., Williams, D.A., 2011. Mapping Vesta: First Results from Dawn's Survey Orbit, European Planetary Science Congress - DPS Joint Meeting 2011, Nantes, France, p. 437.

Kneissl, T., Schmedemann, N., Neesemann, A., Raymond, C.A., Russell, C.T., 2014. Crater Counting on Small Bodies --- The Influence of Topography-Related Distortions, Lunar and Planetary Science Conference, p. 2398.

Kneissl, T., Schmedemann, N., Neukum, G., Williams, D.A., Garry, W.B., Yingst, R.A., Ammannito, E., Jaumann, R., Pieters, C.M., Russell, C.T., Raymond, C.A., Schenk, P., Hiesinger, H., McCord, T.B., Buczkowski, D., Nathues, A., Reddy, V., Büttner, I., Krohn, K., Preusker, F., Giesen, N., 2012. Geologic Mapping of the Av-13 Tuccia Quadrangle of Asteroid 4 Vesta, In: Abbasi, A. (Ed.), EGU General Assembly Conference Abstracts, p. 8239.

Kneissl, T., Schmedemann, N., Neukum, G., Williams, D.A., Garry, W.B., Yingst, R.A., Ammannito, E., Jaumann, R., Pieters, C.M., Russell, C.T., Raymond, C.A., Schenk, P., Hiesinger, H., McCord, T.B., Buczkowski, D.L., Nathues, A., Reddy, V., Büttner, I., Krohn, K., Preusker, F., 2012. Geologic Mapping of the AV-13 Tuccia Quadrangle of Asteroid 4 Vesta, Publication: 43rd Lunar and Planetary Science Conference, held March 19--23, 2012 at The Woodlands, Texas. LPI Contribution No. 1659, id.1899.

Kneissl, T., Schmedemann, N., Walter, S., Williams, D., Garry, W.B., Yingst, R.A., Reddy, V., Jaumann, R., Krohn, K., Preusker, F., Roatsch, T., Buczkowski, D.L., Raymond, C.A., Russell, C.T., 2013. Prominent Impact Craters in the AV-13 Quadrangle Tuccia on Vesta — Morphology, Degradation, and Ages of Tuccia, Eusebia, Vibidia, Galeria, and Antonia. LPI Contributions 1719, 1078.

Krohn, K., Jaumann, R., Elbeshausen, D., Kneissl, T., Wagner, R., Stephan, K., Otto, K., Matz, K.D., Preusker, F., Roatsch, T., Schmedemann, N., Raymond, C.A., Russell, C.T., 2013. Bimodal Craters on Vesta: Impacts on Slopes Studied by Geological Investigations. LPI Contributions 1719, 1949.

Krohn, K., Jaumann, R., Stephan, K., Pieters, C.M., Wagner, R., Yingst, R.A., Williams, D.A., Schenk, P., Neukum, G., Schmedemann, N., Kneissl, T., de Sanctis, M.C., Nathues, A., Buczkowski, D.L., Roatsch, T., Preusker, F., Kersten, E., Russell, C.T., Raymond, C.A., 2012. Geologic Mapping of the Av-12 Sextlia Quadrangle of Asteroid 4 Vesta, Publication: 43rd Lunar and Planetary Science Conference, held March 19--23, 2012 at The Woodlands, Texas. LPI Contribution No. 1659, id.1901.

Krohn, K., Jaumann, R., Stephan, K., Pieters, C.M., Wagner, R., Yingst, R.A., Williams, D.A., Schenk, P., Neukum, G., Schmedemann, N., Kneissl, T., DeSanctis, M.C., Nathues, A., Buczkowski, D.L., Roatsch, T., Preusker, F., Kersten, E., Russell, C.T., Raymond, C.A., Giesen, N., 2012. Geologic Mapping of the Av-12 Sextilia Quadrangle of Asteroid 4 Vesta, In: Abbasi, A. (Ed.), EGU General Assembly Conference Abstracts, p. 8175.

Le Corre, L., Reddy, V., Schmedemann, N., Becker, K.J., O'Brien, D.P., Yamashita, N., Peplowski, P.N., Prettyman, T.H., Li, J.-Y., Cloutis, E.A., Denevi, B.W., Kneissl, T., Palmer, E., Gaskell, R.W., Nathues, A., Gaffey, M.J., Mittlefehldt, D.W., Gary, W.B., Sierks, H., Russell, C.T., Raymond, C.A., 2014. Nature of the ``Orange'' Material on Vesta from Dawn. LPI Contributions 1773, 2048.

Mest, S.C., Yingst, R., Williams, D.A., Garry, W.B., Pieters, C.M., Jaumann, R., Buczkowski, D., Wyrick, D.Y., Schenk, P., Neukum, G., Schmedemann, N., Roatsch, T., Preusker, F., Ammannito, E., Russell, C.T., Raymond, C.A., 2011. Mapping Vesta Mid-Latitude Quadrangle V-11SE: Analysis of Dark "Ribbons" and Bright Rayed Craters. AGU Fall Meeting Abstracts 31, 0019.

Mest, S.C., Yingst, R.A., Williams, D.A., Garry, W.B., Pieters, C.M., Jaumann, R., Buczkowski, D.L., Sykes, M.V., Tricarico, P., Wyrick, D.Y., Schenk, P.M., Russell, C.T., Raymond, C.A., Neukum, G., Schmedemann, N., Roatsch, T., Preusker, F., Ammannito, E., Dawn, T., 2012. Geologic Mapping of the Av-14 Urbinia Quadrangle of Asteroid 4 Vesta, Publication: 43rd Lunar and Planetary Science Conference, held March 19--23, 2012 at The Woodlands, Texas. LPI Contribution No. 1659, id.2375.

Mest, S.C., Yingst, R.A., Williams, D.A., Garry, W.B., Pieters, C.M., Jaumann, R., Buczkowski, D.L., Sykes, M.V., Wyrick, D.Y., Schenk, P.M., Russell, C.T., Raymond, C.A., Neukum, G., Schmedemann, N., Roatsch, T., Preusker, F., Ammannito, E., Giesen, N., 2012. Geologic Mapping of the Av-14 Urbinia Quadrangle of Asteroid 4 Vesta, In: Abbasi, A. (Ed.), EGU General Assembly Conference Abstracts, p. 9611.

Michael, G.G., Platz, T., Kneissl, T., Schmedemann, N., 2012. Planetary Surface Dating from Crater Size-Frequency Distribution Measurements: Spatial Randomness and Clustering, Lunar and Planetary Institute Science Conference Abstracts, p. 2486.

Nathues, A., Sykes, M.V., Büttner, I., Buczkowski, D.L., Carsenty, U., Castillo-Rogez, J., Christensen, U., Gutiérrez Marqués, P., Hall, I., Hoffmann, M., Jaumann, R., Joy, S., Keller, H.U., Kersten, E., Krohn, K., Li, J.-Y., Marchi, S., Matz, K.-D., McCord, T.B., McFadden, L.A., Mengel, K., Mertens, V., Mottola, S., Neumann, W., Mastrodemos, N., O'Brien, D.P., Otto, K., Pieters, C., Pieth, S., Polanskey, C., Preusker, F., Rayman, M.D., Raymond, C., Reddy, V., Ripken, J., Roatsch, T., Russell, C.T., Schäfer, M., Schäfer, T., Schenk, P., Schmedemann, N., Scholten, F., Schröder, S.E., Schulzeck, F., Sierks, H., Smith, D., Stephan, K., Thangjam, G., Weiland, M., Williams, D., Zuber, M., 2015. Dawn Framing Camera Clear Filter Imaging on Ceres Approach, Lunar and Planetary Science Conference, p. 2069.

Neesemann, A., Kneissl, T., Schmedemann, N., Walter, S., Raymond, C., Russell, C.T., 2014. Size-Frequency Distributions of Small Impact Craters on Vesta - Implications for Secondary Cratering, Lunar and Planetary Science Conference, p. 1712.

Neesemann, A., Kneissl, T., Schmedemann, N., Walter, S.H.G., van Gasselt, S., Hiesinger, H., Jaumann, R., Raymond, C., Russell, C.T., 2015. Crater Size-Frequency Distributions Accumulated on Ejecta Blankets of Fresh Primary Craters on Vesta, Lunar and Planetary Science Conference, p. 2814.

Neukum, G., Schenk, P., Schmedemann, N., Michael, G., Jaumann, R., Scully, J., Russell, C.T., O'Brien, D.P., Hiesinger, H., Nathues, A., Wagner, R., Marchi, S., 2011. Chronology and Cratering at Vesta: First Results from Dawn's Survey Orbit, European Planetary Science Congress - DPS Joint Meeting 2011, Nantes, France, p. 501.

Ruesch, O., Hiesinger, H., Schmedemann, N., Kneissl, T., Blewett, D.T., Williams, D.A., Russell, C.T., Raymond, C.A., 2012a. Geologic Mapping of the Av-2 Bellicia Quadrangle of 4 Vesta, Publication: 43rd Lunar and Planetary Science Conference, held March 19--23, 2012 at The Woodlands, Texas. LPI Contribution No. 1659, id.2160.

Ruesch, O., Hiesinger, H., Schmedemann, N., Kneissl, T., Blewett, D.T., Williams, D.A., Russell, C.T., Raymond, C.A., 2012. Geologic mapping of the Av-2 Bellicia quadrangle of asteroid 4 Vesta. EGU General Assembly 2012, held 22-27 April, 2012 in Vienna, Austria., 9122.

Schäfer, M., Nathues, A., Hoffmann, M., Cloutis, E.A., Reddy, V., Christensen, U., Sierks, H., Thangjam, G.S., Le Corre, L., Mengel, K., Vincent, J.B., Russel, C.T., Schmedemann, N., Kneissl, T., Raymond, C., 2014. Serpentine in Exogenic Carbonaceous Chondrite Material on Vesta Detected by Dawn FC, Lunar and Planetary Science Conference, p. 1745.

Schenk, P., Jaumann, R., Pieters, C.M., Neukum, G., Schmedemann, N., Yingst, R., Williams, D.A., Garry, W.B., Buczkowski, D., McCord, T.B., Sykes, M.V., O'Brien, D.P., Blewett, D.T., Asmar, S., Ermakov, A., Gaskell, R.W., Raymond, C.A., Polanskey, C., Marchi, S., Mottola, S., Prettyman, T.H., Roatsch, T., Preusker, F., Nathues, A., DeSanctis, C., McSween, H.Y., Russell, C.T., 2011. The South Polar Structure on Vesta from Dawn: Using Geologic, Topographic and Compositional Mapping and Planetary Analogs to Test Origin Models. AGU Fall Meeting Abstracts 21, 03.

Schmedemann, N., Denk, T., Wagner, R., Neukum, G., 2007. Stratigraphy and Surface Ages on Iapetus. Bulletin of the American Astronomical Society 39, 418.

Schmedemann, N., Denk, T., Wagner, R., Neukum, G., 2007. Stratigraphy and surface ages on Iapetus, European Planetary Science Congress 2007, Potsdam, Germany, p. 667.

Schmedemann, N., Galuba, G., Neukum, G., Denk, T., Wagner, R., Hartmann, O., 2010. Size-Frequency Distributions (SFD) of Impact Craters on Saturnian Satellites and of the Body Diameters of Possible Impactors, Lunar and Planetary Science Conference, 1533 ed, The Woodlands, Texas, p. 1989.

Schmedemann, N., Kneissl, T., Ivanov, B.A., Michael, G.G., Neukum, G., Nathues, A., Sierks, H., Wagner, R., Krohn, K., Le Corre, L., Reddy, V., Ruesch, O., Hiesinger, H., Jaumann, R., Raymond, C.A., Russell, C.T., 2013. Crater Retention Ages from (4) Vesta Matching Independent Ar-Ar Ages of HED Meteorites, EGU General Assembly Conference Abstracts, p. 5741.

Schmedemann, N., Kneissl, T., Ivanov, B.A., Michael, G.G., Neukum, G., Nathues, A., Sierks, H., Wagner, R., Krohn, K., Le Corre, L., Reddy, V., Ruesch, O., Hiesinger, H., Jaumann, R., Raymond, C.A., Russell, C.T., 2013. Lunar-Like Chronology for Vesta — Crater Retention Ages Matching Independent Ar-Ar HED Ages. LPI Contributions 1719, 2155.

Schmedemann, N., Kneissl, T., Michael, G., Neukum, G., Nathues, A., Sierks, H., Wagner, R., Krohn, K., Reddy, V., Hiesinger, H., Jaumann, R., Raymond, C.A., Russell, C.T., 2012. Crater Size-Frequency Distribution (CSFD) and Chronology of Vesta — Crater Counts Matching HED Ages, Lunar and Planetary Science Conference, 1659 ed, The Woodlands, Texas, p. 2544.

Schmedemann, N., Kneissl, T., Michael, G., Neukum, G., Nathues, A., Sierks, H., Wagner, R., Krohn, K., Reddy, V., Hiesinger, H., Jaumann, R., Raymond, C.A., Russell, C.T., Giesen, N., 2012. Cratering on 4 Vesta - Comparison of Crater Retention Ages and Ar-Ar Ages of HED Meteorites, In: Abbasi, A. (Ed.), EGU General Assembly Conference Abstracts, p. 9055.

Schmedemann, N., Kneissl, T., Michael, G., Wagner, R., Neukum, G., Nathues, A., Sierks, H., 2012. Crater Size-Frequency Distributions and Chronologies of Asteroids, Workshop on the Early Solar System Bombardment II, held 1-3 February 2012, in Houston, Texas. LPI Contribution No. 1649, pp. 75-76.

Schmedemann, N., Kneissl, T., Neesemann, A., Michael, G., Hiesinger, H., Jaumann, R., Raymond, C.A., Russell, C.T., 2015. The Age of the Rheasilvia Basin --- How the two Geological Interpretations and Chronology Systems Differ. LPI Contributions 1826, 3006.

Schmedemann, N., Kneissl, T., Neesemann, A., Michael, G., Wagner, R.J., Raymond, C.A., Russell, C.T., 2014. The Signature of Secondary Cratering on 4 Vesta and Tethys, Lunar and Planetary Science Conference, p. 1960.

Schmedemann, N., Michael, G., Ivanov, B.A., Kneissl, T., Neesemann, A., Hiesinger, H., Jaumann, R., Raymond, C.A., Russell, C.T., 2015. A Preliminary Chronology for Ceres, Lunar and Planetary Science Conference, p. 1418.

Schmedemann, N., Michael, G., Ivanov, B.A., Kneissl, T., Neesemann, A., Hiesinger, H., Jaumann, R., Raymond, C.A., Russell, C.T., 2015. Preliminary Results from Initial Investigations of Ceres' Cratering Record from Dawn Imaging Data, EGU General Assembly Conference Abstracts, p. 6486.

Schmedemann, N., Michael, G.G., Ivanov, B.A., Murray, J., Neukum, G., 2013. Crater Retention Ages of Phobos Based on a Lunar-Like Chronology, Lunar and Planetary Science Conference, p. 2193.

Schmedemann, N., Neukum, G., 2011. Impact Crater Size-Frequency Distribution (SFD) and Surface Ages on Mimas, Lunar and Planetary Science Conference, 1608 ed, The Woodlands, Texas, p. 2772.

Schmedemann, N., Neukum, G., Denk, T., Michael, G., Wagner, R., 2008. Improvement of the Crater Size-Frequency Distributon and Results on Surface Ages of the Saturnian Satellites, European Planetary Science Congress 2008, Proceedings of the conference held 21-25 September, 2008 in Münster, Germany. Muenster, Germany, p. 852.

Schmedemann, N., Neukum, G., Denk, T., Wagner, R., 2009. Impact Crater Size-Frequency Distribution (SFD) on Saturnian Satellites and Comparison with Other Solar-System Bodies, Publication: 40th Lunar and Planetary Science Conference, (Lunar and Planetary Science XL), held March 23-27, 2009 in The Woodlands, Texas, id.1941.

Schmedemann, N., Neukum, G., Denk, T., Wagner, R., Hartmann, O., 2009. Impact Crater Size-Frequency Distributions (SFD) on Saturnian Satellites and Other Solar-System Bodies, European Planetary Science Congress 2009, held 14-18 September in Potsdam, Germany. Potsdam, Germany, p. 365.

Schmedemann, N., Neukum, G., Denk, T., Wagner, R., Hartmann, O., 2010. Impact Crater Size-Frequency Distributions (SFD) on Saturnian Satellites in Comparison with Possible Impactor Populations. EGU General Assembly 2010, held 2-7 May, 2010 in Vienna, Austria, 4308.

Schmedemann, N., Neukum, G., Denk, T., Wagner, R., Hartmann, O., Michael, G., 2008. Comparison of the Production Size-frequency Distribution (SFD) of Craters on Saturnian Satellites With the Lunar Crater SFD and Asteroid Diameter SFD, American Astronomical Society - DPS meeting, 40 ed, p. 511.

Schmedemann, N., Neukum, G., Denk, T., Wagner, R., Hartmann, O., Tscherning, C.C., 2009. Comparison of Impact Crater Size-Frequency Distributions (SFD) on Saturnian Satellites with Other Solar-System Bodies, In: Arabelos, D.N. (Ed.), EGU General Assembly Conference Abstracts, p. 7702.

Schmedemann, N., Neukum, G., Denk, T., Wagner, R.J., 2008. Stratigraphy and Surface Ages on Iapetus and Other Saturnian Satellites, Lunar and Planetary Science Conference, 1391 ed, League City, Texas, p. 2070.

Schmedemann, N., Neukum, G., Kneissl, T., Williams, D.A., Garry, W.B., Yingst, R., Ammannito, E., Jaumann, R., Pieters, C.M., Russell, C.T., Raymond, C.A., Schenk, P., Hiesinger, H., McCord, T.B., Buczkowski, D., Nathues, A., Büttner, I., Krohn, K., 2011. Mapping Vesta Southern Quadrangle V-14SW: Identification of Dark and Bright Features. AGU Fall Meeting Abstracts 31, 0022.

Schmedemann, N., Wagner, R.J., Michael, G., Denk, T., Kneissl, T., 2015. The Crater Production Functions for Mimas. LPI Contributions 1826, 3021.

Sierks, H., Raymond, C.A., Nathues, A., Jaumann, R., Christensen, U., Vincent, J.B., Mattola, S., Gutierréz Marqués, P., Maue, T., Büttner, I., Hall, I., Schmedemann, N., Hiesinger, H., 2011. The Surface Features of Vesta: First Results from Dawn's Surbey Orbit, European Planetary Science Congress - DPS Joint Meeting 2011, Nantes, France, p. 1006.

Wagner, R., Schmedemann, N., Werner, S., Ivanov, B., Stephan, K., Jaumann, R., 2015. Crater size distributions on Ganymede and Callisto: fundamental issues, EGU General Assembly Conference Abstracts, p. 11785.

Wagner, R., Schmedemann, N., Neukum, G., Werner, S.C., Ivanov, B.A., Stephan, K., Jaumann, R., Palumbo, P., 2014. Reassessing the Crater Distributions on Ganymede and Callisto: Results from Voyager and Galileo, and an Outlook to ESA's JUICE Mission to Jupiter, AAS/Division for Planetary Sciences Meeting Abstracts.

Wagner, R., Stephan, K., Schmedemann, N., Roatsch, T., Kersten, E., Neukum, G., Denk, T., Porco, C.C., 2014. Large impacts and tectonism: the relative ages of the basin Odysseus and Ithaca Chasma on Saturn's icy moon Tethys, EGU General Assembly Conference Abstracts, p. 15716.

Wagner, R.J., Neukum, G., Schmedemann, N., 2012. Double and Multiple Craters on the Satellites of Saturn and Their Size Distribution, Publication: 43rd Lunar and Planetary Science Conference, held March 19--23, 2012 at The Woodlands, Texas. LPI Contribution No. 1659, id.2469.

Wagner, R.J., Neukum, G., Schmedemann, N., 2012. Identification, mapping and size distribution of double and multiple craters on satellites of Saturn. EGU General Assembly 2012, held 22-27 April, 2012 in Vienna, Austria., 10505.

Wagner, R.J., Neukum, G., Schmedemann, N., Hartmann, O., Wolf, U., 2010. Crater chains, double and multiple craters on the satellites of Saturn: morphology and stratigraphy, European Planetary Science Congress 2010, held 20-24 September in Rome, Italy. Rome, Italy, p. 676.

Wagner, R.J., Neukum, G., Wolf, U., Schmedemann, N., Denk, T., Stephan, K., Roatsch, T., Porco, C.C., 2011. Bright Ray Craters on Rhea and Dione, Lunar and Planetary Science Conference, 1608 ed, The Woodlands, Texas, p. 2249.

Wagner, R.J., Stephan, K., Huszmann, H., Roatsch, T., Jaumann, R., Neukum, G., Schmedemann, N., Wolf, U., 2009. Candidate imaging target areas of Ganymede and Callisto for geologic investigations and crater size-frequency measurements in a future mission to Jupiter and its satellites, European Planetary Science Congress 2009, held 14-18 September in Potsdam, Germany. Potsdam, Germany, p. 557.

Wagner, R.J., Stephan, K., Neukum, G., Schmedemann, N., Hartmann, O., Roatsch, T., Wolf, U., 2011. Ray craters on the satellites of Jupiter and Saturn, European Planetary Science Congress - DPS Joint Meeting 2011, Nantes, France, p. 1335.

White, O.L., Yingst, R.A., Berman, D., Frigeri, A., Jaumann, R., Le Corre, L., Mest, S., Pieters, C.M., Preusker, F., Raymond, C.A., Reddy, V., Roatsch, T., Russell, C.T., Schenk, P.M., Schmedemann, N., 2012. Geologic Mapping of the AV-15 Rheasilvia Quadrangle of Asteroid 4 Vesta, Publication: 43rd Lunar and Planetary Science Conference, held March 19--23, 2012 at The Woodlands, Texas. LPI Contribution No. 1659, id.1264.

Williams, D.A., Blewett, D.T., Buczkowski, D.L., Garry, W.B., Kneissl, T., Krohn, K., Mest, S.C., Ruesch, O., Schaefer, M., Scully, J.E.C., Yingst, R.A., Pieters, C.M., Jaumann, R., Raymond, C.A., McSween, H.Y., Marchi, S., Schmedemann, N., Russell, C.T., 2015. Complete Global Geologic Map of Vesta from Dawn and Mapping Plans for Ceres, Lunar and Planetary Science Conference, p. 1126.

Williams, D.A., Hiesinger, H., Garry, W.B., Buczkowski, D., McCord, T.B., Combe, J., Schenk, P., Jaumann, R., Pieters, C.M., Bleacher, J.E., Nathues, A., Le Corre, L., Hoffmann, M., Reddy, V., Roatsch, T., Preusker, F., Marchi, S., Russell, C.T., Raymond, C.A., Neukum, G., Schmedemann, N., Ammannito, E., 2011. Mapping Vesta Equatorial Quadrangle V-10EW: Identification of Dark (Volcanic?) Features. AGU Fall Meeting Abstracts 31, 0018.

Williams, D.A., Hiesinger, H., Schenk, P.M., Jaumann, R., Buczkowski, D.L., McCord, T.B., Yingst, R.A., Garry, W.B., Combe, J.P., Pieters, C.M., Nathues, A., Le Corre, L., Reddy, V., Roatsch, T., Preusker, F., Schmedemann, N., Neukum, G., Raymond, C.A., Ammannito, E., De Sanctis, M.C., 2012. Geologic Mapping of the Av-8 Marcia Quadrangle of Asteroid 4 Vesta. EGU General Assembly 2012, held 22-27 April, 2012 in Vienna, Austria., 5686.

Williams, D.A., Schenk, P.M., Jaumann, R., Buczkowski, D.L., McCord, T.B., Yingst, R.A., Hiesinger, H., Garry, W.B., Combe, J.P., Pieters, C.M., Nathues, A., Le Corre, L., Hoffmann, M., Reddy, V., Roatsch, T., Preusker, F., Marchi, S., Russell, C.T., Raymond, C.A., Neukum, G., Schmedemann, N., Ammannito, E., de Sanctis, M.C., 2012. Geologic Mapping of the Av-8 Marcia Quadrangle of Asteroid 4 Vesta, Publication: 43rd Lunar and Planetary Science Conference, held March 19--23, 2012 at The Woodlands, Texas. LPI Contribution No. 1659, id.1534.

Yingst, R.A., Ammannito, E., Berman, D., De Sanctis, M.C., Capaccioni, F., Frigeri, A., Jaumann, R., Le Corre, L., Mest, S., Palomba, E., Pieters, C.M., Preusker, F., Reddy, V., Roatsch, T., Russell, C.T., Schenk, P.M., Schmedemann, N., Williams, D.A., Tosi, F., Zambon, F., 2012. Geologic Mapping of the Av-15 Rheasilvia Quadrangle of Asteroid 4 Vesta. EGU General Assembly 2012, held 22-27 April, 2012 in Vienna, Austria., 6349.